Week 11: Project 2 - Emission characterization on a CAT3410 engine

In the following link, the bowl profile for the baseline engine and 3D geometry of the open-w piston are provided. Baseline input files that contain critical information are also provided.

07 CAT diesel engine project - Google Drive

Your job is to run simulations with both these pistons and characterize the emissions (NO_x, Soot, CO)

- Create cut-plan animations showing NO_x, Soot, carbon monoxide (CO) and compare them between the Open-W and Omega pistons.
    - Upload animations on YouTube and provide the YouTube link for animations in your report.
- Compare the indicated mean effective pressure (IMEP) and power values graphically.

NOTE:

- Make sure that the sector angle and periodic angle are 60°.
- Make sure to go through the setup once to check if all parameters are provided logically.

Solution

This project aims to characterize emissions and evaluate engine performance for Open-W and Omega piston configurations in a CAT3410 engine using CONVERGE CFD.

Objectives

- Create the engine sector surface (60°) using the provided bowl profiles, optimizing computational efficiency by simulating only one sector instead of the entire domain.
- Set up simulations for spray, combustion, and emissions modeling.
- Post-process the simulation results and conduct a comparative analysis of the selected bowl configurations.
- Assess engine performance parameters for both Open-W and Omega piston bowl geometries of the CAT3410 engine.
- Evaluate and compare the emissions of NO_x, Soot, and CO.

Theory

In internal combustion engines, the piston bowl design plays a critical role in determining combustion characteristics, emissions, and overall engine efficiency [1]. The geometry of the piston bowl influences air-fuel mixing, combustion timing, and heat transfer within the engine cylinder. Figure 1 shows the two piston bowl profiles used in the current study: the Open-W and Omega designs.

(a) **(b)**

Figure 1: Piston bowl profiles with (a) Open-W [Source] and (b) Omega designs [Source].

The **Open-W piston bowl** (Figure 1a) features a sharp, angular structure with multiple ridges forming a "W-like" pattern [2]. This open and intricate design enhances air-fuel mixing by promoting high turbulence and swirling motions within the combustion chamber. Such a geometry is particularly effective for engines operating under high-load conditions, optimizing combustion efficiency and reducing emissions, including soot and NO_x.

In contrast, the **Omega piston bowl** (Figure 1b) exhibits a smooth, rounded combustion chamber that resembles the Greek letter Omega (Ω) [3]. Its centralized and symmetrical structure ensures consistent flame propagation and controlled combustion. This design is best suited for applications that prioritize fuel efficiency, reduced peak pressures, and stable combustion under medium to low load conditions.

By comparing these two configurations, this study evaluates the influence of piston bowl geometry on key parameters such as emissions (NO_x, Soot, CO) and engine performance metrics, including indicated mean effective pressure (IMEP) and power. These profiles are applied in the CAT3410 engine model for further analysis using CONVERGE CFD. The following sections outline the practical setup, simulation parameters, and methodologies used for assessing these designs.

Geometry

The given geometry does not include any exhaust or inlet valves, representing a closed cycle system. To enhance computational efficiency and reduce simulation time, a 60-degree sector of geometry is used. The sectors can be defined based on the spray-to-angle ratio. For example, if the cylinder has 8 nozzles, each nozzle covers an angle of 45 degrees (360°/8). Similarly, if there are 6 nozzles, each covers 60 degrees (360°/6). Each sector, such as the one covering 60 degrees, represents $1/6^{th}$ of the entire geometry. This segmentation is employed to ensure smooth simulation performance and enhance computational efficiency.

Using Tools > Utilities > Make engine sector surface tool is employed to extract these sectors, with the bowl profiles for both the Open-W and Omega configurations loaded to obtain the respective sectors. The engine's geometric parameters are set as follows:

- **Bore:** 0.13716 m
- **Stroke:** 0.1651 m
- **Connecting rod length:** 0.263 m
- **Wrist pin offset:** 0
- **Compression ratio:** 17.5
- **Sector angle:** 60.0^o

Following that, the Open-W and Omega piston profiles are set as:

1. Open-W Piston

Follow these steps to create the Open-W piston geometry:

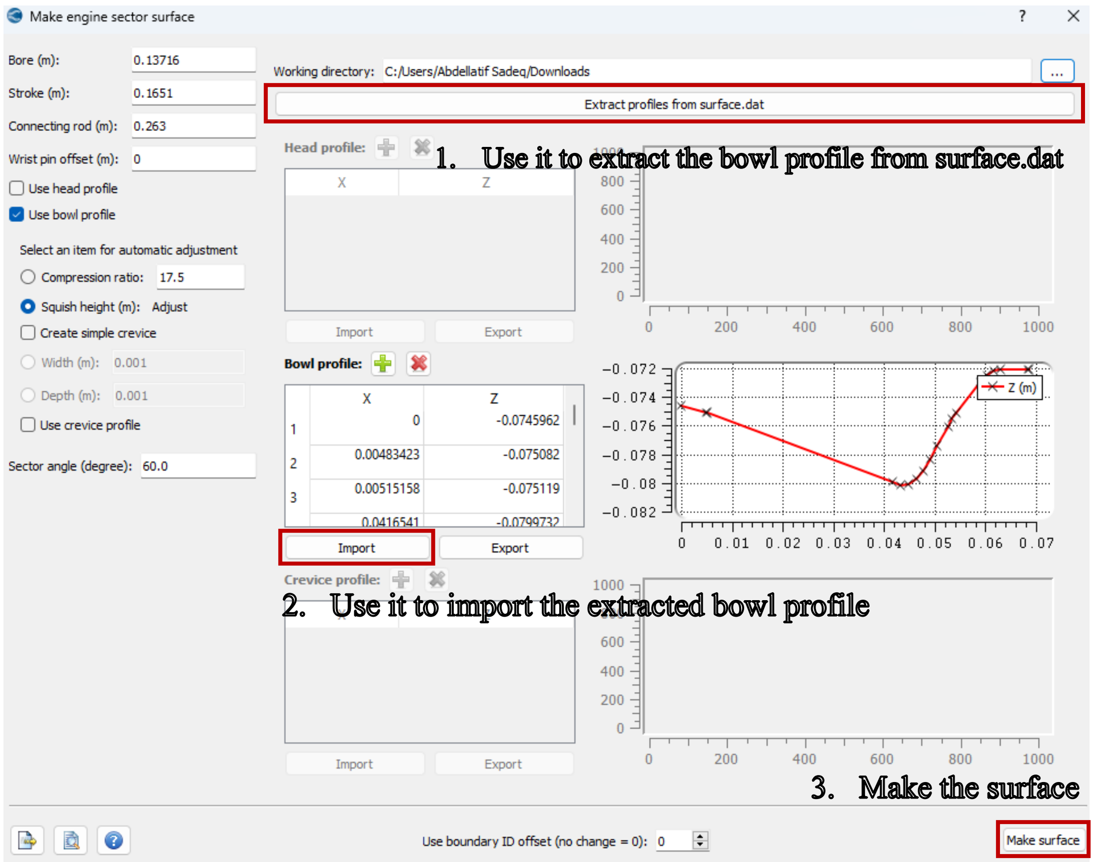

2. Omega Piston

Since the bowl profile for the Omega piston is provided, proceed to import it and generate the surface geometry.

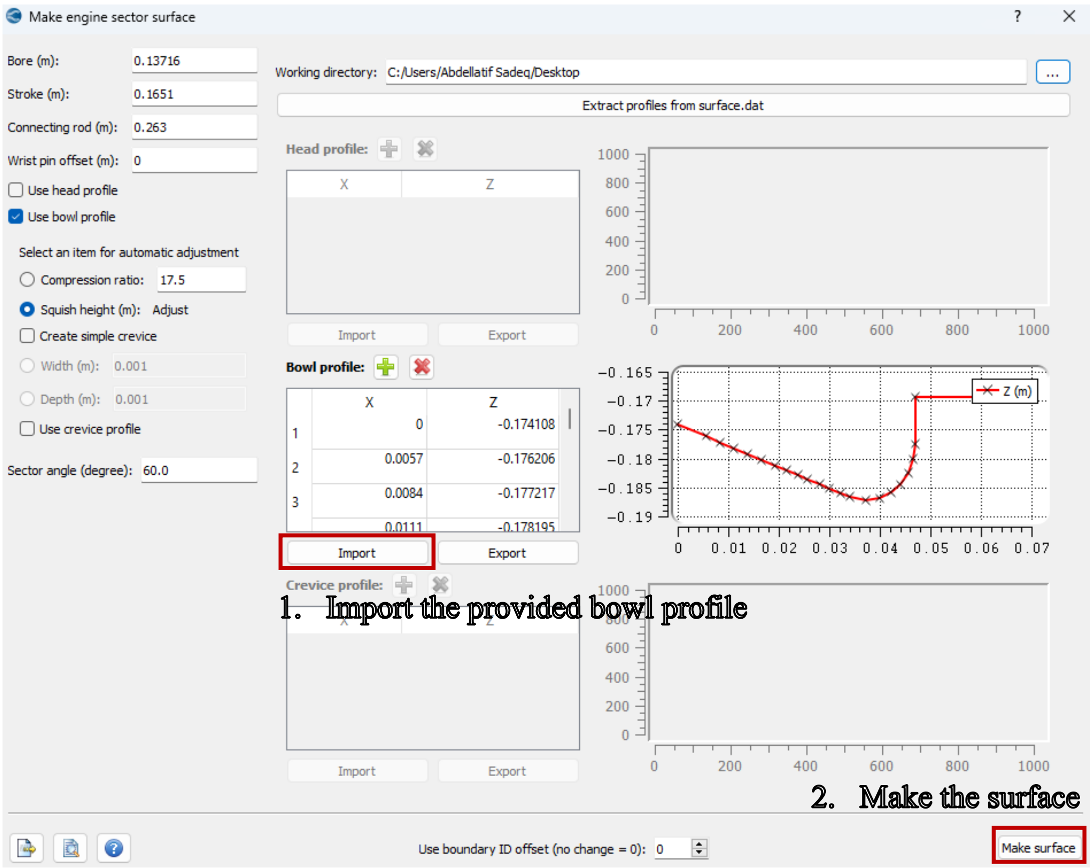

The surface geometries generated using this tool are displayed below:

1. Open-W Piston

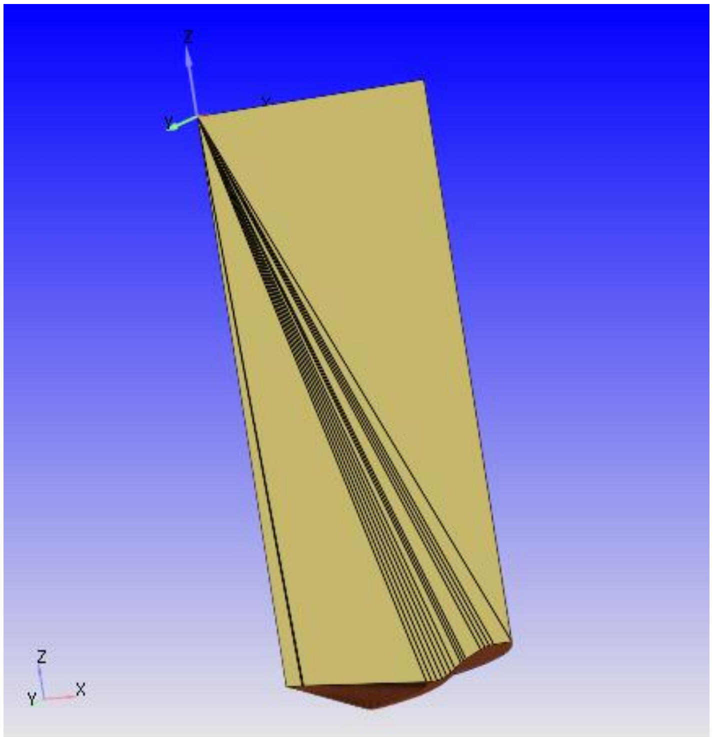

2. Omega Piston

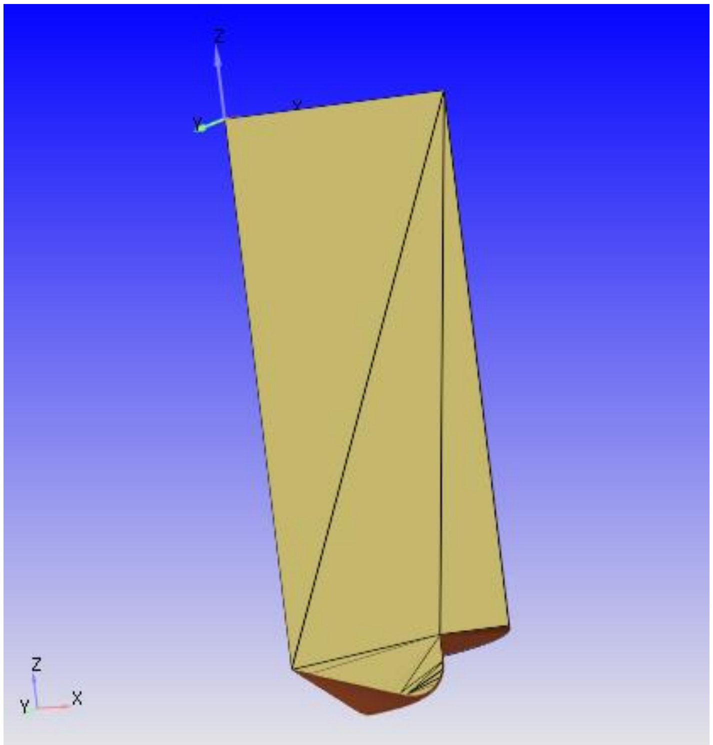

Boundary Flagging

CONVERGE CFD automatically flags the boundaries once the sector is generated as follows:

1. Open-W Piston

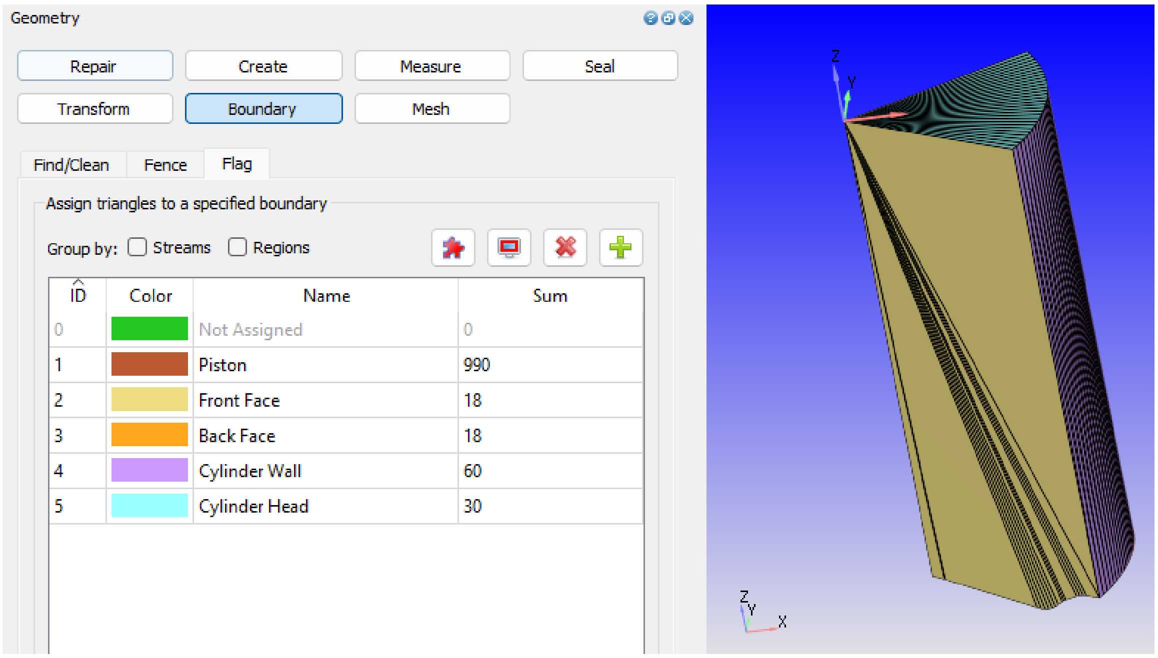

2. Omega Piston

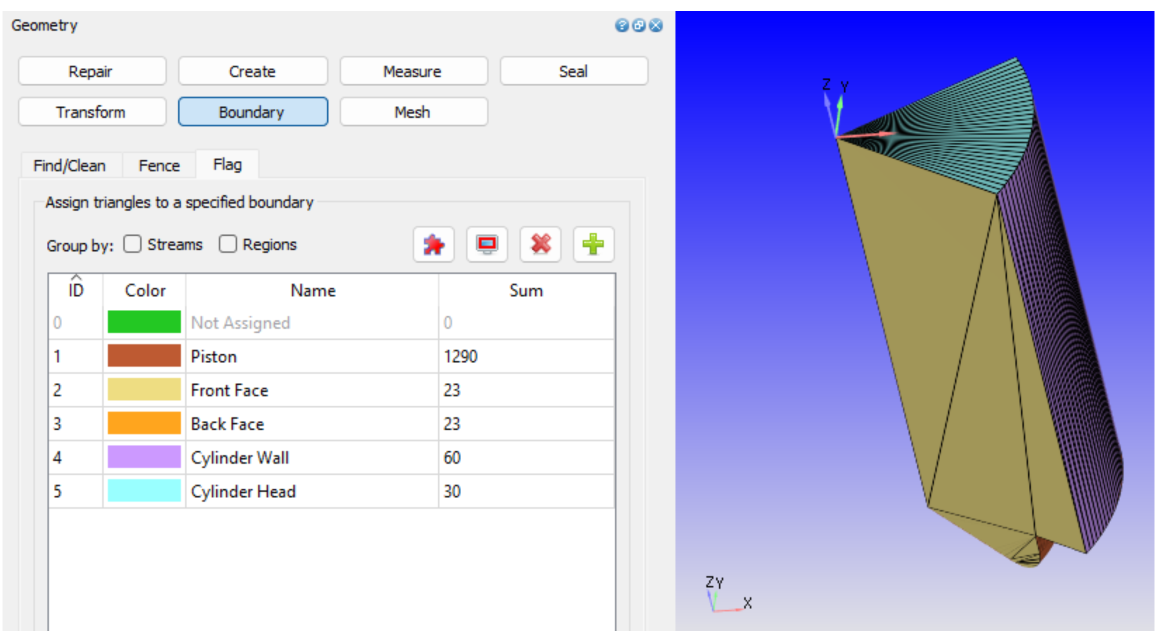

Case Setup

After creating the geometric sectors for both piston profiles and flagging the boundaries, a diagnostic check was performed to identify any potential errors.

Diagnosis Check-up

It was ensured that both geometries are free from problem triangles.

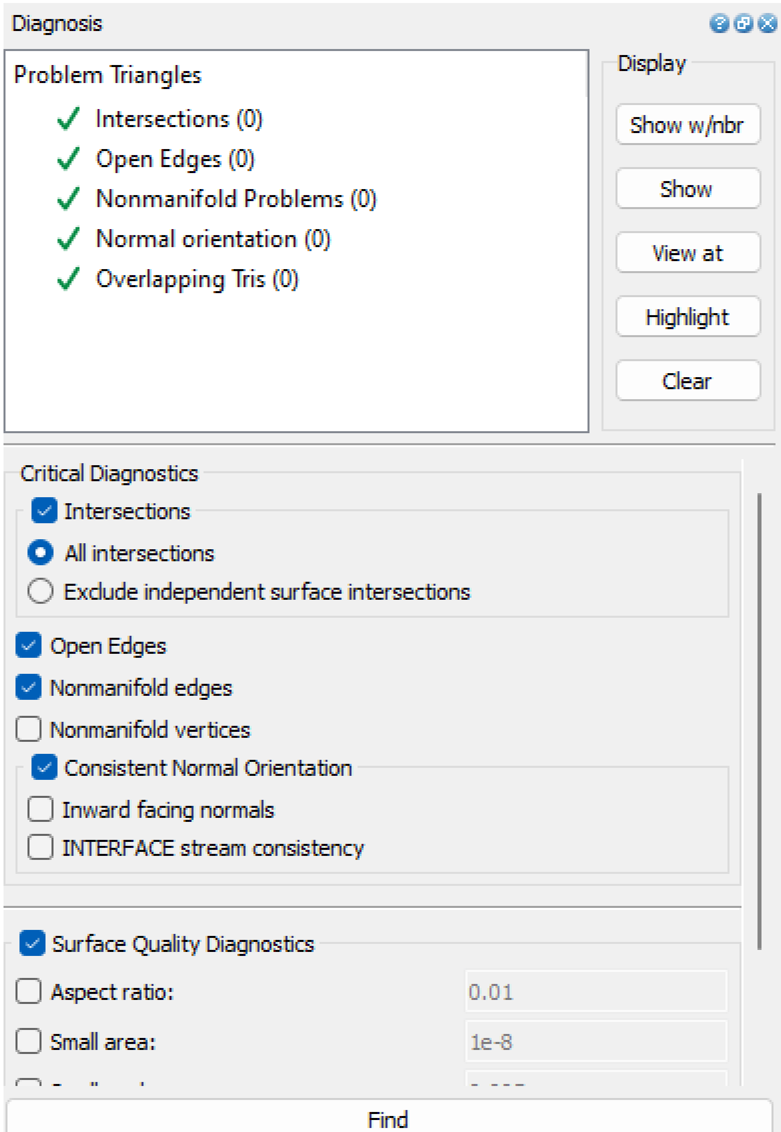

The case will then be set up for both geometries using the provided input files. While these files can be used directly for automatic case setup, the following explanations outline the steps for proceeding manually too.

Case Setup

Application Type

A crank angle-based IC engine application type is selected for this simulation.

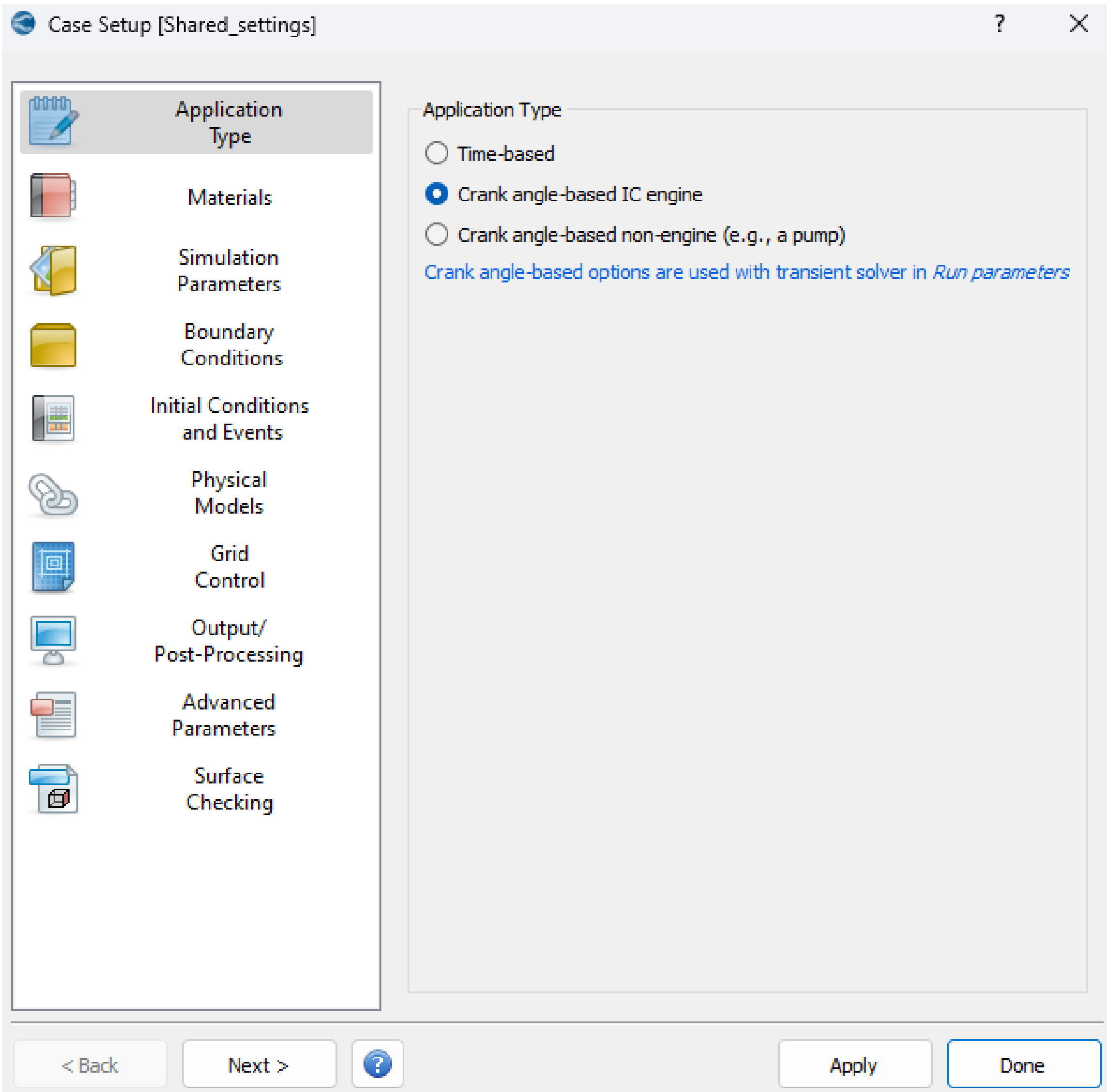

- Crank angle-based (e.g., IC engine)

The parameters for the IC engine are configured as follows:

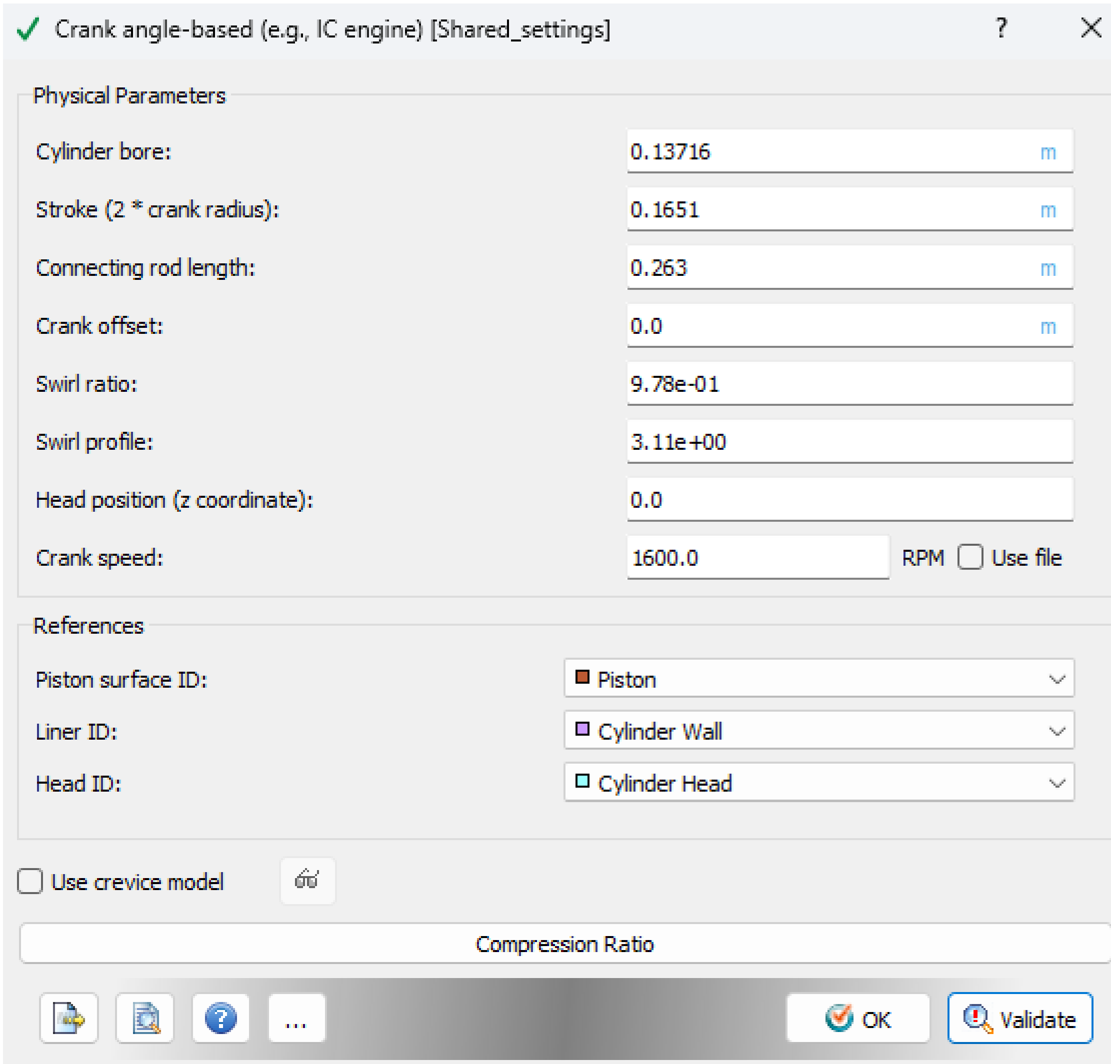

Materials

In the materials section, air is selected as the predefined mixture. Additionally, gas simulation, liquid parcel simulation, and reaction mechanisms are chosen.

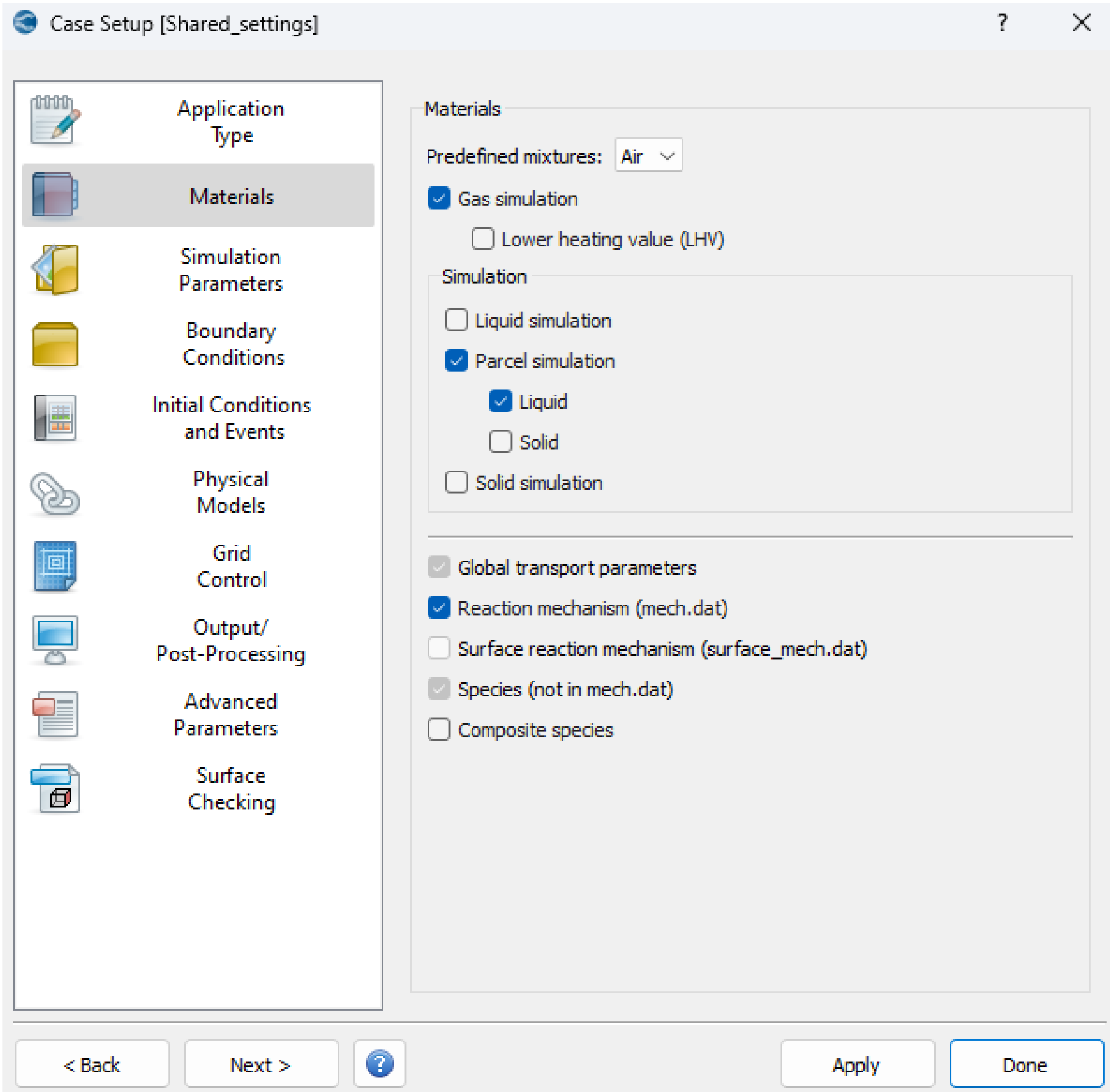

- Gas simulation

Gas thermodynamic data are imported using the provided ‘therm.in’ file.

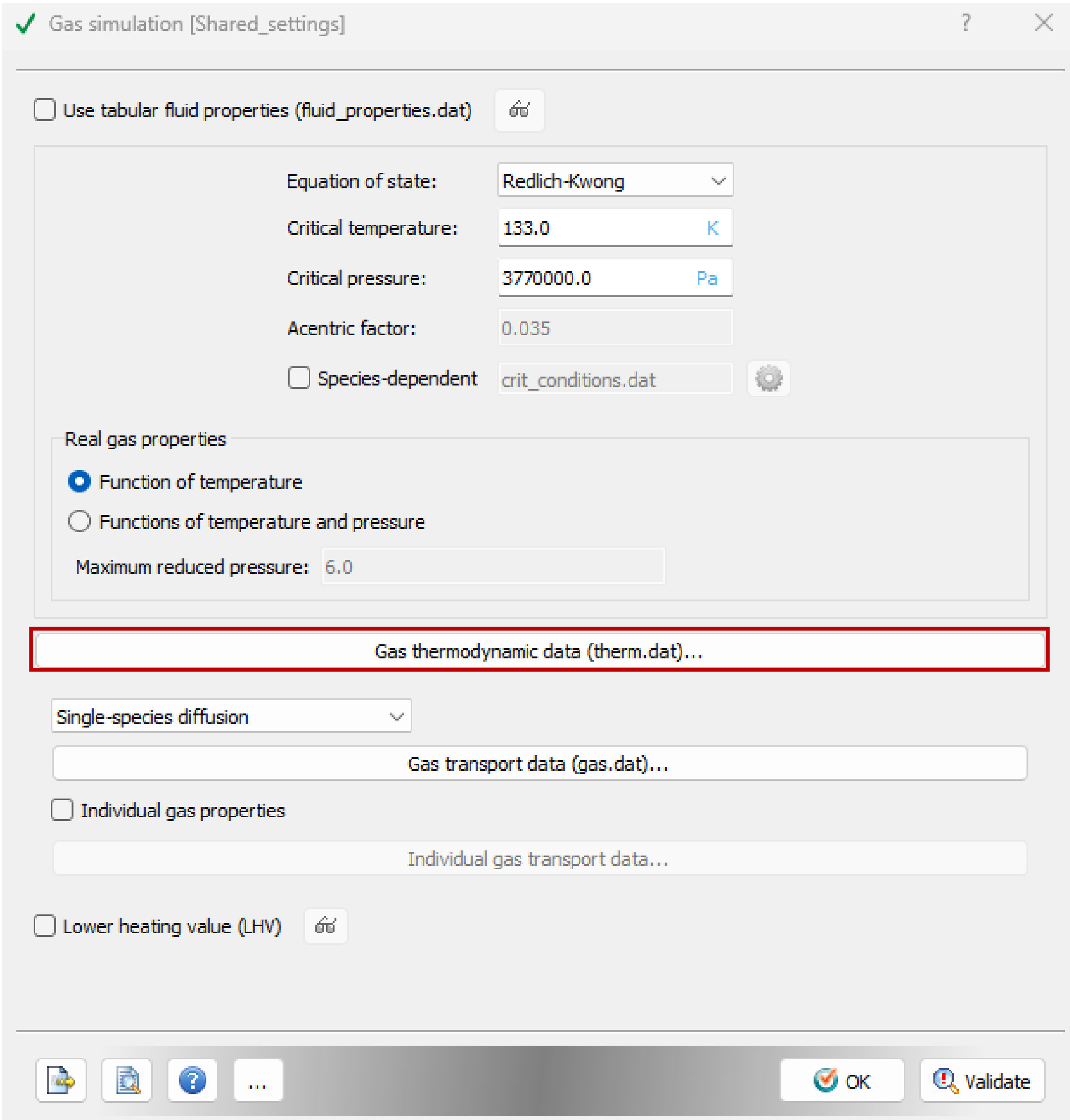

- Parcel simulation

For the parcel simulations, 'DIESEL 2' species is chosen due to its properties closely matching those of diesel.

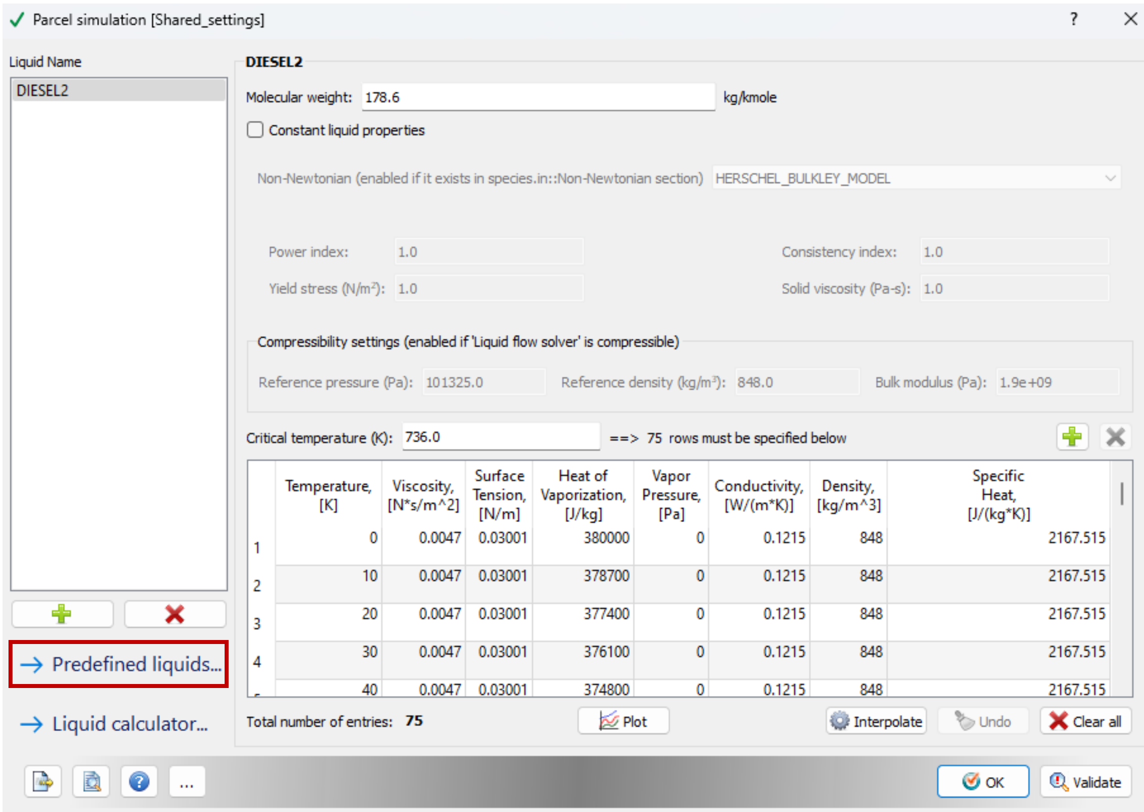

- Global transport parameters

Use default parameters.

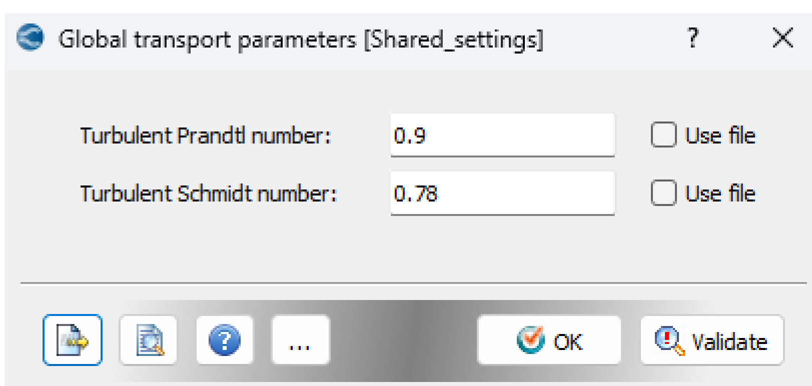

Reaction mechanism

The reaction mechanism is configured using the provided 'mech.in' file.

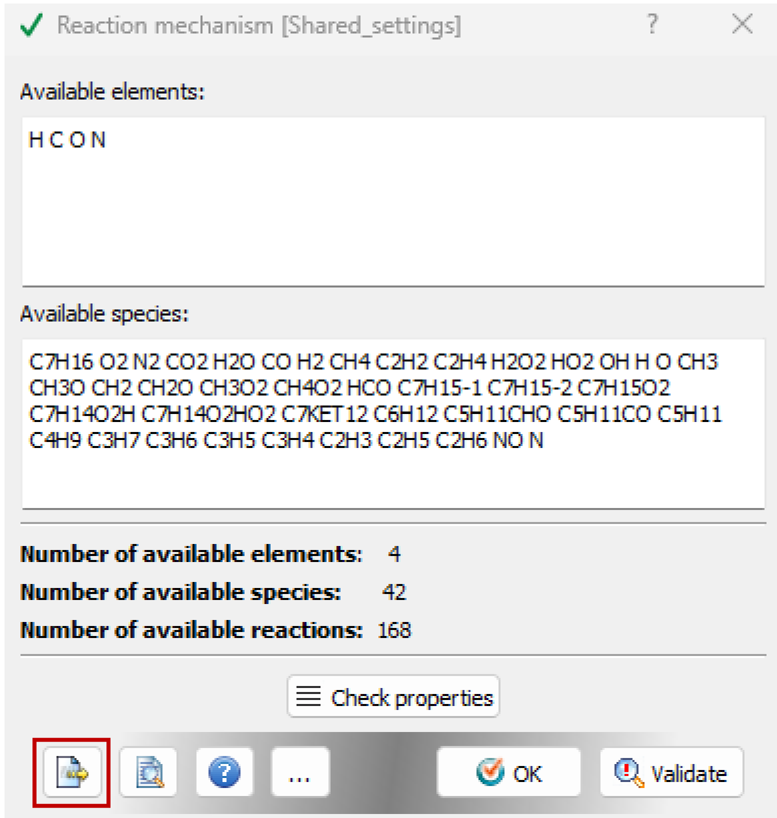

Species

The gas species are automatically handled within the reaction mechanism, so for the liquid parcel species, select DIESEL2.

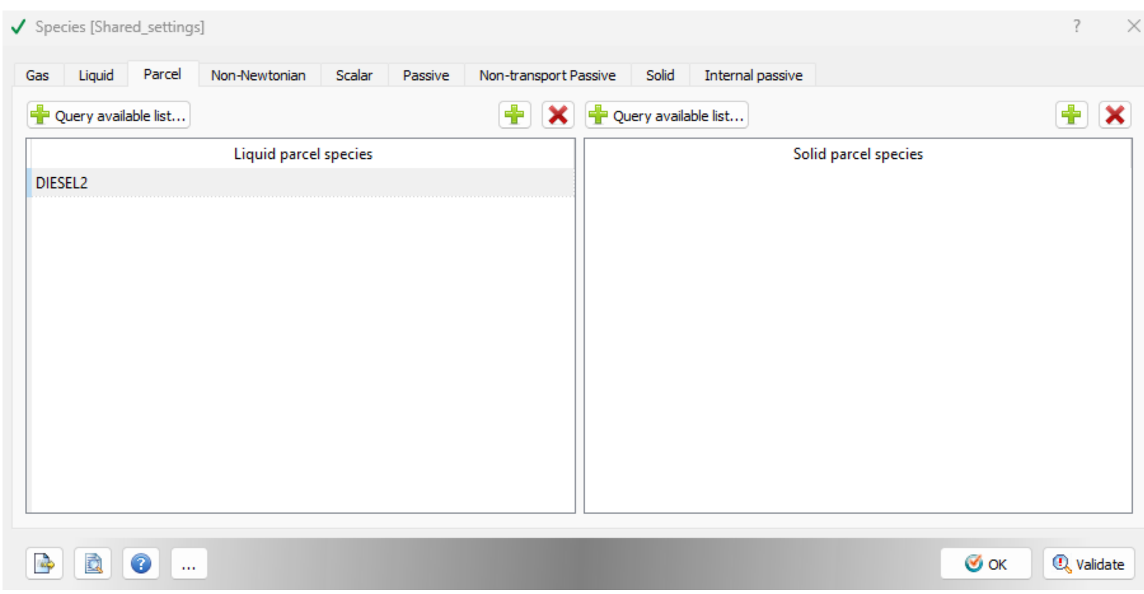

Simulation Parameters

- Run parameters

The run parameters are set for a transient simulation using a crank angle-based engine simulation type. The simulation mode is set to "Full hydrodynamic," which includes fluid dynamics without specific modeling of spray and combustion. This setting is useful for verifying the motion of surfaces and the accuracy of mesh generation without the added complexity of transport equations for sprays and combustion, thus reducing computational time. The gas flow solver is configured as "Compressible," and the liquid flow solver is set to "Incompressible."

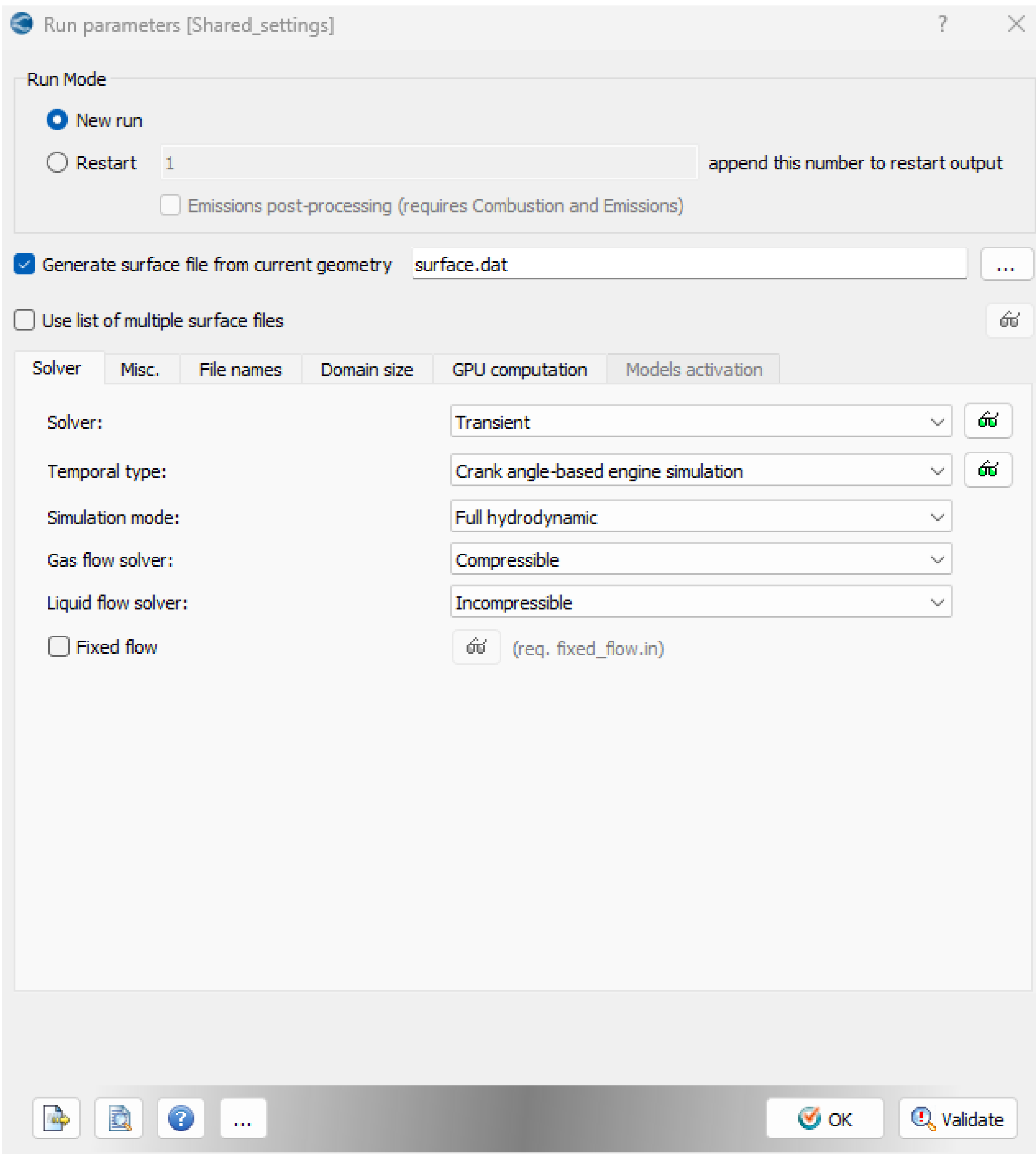

- Simulation time parameters

The simulation time parameters are configured as follows:

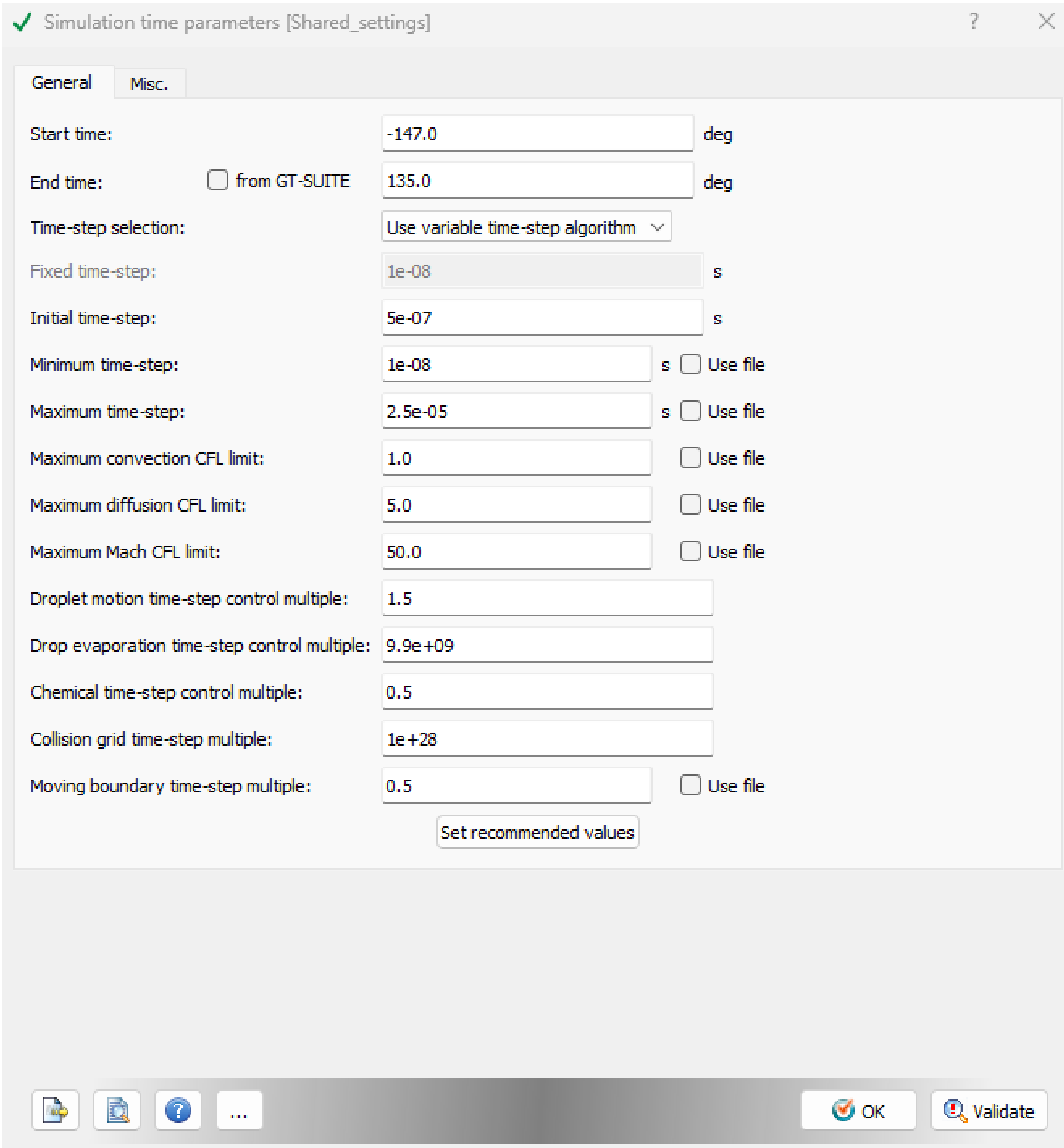

- Solver parameters [Transient]

The Navier-Stokes solver is set to density-based. The remaining parameters in the dialog box are automatically configured by CONVERGE CFD and do not require any modifications.

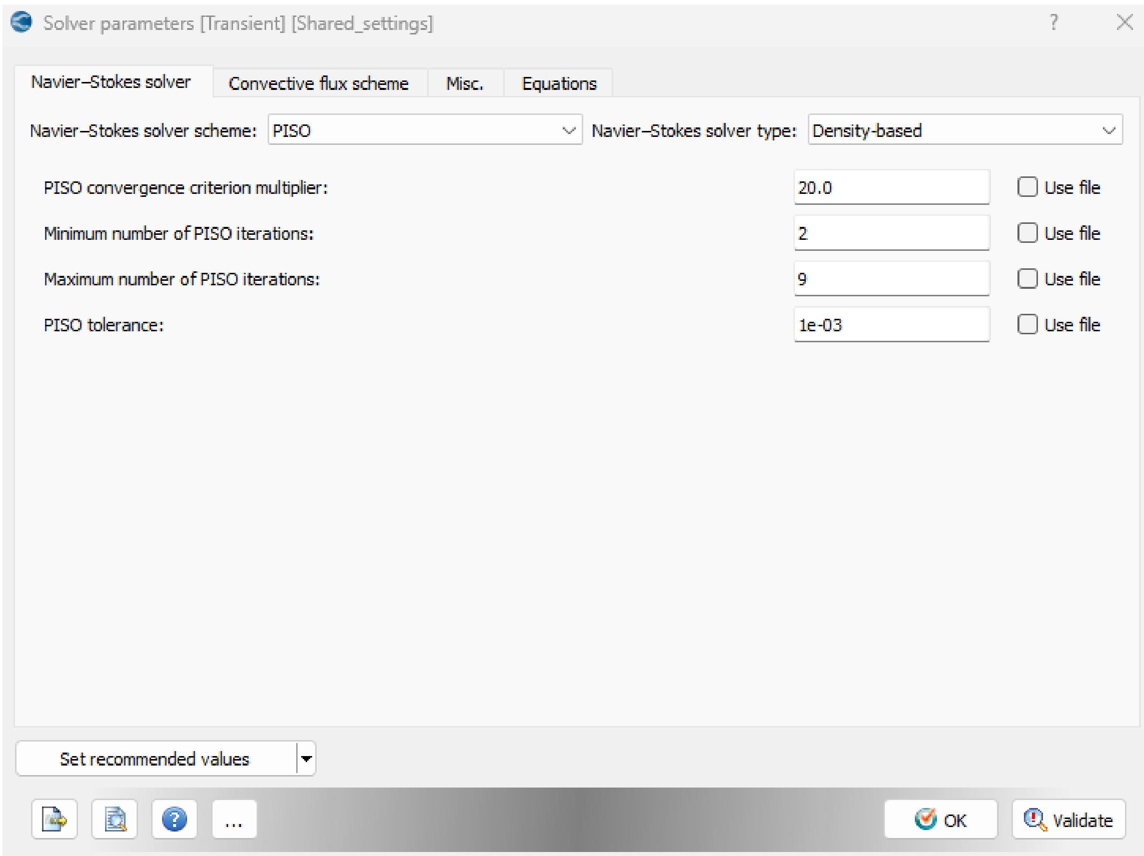

Initial Conditions and Events

- Regions and initialization

Use the provided 'initialize.in' file to configure the initialization. Alternatively, the parameters and values can be set manually as displayed.

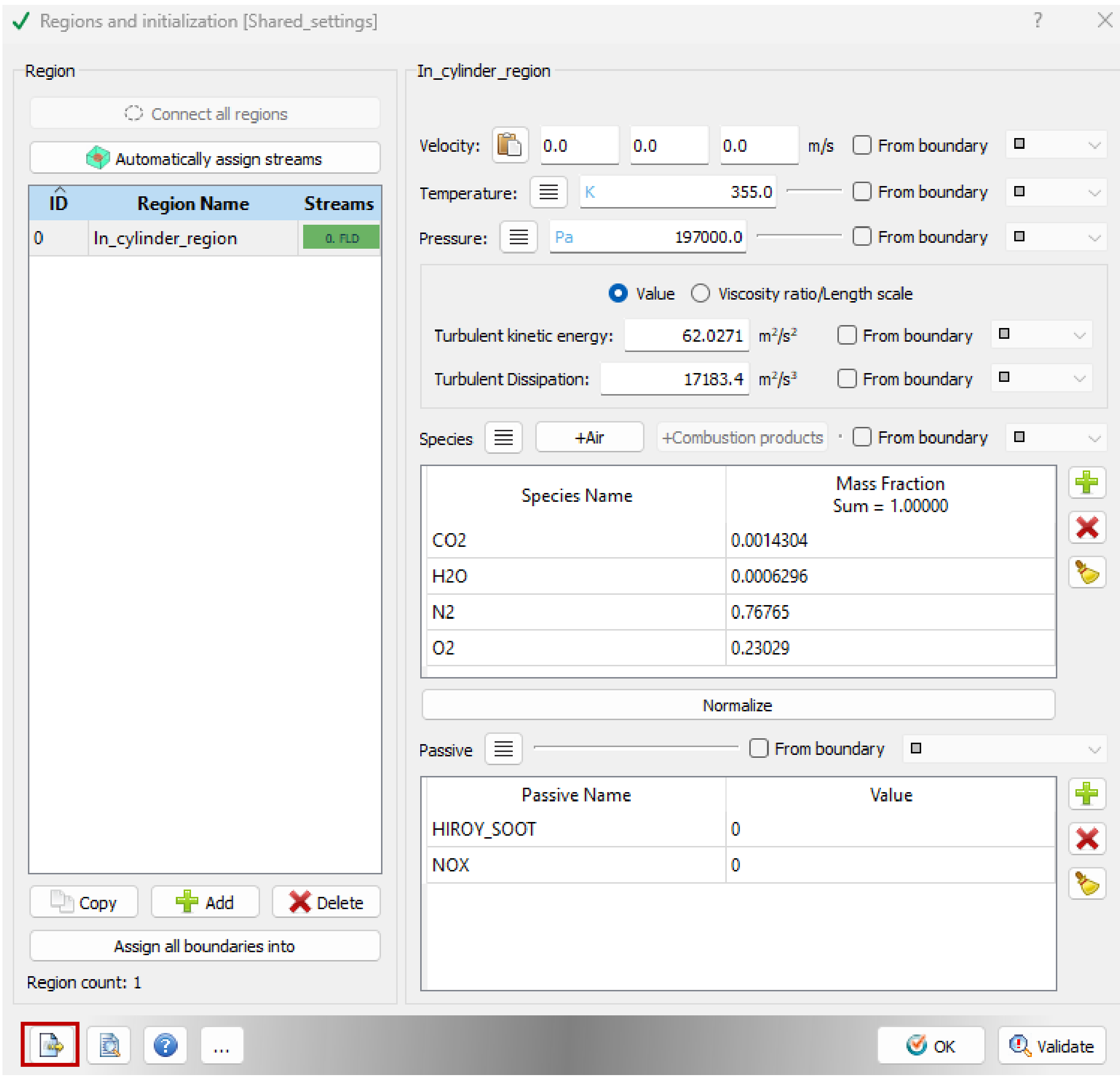

Boundary Conditions

- Boundary

Use the provided 'boundary.in' file to configure the boundary conditions or manually set them up as shown.

- Piston

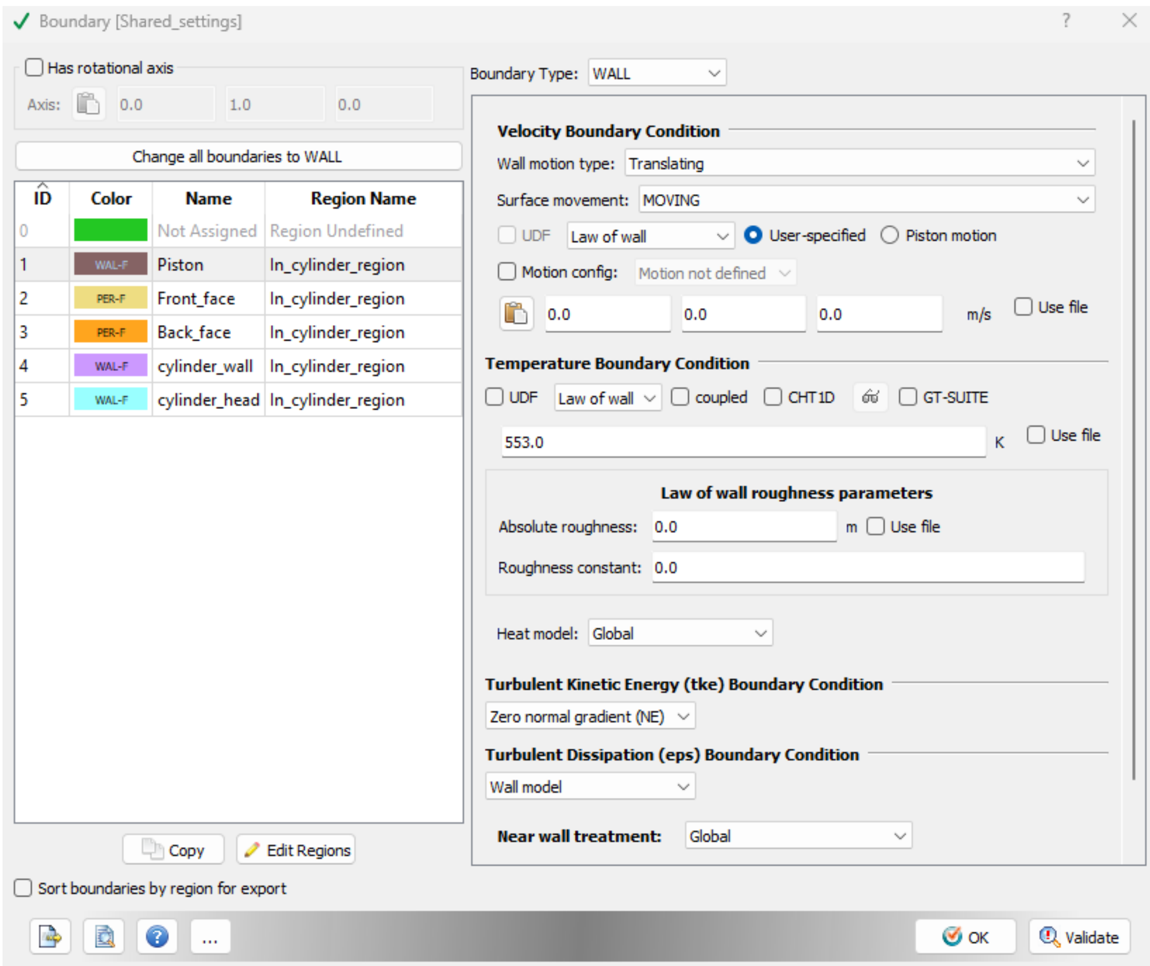

- Front face

Make sure to set the periodic angle at 60 degrees.

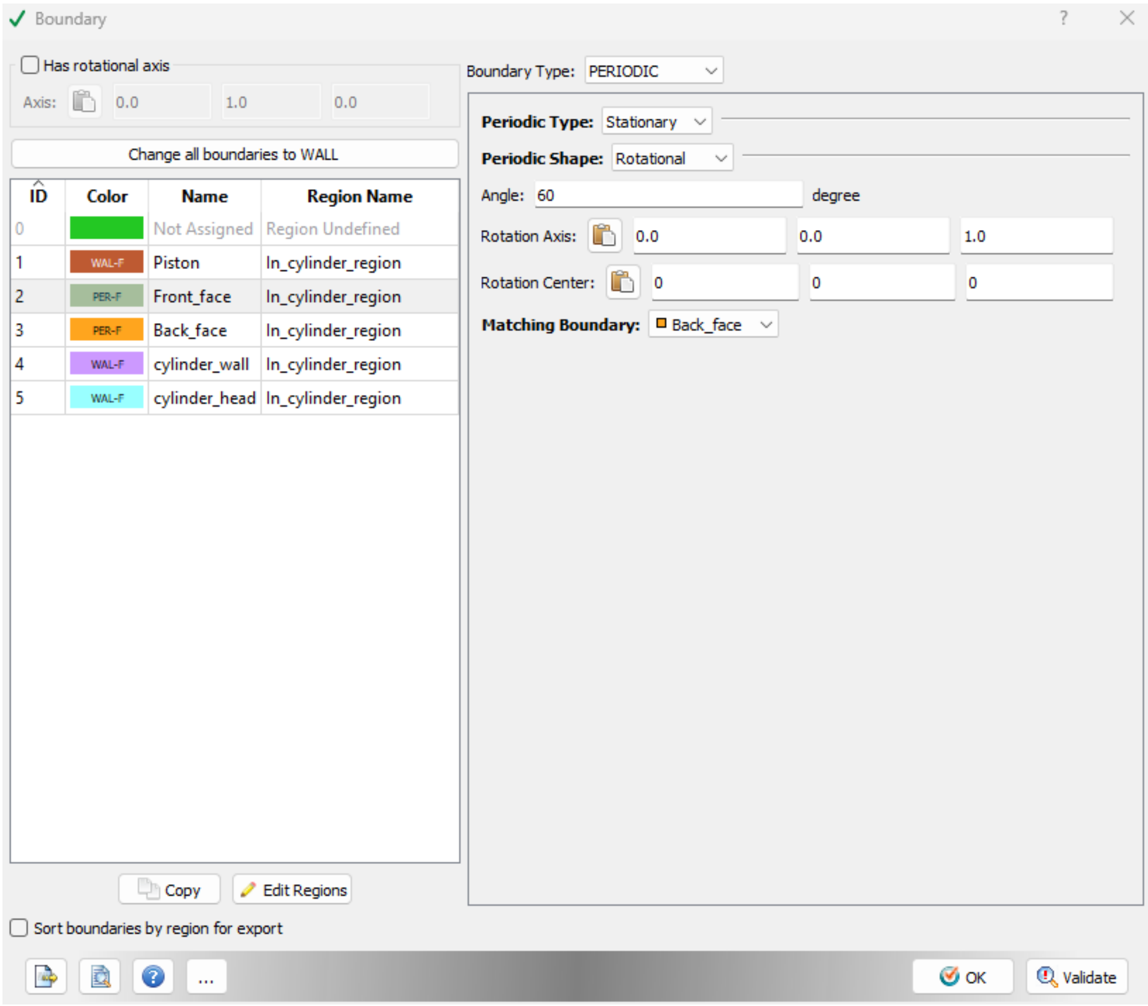

- Back face

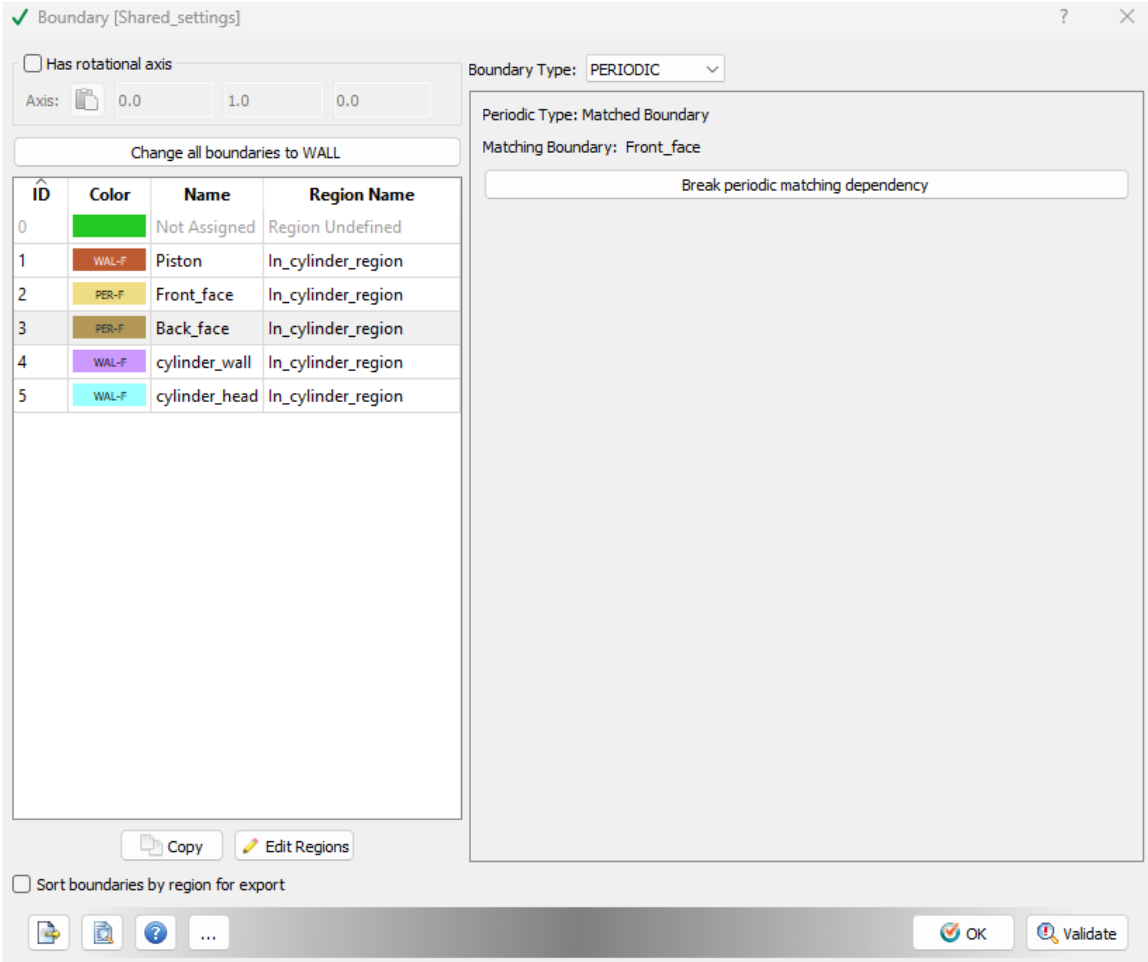
Boundary [Shared_settings]
Has rotational axis
Axis: 0.0 1.0 0.0
Change all boundaries to WALL
ID Color Name Region Name
0 Not Assigned Region Undefined
1 WAL-F Piston In_cylinder_region
2 PER-F Front_face In_cylinder_region
3 PER-F Back_face In_cylinder_region
4 WAL-F cylinder_wall In_cylinder_region
5 WAL-F cylinder_head In_cylinder_region
Copy
Edit Regions
Sort boundaries by region for export
Boundary Type: PERIODIC
Periodic Type: Matched Boundary
Matching Boundary: Front_face
Break periodic matching dependency
OK
Validate

- Cylinder wall

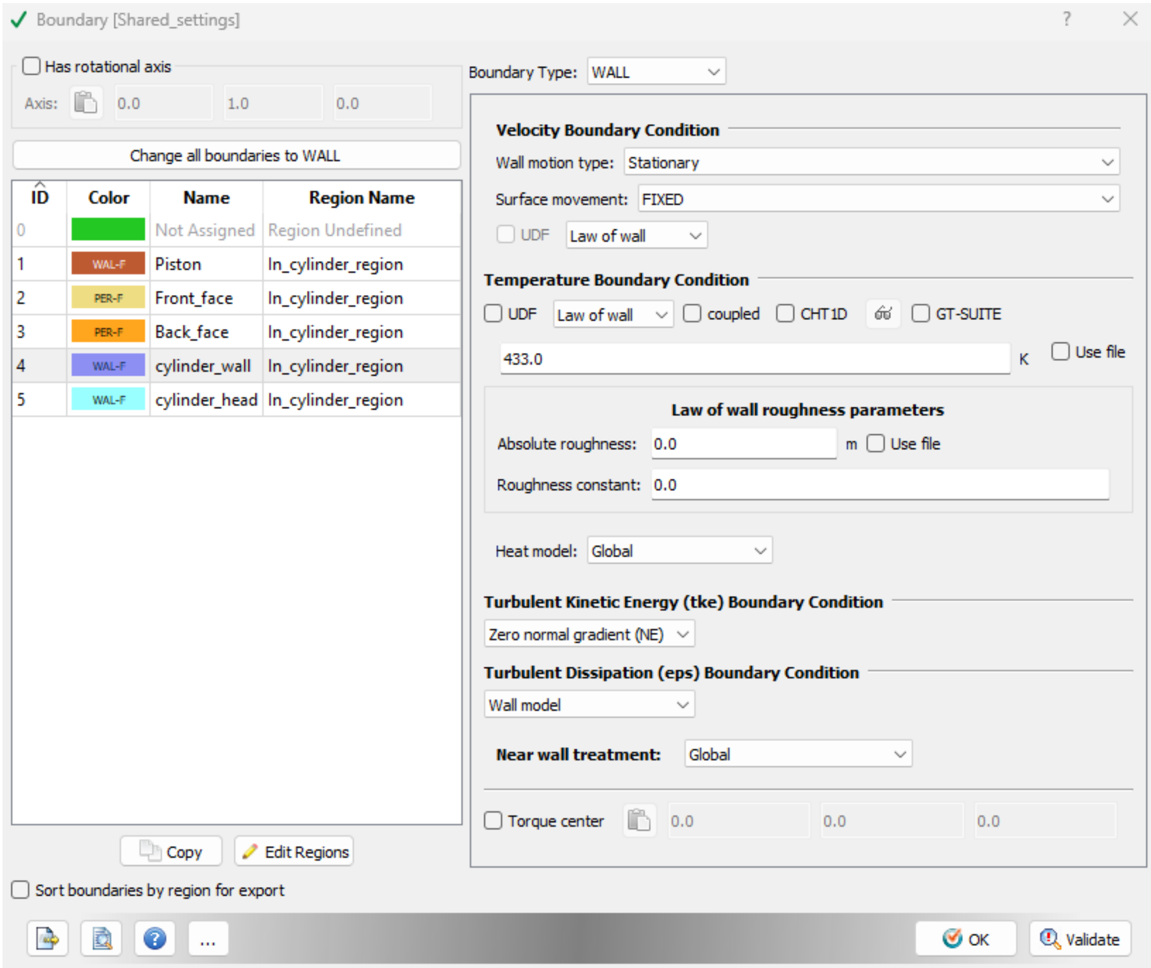

- Cylinder head

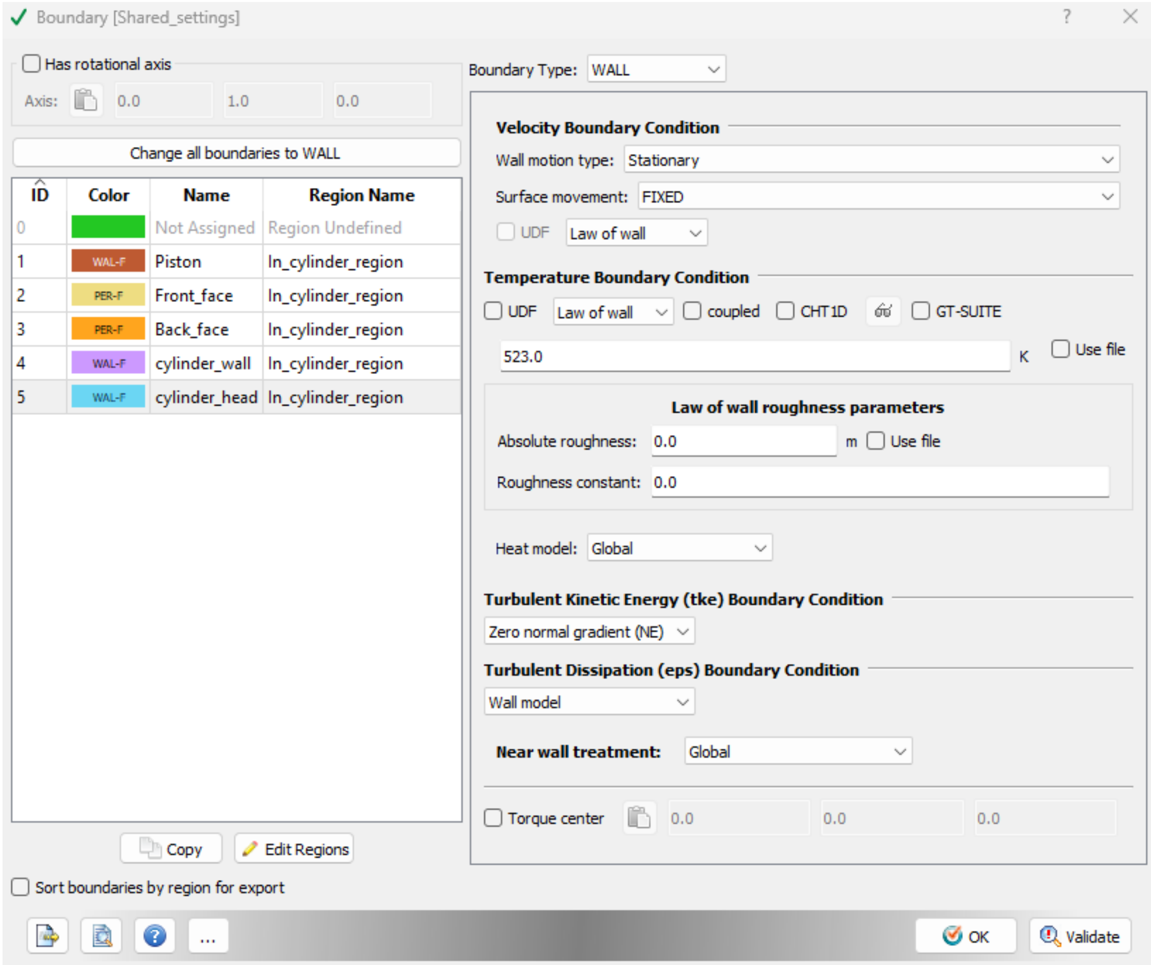

Physical Models

- Parcel configuration

Under the General tab of the Parcels configuration, custom collision control is left unchecked, and the level for collision is set to 2. This configuration indicates that detailed collision modeling is enabled, allowing for more accurate simulation of parcel interactions. The Level 2 collision model considers sub-grid-scale effects, particle size, velocity, and interaction probabilities, which are crucial for capturing realistic spray or particle behaviors in dense flow fields or high-collision environments.

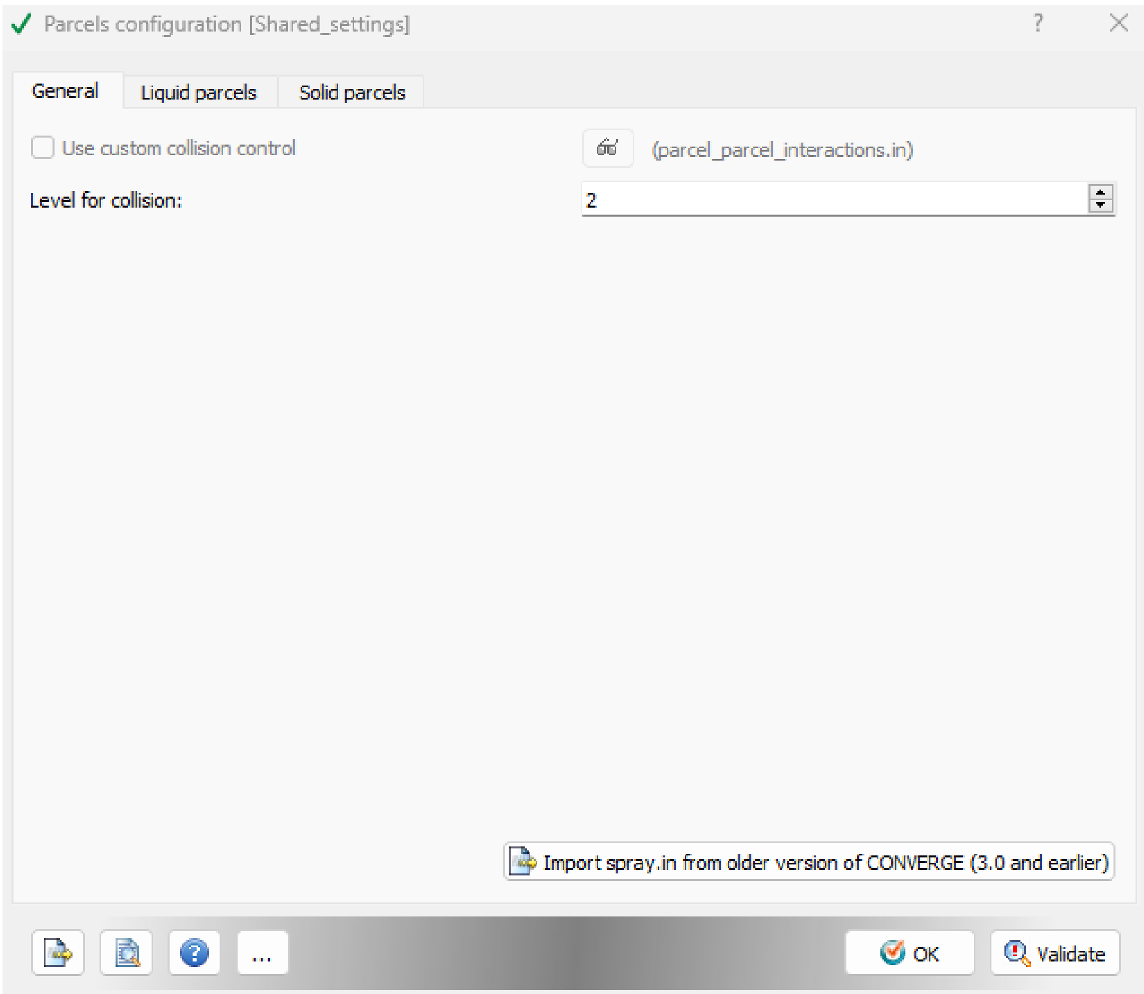

Under the Liquid Parcels tab, the No Time Counter (NTC) collision model is selected for efficiently handling droplet collisions using a probabilistic approach. It is paired with Post-Collision Outcomes to accurately model coalescence, bounce, or fragmentation [4]. The Wall Interaction Model is set to Rebound/slide, simulating droplets bouncing or sliding on surfaces without forming a liquid film. The MOD-KH-RT breakup model combines Kelvin-Helmholtz (KH) and Rayleigh-Taylor (RT) instabilities for realistic droplet breakup, ensuring accurate spray dynamics in turbulent flows [5].

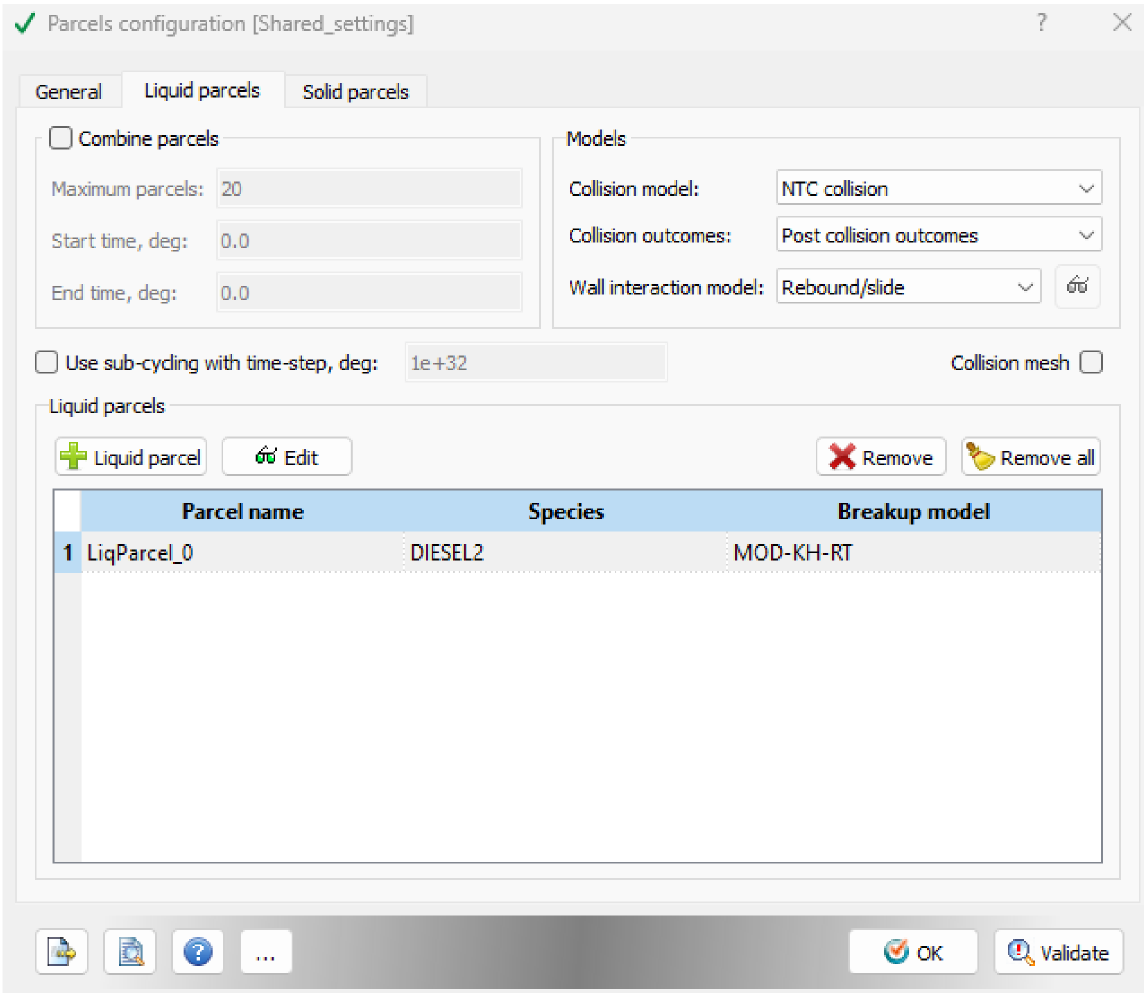

This window displays the configuration for the 'General' settings of the liquid parcel editor. The O'Rourke turbulent dispersion model is selected, which is designed to model the spread of parcels due to turbulence in the gas phase [6]. This model is suitable for cases where turbulence plays a significant role in spray dispersion, such as in combustion or high-velocity injections. The mass ratio and radius cutoff values are set to conservative defaults (0.001 and 1e^{-20} m, respectively), ensuring that only parcels with significant mass and size are tracked, thus maintaining computational efficiency while capturing the essential physics of the spray.

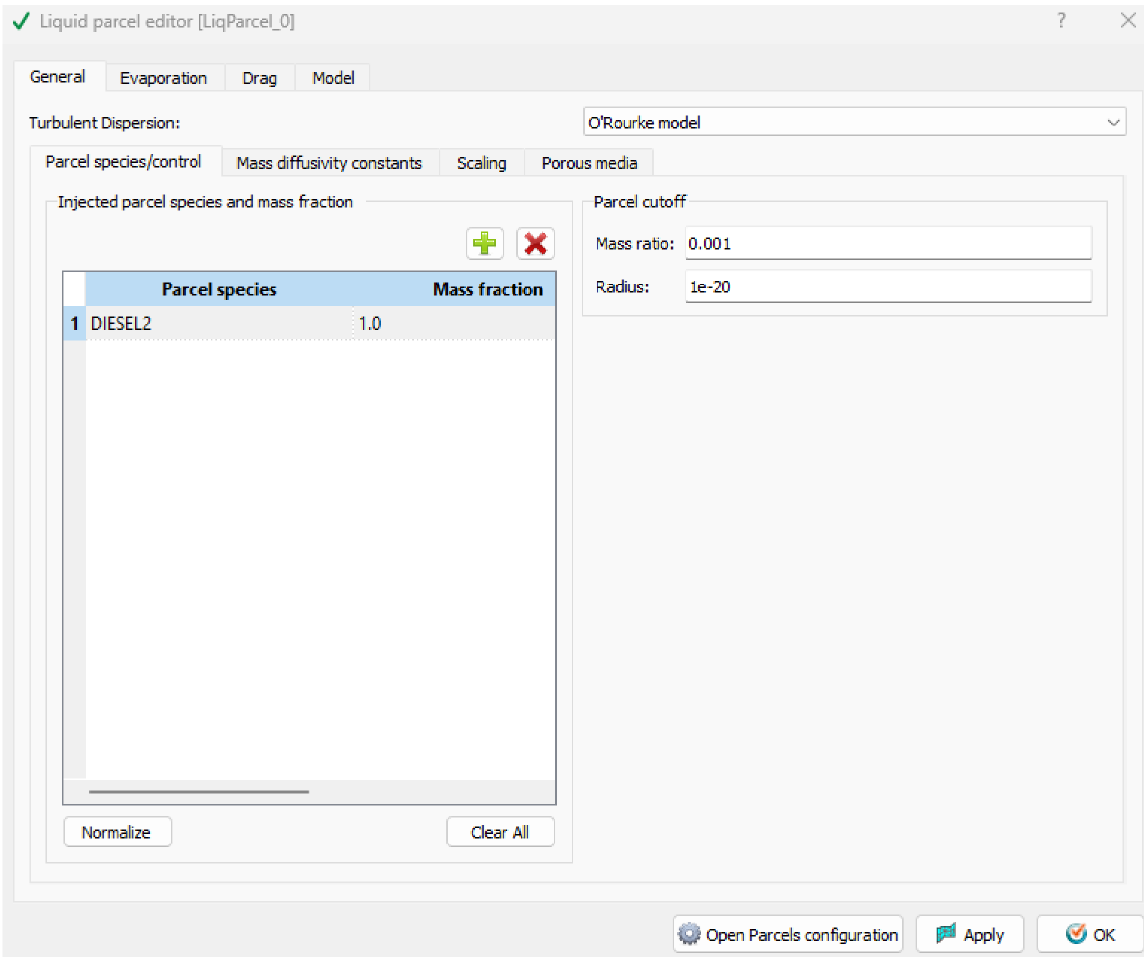

In this window, the 'Mass diffusivity constants' tab shows values specific to the DIESEL2 species, with constants set to default values typically associated with kerosene-like fuels. The diffusivity constants (D_0 and n_0) control how quickly species diffuse through the gas phase, which is crucial for accurate representation of fuel vapor mixing with air. Using these values helps in accurately simulating the physical processes occurring during the fuel evaporation and combustion stages, contributing to realistic predictions of combustion efficiency and emissions.

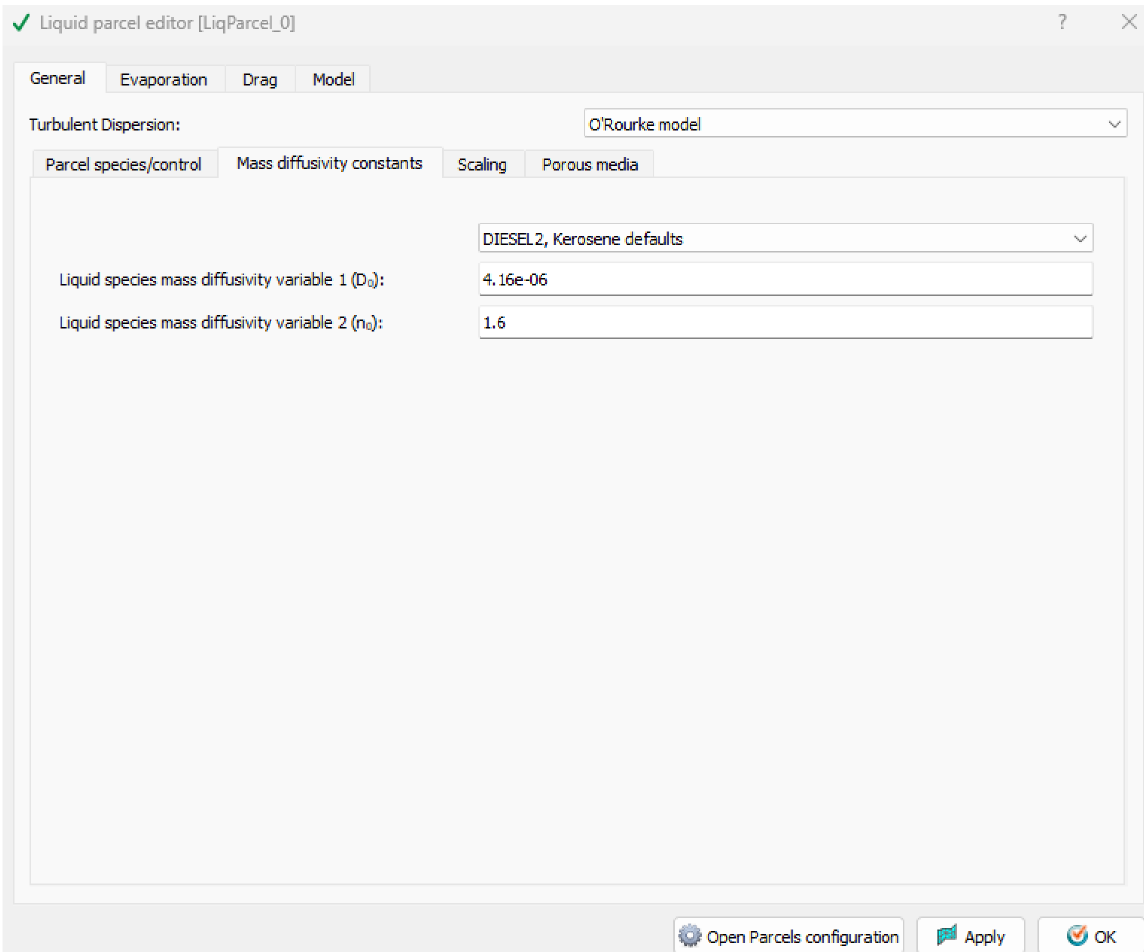

This window highlights the 'Scaling' settings for droplet heat and mass transfer coefficients. Both coefficients are set to a scaling factor of 1.0, indicating that no additional scaling is applied beyond the default model behavior. This choice ensures that the simulation closely follows the physical models implemented in CONVERGE CFD without artificial enhancement or suppression of heat and mass transfer effects. This approach is justified when the built-in models are well-validated for the conditions being simulated, allowing for accurate thermal and compositional changes in the droplets during the simulation.

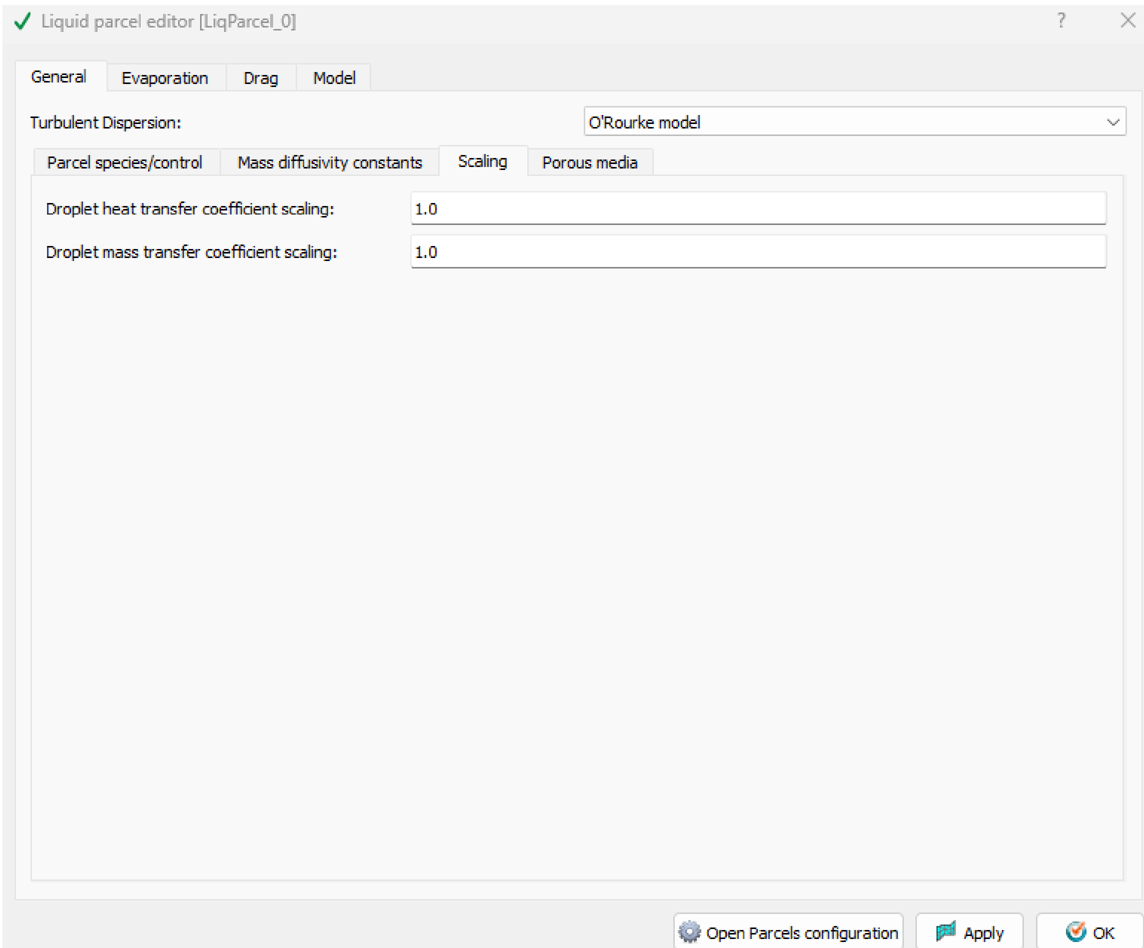

Under the 'Porous media' tab, the control behavior is set to 'Off,' with a ratio to break up trapped parcels of 0.1. This configuration indicates that interaction between spray parcels and porous media, such as fuel injectors with porous filters, is not modeled in this case. This setting is appropriate when the simulation does not involve significant porous media interactions or when focusing on other aspects of the spray behavior. The ratio to break up trapped parcels is a parameter that would be relevant if porous interaction were enabled, dictating how aggressively trapped parcels are broken up, but with the control turned off, this parameter does not affect the current simulation.

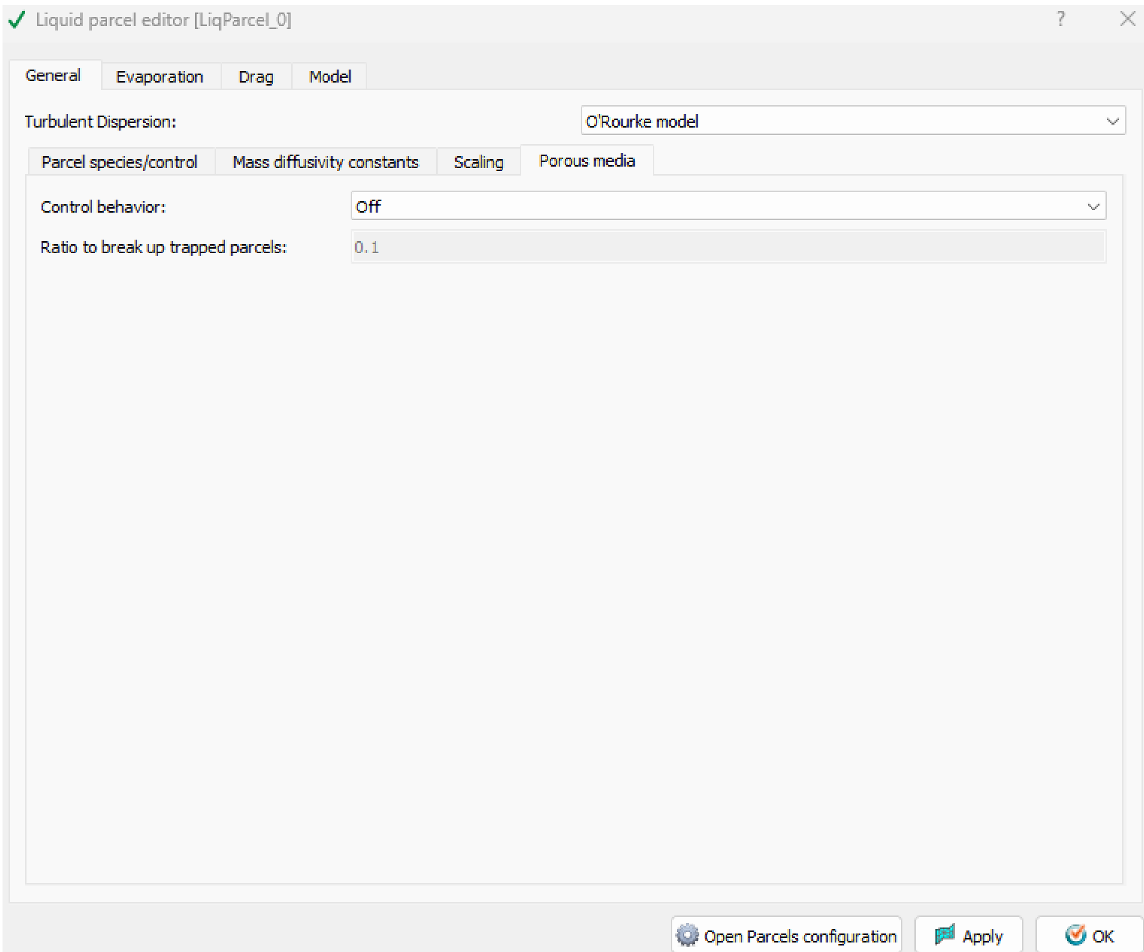

The Frossling evaporation model provides a robust framework for simulating the heat and mass transfer processes governing droplet evaporation, particularly in conditions dominated by convective heat transfer [7]. By specifying C_7H_{16} (a heptane surrogate) as the sourced species, the model ensures accurate representation of phase transition into the gas phase. Enabling temperature discretization enhances thermal resolution within larger droplets, accounting for internal temperature gradients and ensuring realistic evaporation behavior. This approach is essential for capturing the interplay between droplet size, heat diffusion, and evaporation rates. Selecting the thermal conductivity as "Physical" allows for accurate representation of the fuel’s material properties, critical for achieving credible evaporation dynamics.

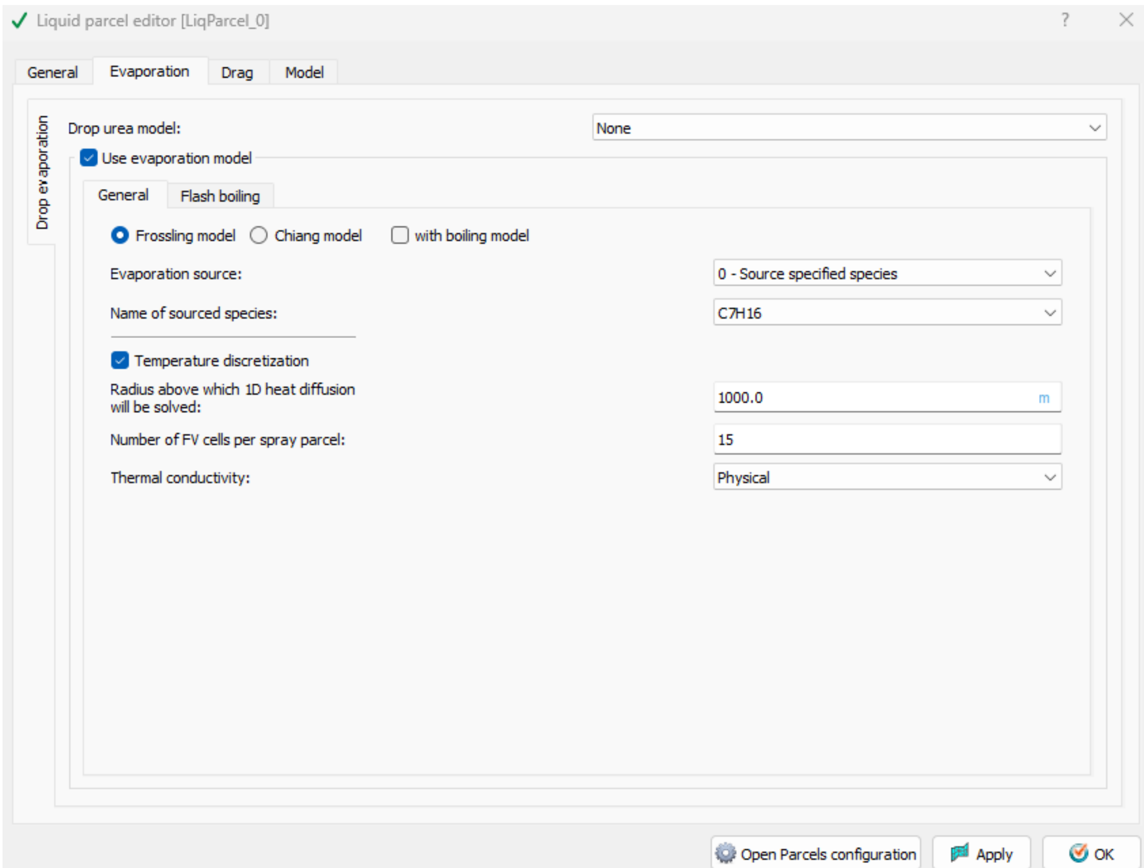

The dynamic drop drag model reflects the deformation of droplets under aerodynamic forces, ensuring an accurate calculation of drag forces in high-pressure and high-velocity flows typical of diesel sprays. The parameterization of the dynamic drag variables accounts for the Weber and Reynolds number influences, capturing the transitional behavior between droplet stability and breakup. These settings provide a balance between computational efficiency and the realism needed to simulate droplet motion and its response to flow turbulence and deformation.

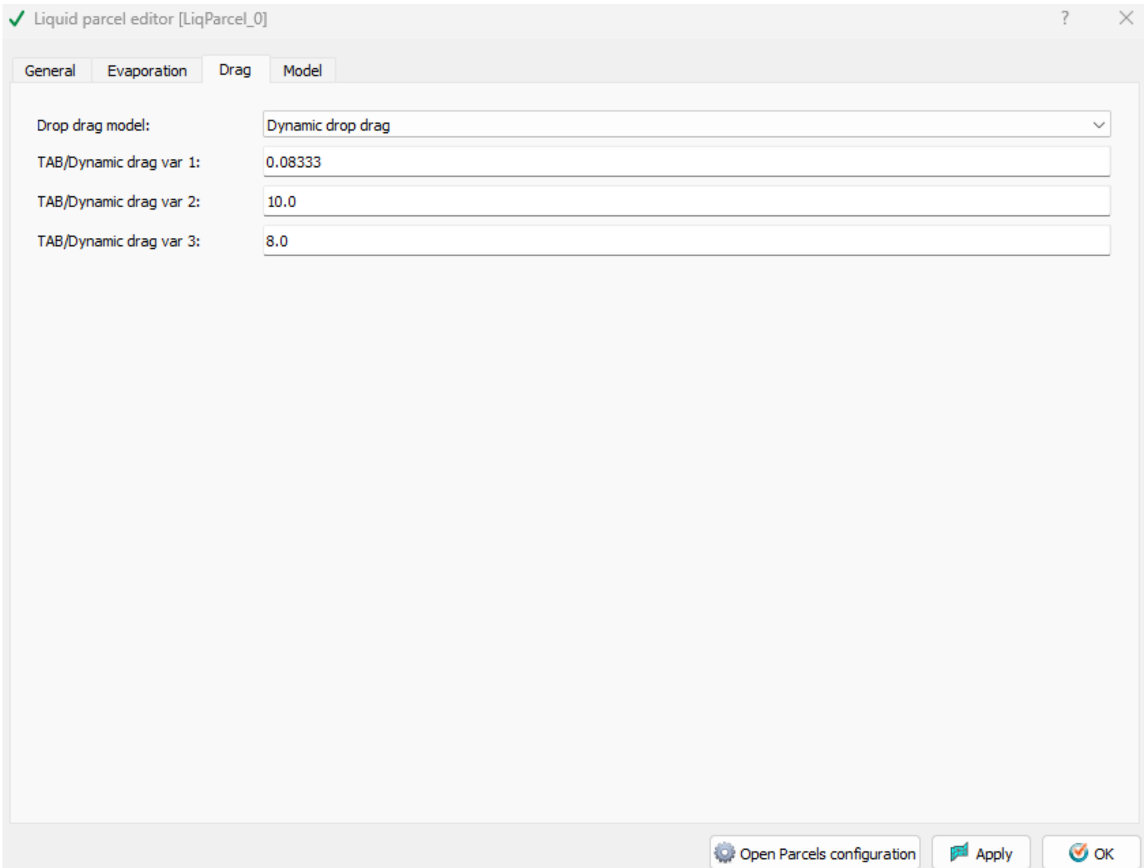

The Kelvin-Helmholtz (KH) and Rayleigh-Taylor (RT) models collectively simulate the breakup of liquid parcels in primary and secondary atomization stages, ensuring a detailed representation of spray behavior [5]. The KH model governs the disintegration of liquid sheets into droplets, driven by aerodynamic instabilities, while the RT model addresses the secondary fragmentation caused by inertia and surface tension effects. The calibrated constants for breakup time, mass shedding, and droplet size reflect a focus on achieving realistic droplet distributions, crucial for simulating fuel-air mixing and combustion efficiency. By omitting the Taylor Analogy Breakup (TAB) and Linearized Instability Sheet Atomization (LISA) models, the setup simplifies the simulation without compromising its ability to capture critical spray characteristics.

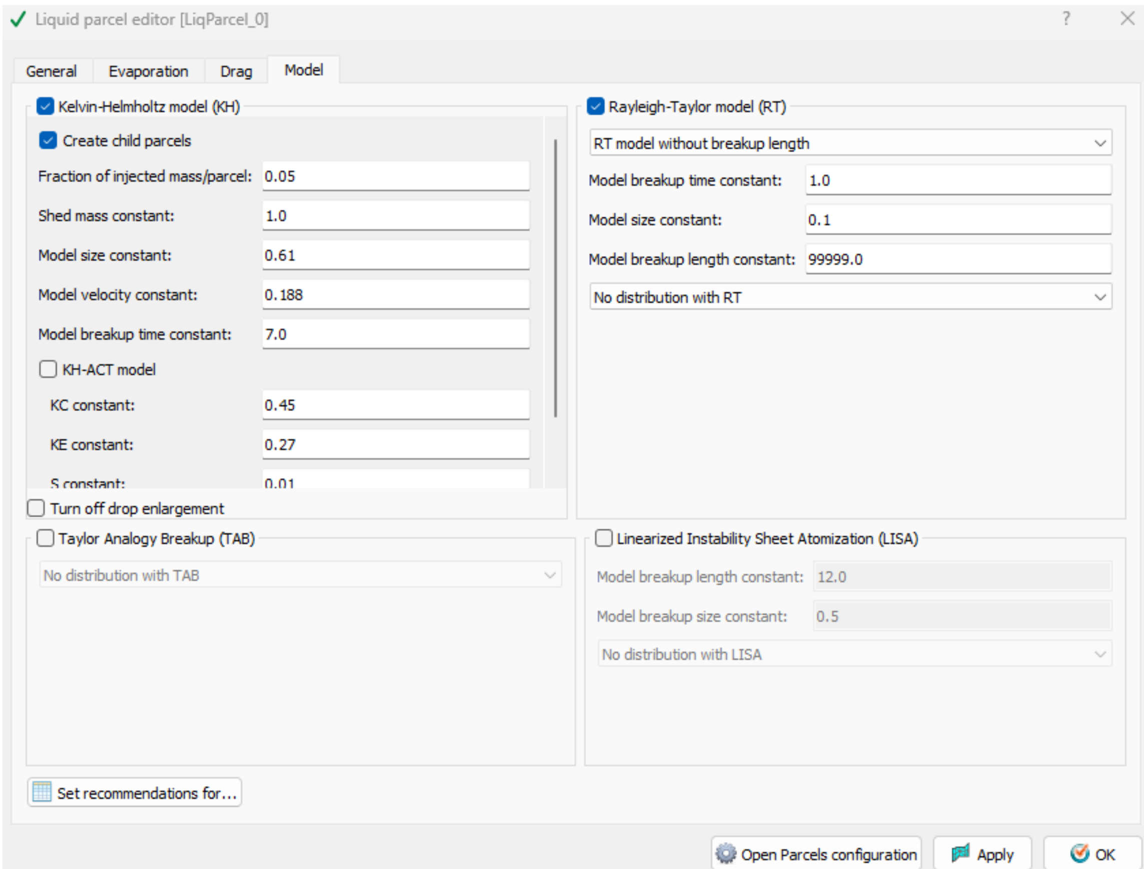

- Parcel introduction

In this window under 'Parcel introduction', the configuration shows that Injector_0 is set up with a single stream (Stream ID: 0) using Liquid parcel type with a reference to LiqParcel_0. The injection distribution method selected is BLOB, meaning that parcels are injected as spherical blobs with sizes directly proportional to the specified nozzle diameter [8]. This approach simplifies the initial representation of parcel size distribution by correlating it to the physical characteristics of the nozzle. Essentially, each injected blob represents a group of fuel droplets, making the initialization process computationally efficient while ensuring that the spray characteristics align with the nozzle's dimensions. This is particularly useful in scenarios where the precise initial size and shape of the spray are critical for accurate downstream modeling of spray breakup and dispersion.

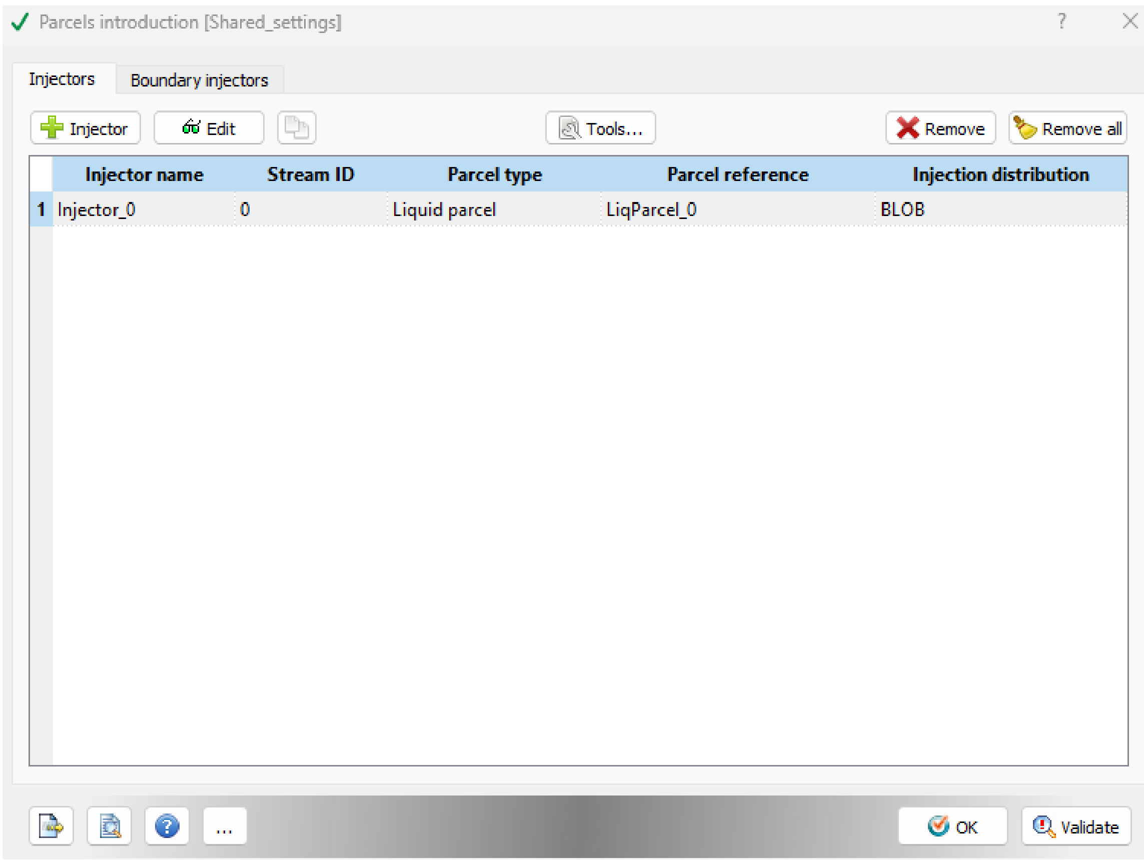

The injector configuration clusters parcels near the spray cone center, simulating realistic fuel distribution for high-pressure injection systems. The injection rate-shape uses rate_shape.in to replicate time-dependent injection profiles, improving accuracy in modeling ramp-up and ramp-down phases. Velocity control is set to RATE_SHAPE, aligning droplet velocities with the mass injection rate, while a small randomness factor of 0.01 introduces variability to replicate physical spray irregularities. Each parcel's mass is defined as $1e^{-12}$ kg, and the mass ratio type is set to MASS with a value of 0.1 kg, providing precise control over the fuel injection process for enhanced simulation fidelity.

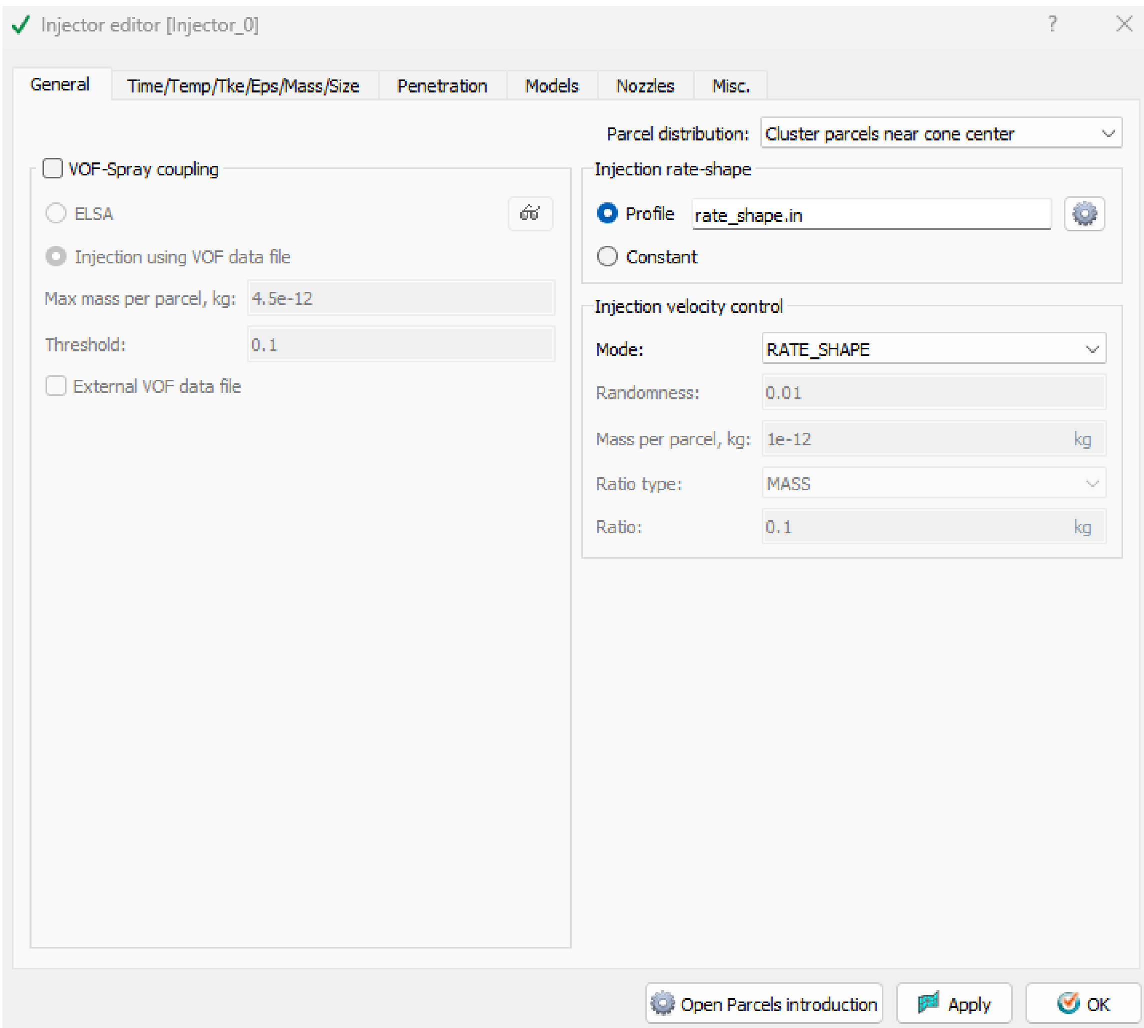

The rate shape profile, as seen in the configuration and the plotted data, shows a sequential rise and fall in injection rate corresponding to the crank angle. This shape accurately represents the dynamic nature of the injection process, particularly for internal combustion engines where the fuel delivery rate varies significantly over a single cycle. This detailed setup enables the simulation to replicate the transient injection behavior accurately, providing insights into how variations in injection timing and rate affect engine performance.

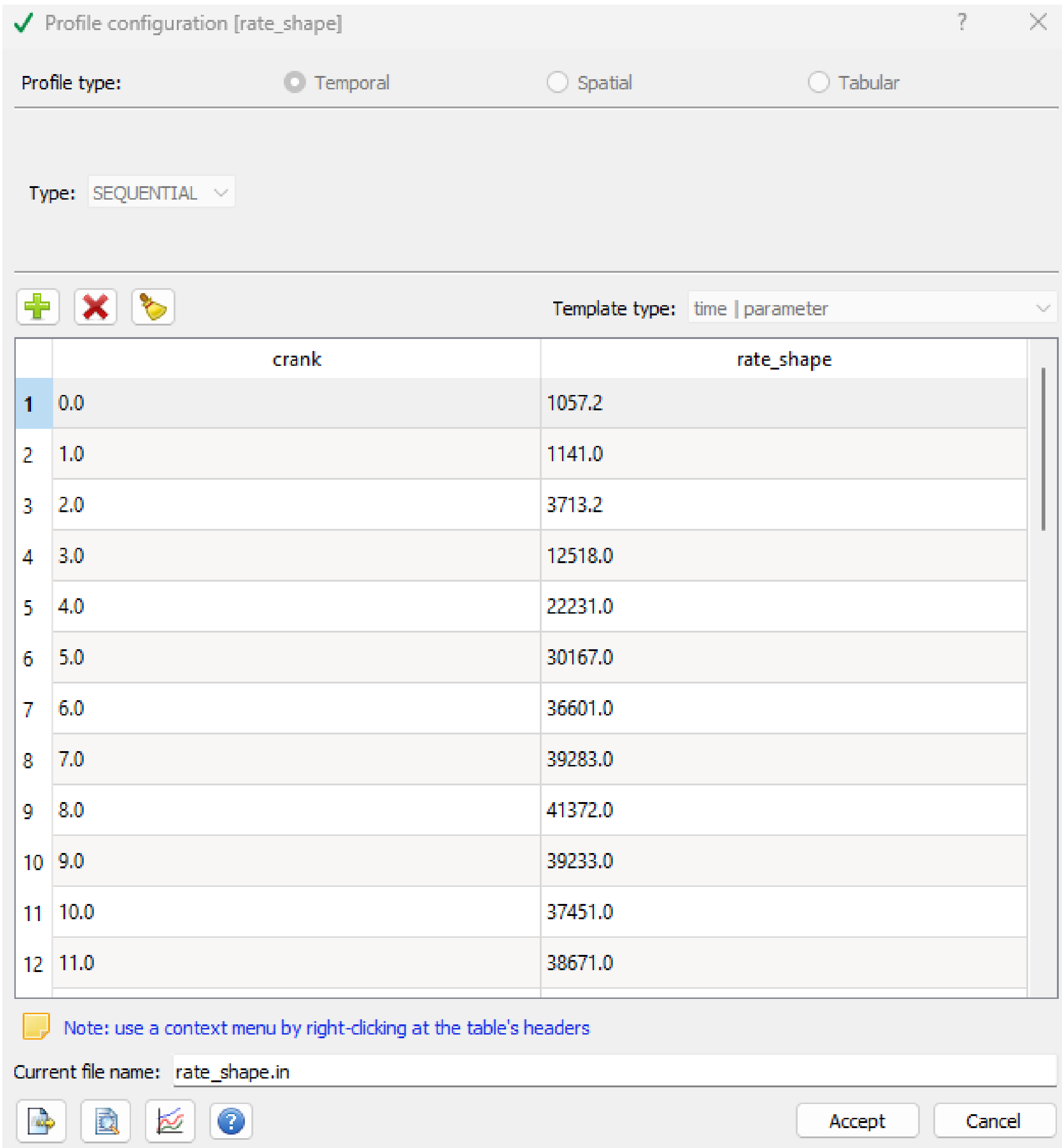

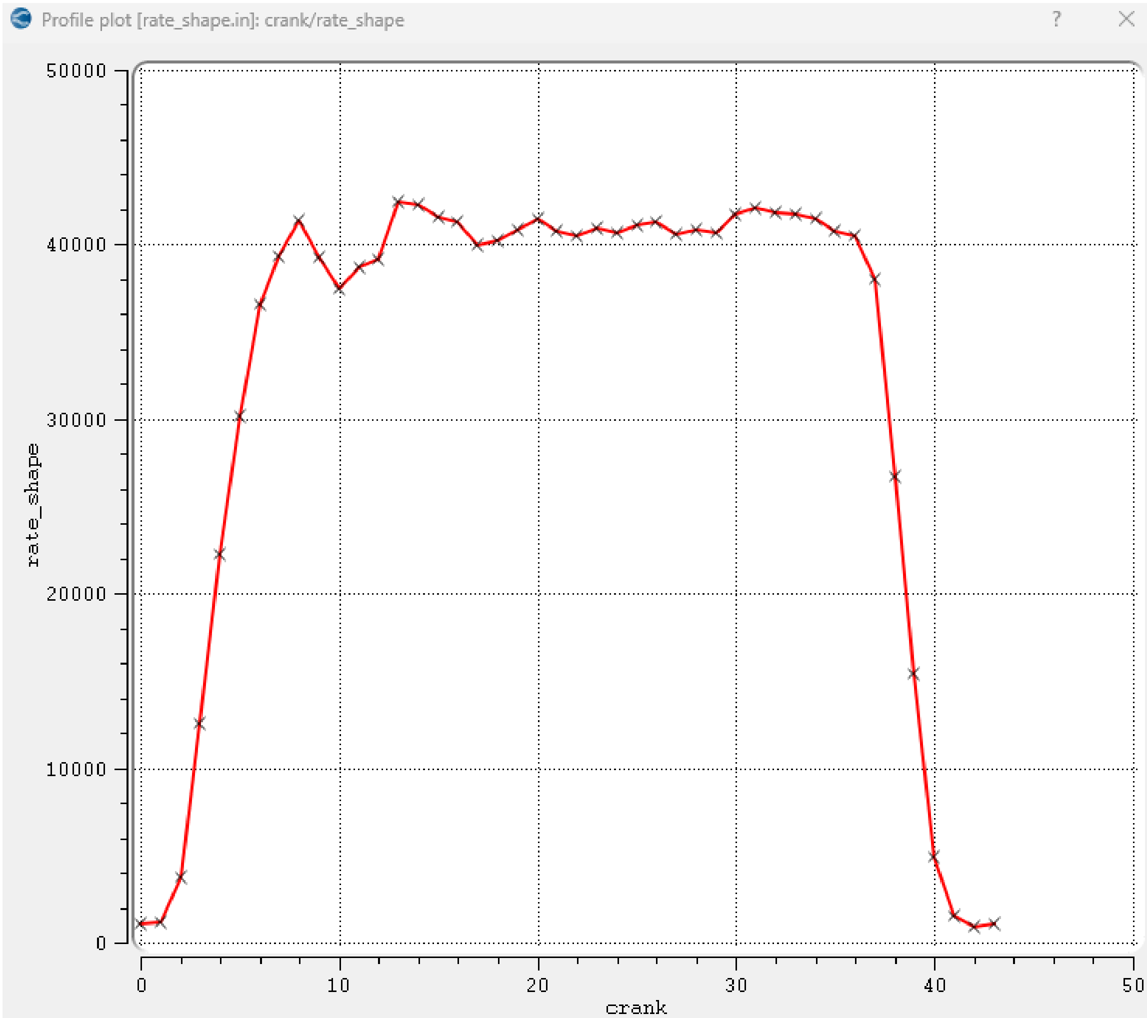

Profile plot [rate_shape.in]: crank/rate_shape
50000
40000
30000
20000
10000
0
rate_shape
0
10
20
30
40
50
crank

The following window outlines the cyclic nature of the injection with a period of 720 degrees, reflecting the full cycle of a four-stroke diesel engine. The start of injection is set at -9.0 degrees, with a duration of 21.0 degrees, and a total injected mass of $2.70167e^{-05}$ kg. The number of parcels per nozzle is set to 50,000, which balances computational cost with the need for enough parcels to accurately model spray interactions. The injection drop distribution is set to predefined as a Blob, which correlates parcel size directly with the physical nozzle characteristics, thereby streamlining the initialization of parcel sizes and ensuring consistency with real-world injector performance [8].

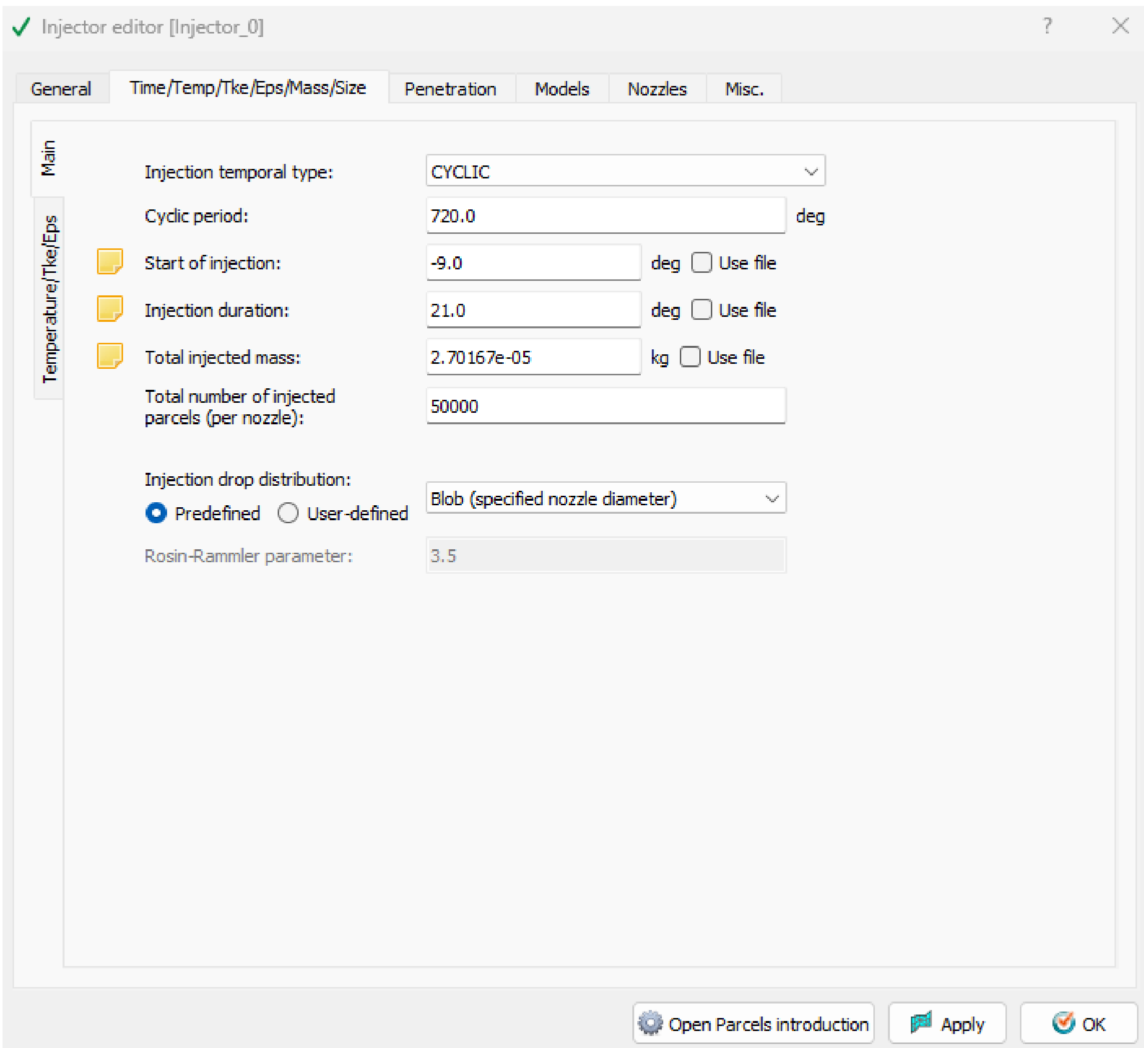

In this window, the injector temperature is set to a constant value of 341 K, while the turbulent kinetic energy (tke) and turbulent dissipation (eps) are set to 3000 m^2/s^2 and 300 m^2/s^3, respectively [9]. These values are crucial for accurately modeling the thermal and turbulence conditions within the spray, which significantly impact droplet evaporation rates and spray dispersion. The constant values are selected based on typical operational conditions for diesel injection, ensuring that the thermal environment around the injector is realistically represented in the simulation.

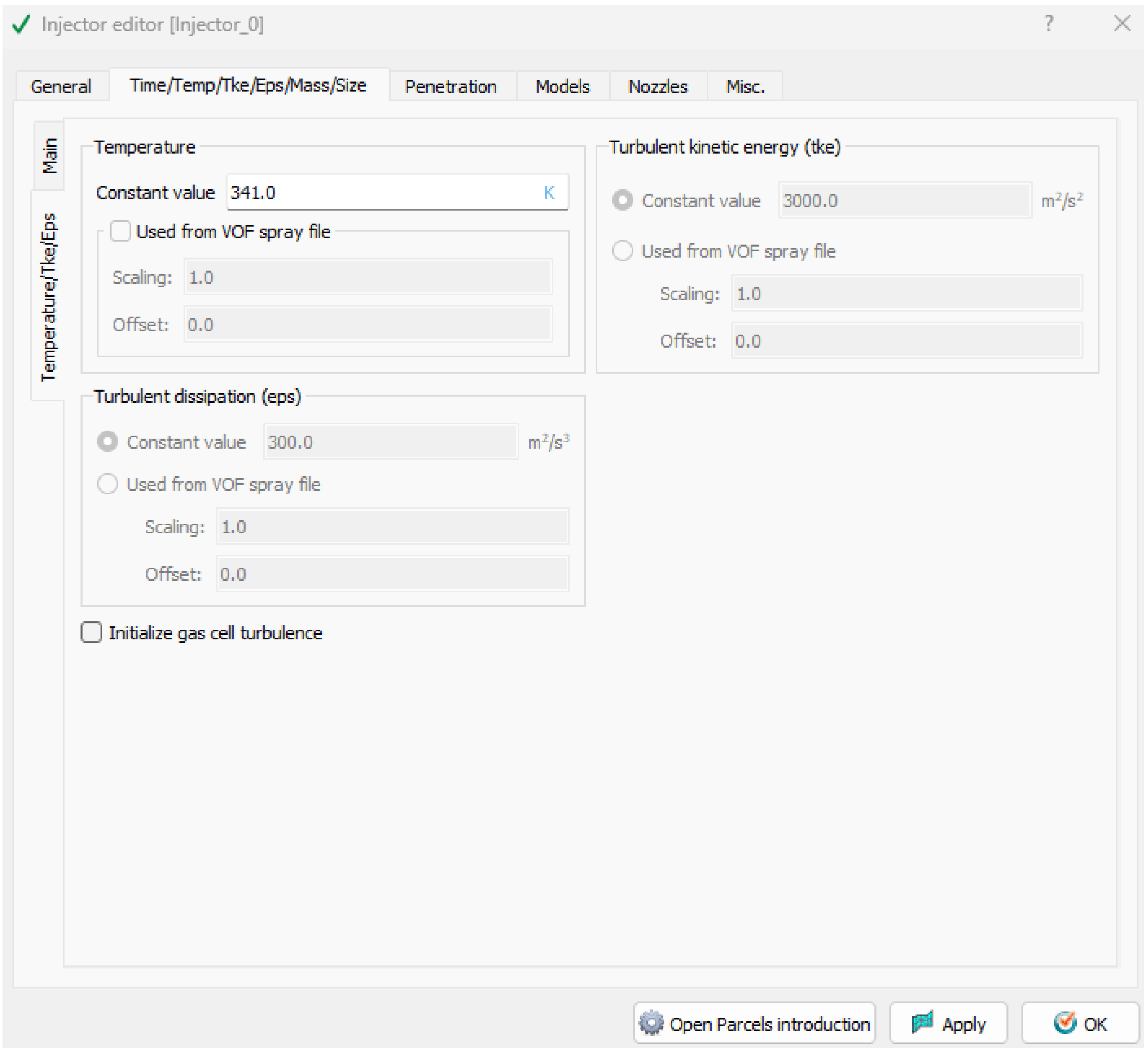

This window focuses on the penetration settings, with a liquid fuel mass fraction of 0.97 for calculating spray penetration and a fuel vapor mass fraction of 0.001 for vapor penetration, using a bin size of 0.001 m. These parameters are used to define the criteria for determining how far liquid droplets and vapor can penetrate the combustion chamber, which is essential for evaluating the mixing efficiency and combustion quality [10]. The selected values ensure a detailed representation of spray and vapor interactions, providing insights into the distribution and phase change processes within the chamber.

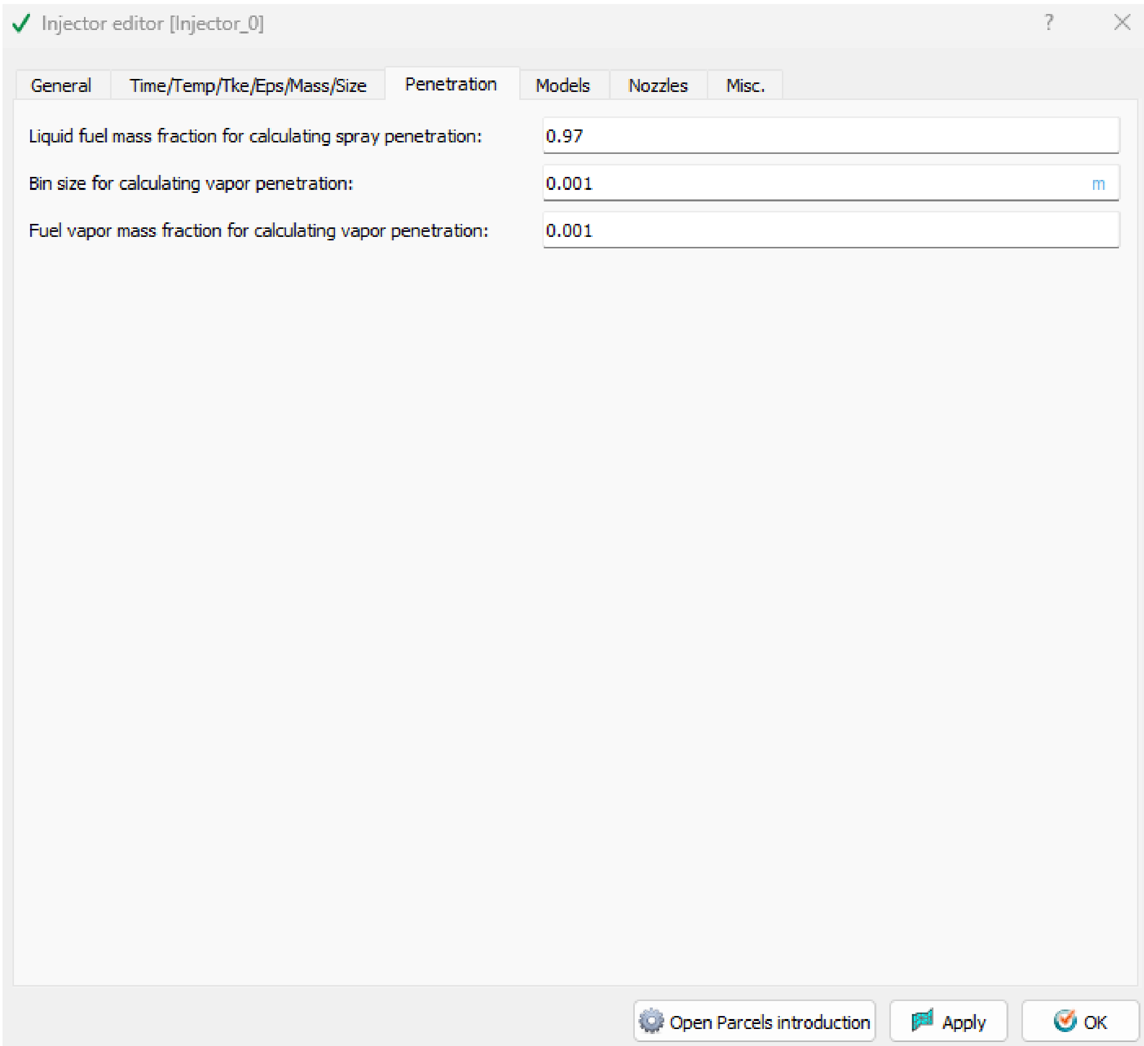

In this window, the discharge coefficient model is activated with specific values set for the discharge coefficient (0.7) and velocity coefficient (1.0). The use of the discharge coefficient model helps in adjusting the flow characteristics of the injector to account for variations in flow resistance and velocity profiles, which can significantly influence spray formation [11]. By correlating the discharge coefficient with the velocity coefficient, the simulation can more accurately reflect the influence of injector design and flow conditions on the spray dynamics, leading to more realistic predictions of spray behavior and subsequent combustion performance.

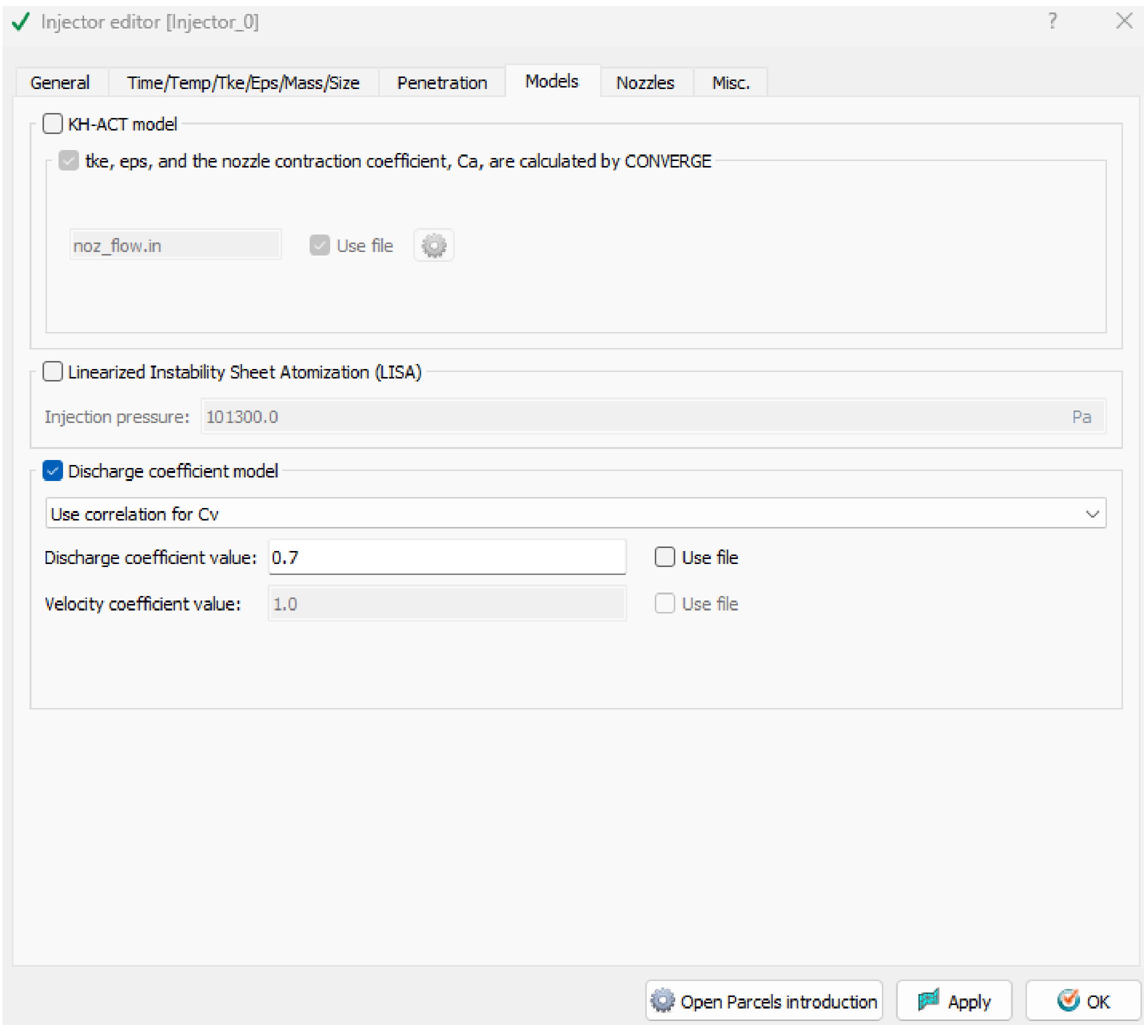

The nozzle configuration defines the injector's spray characteristics and spatial alignment. The polar orientation with 2 holes ensures evenly distributed injection, spanning an azimuth angle of 0° to 360° for symmetrical spray patterns. The nozzle coordinates precisely with the domain's Z-axis at (0.0, 0.0, -0.0032208), positioning the injector at a realistic starting point for spray propagation. The clock angle of 0° maintains uniform spray alignment without angular offsets.

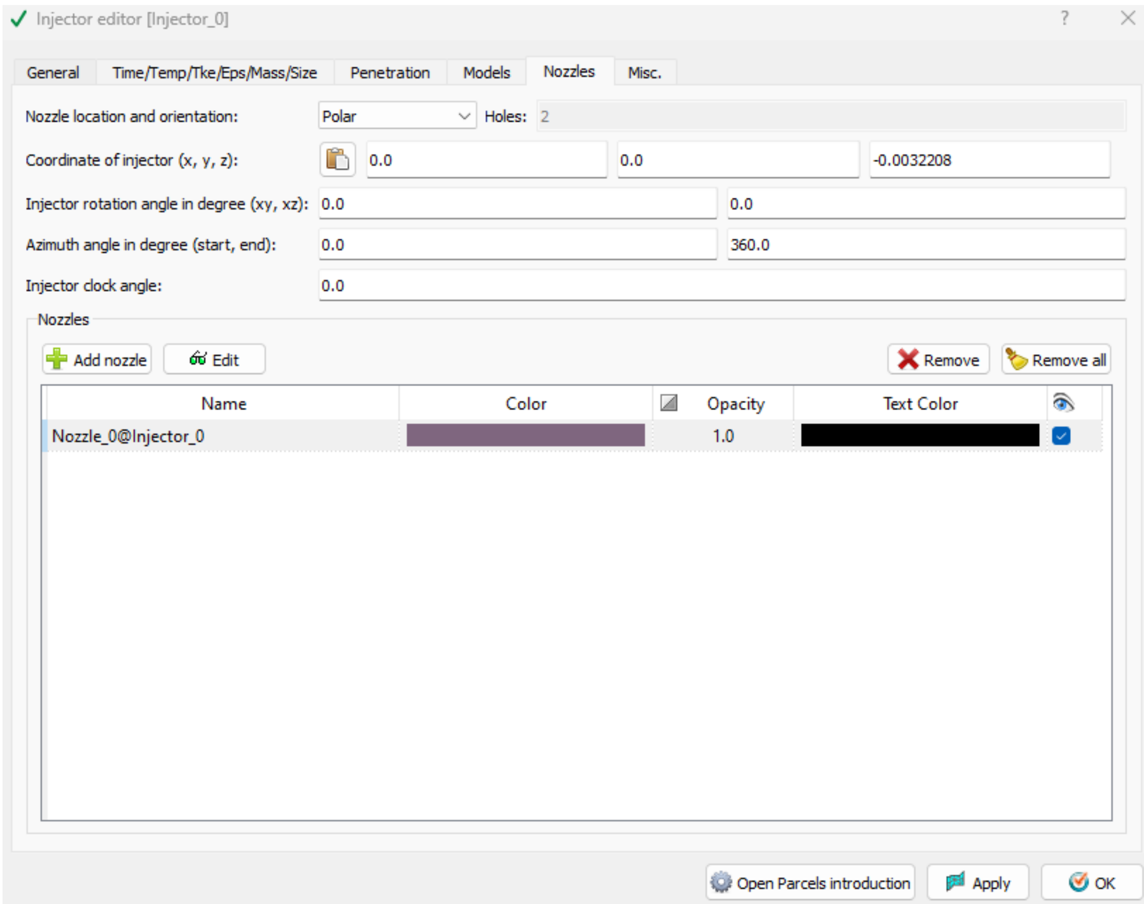

The nozzle configuration specifies the nozzle diameter as 0.000259 m and the circular injection radius as 0.0001295 m, with a spray cone angle of 9 degrees. These parameters define the physical attributes of the injector nozzle, directly influencing the initial characteristics of the spray such as droplet size and spread angle. The specified values are selected to match realistic injector dimensions, ensuring that the initial conditions of the spray are consistent with real-world injector performance [12]. The chosen spray cone angle helps in controlling the spread of the spray, which is crucial for optimizing the air-fuel mixture formation within the combustion chamber.

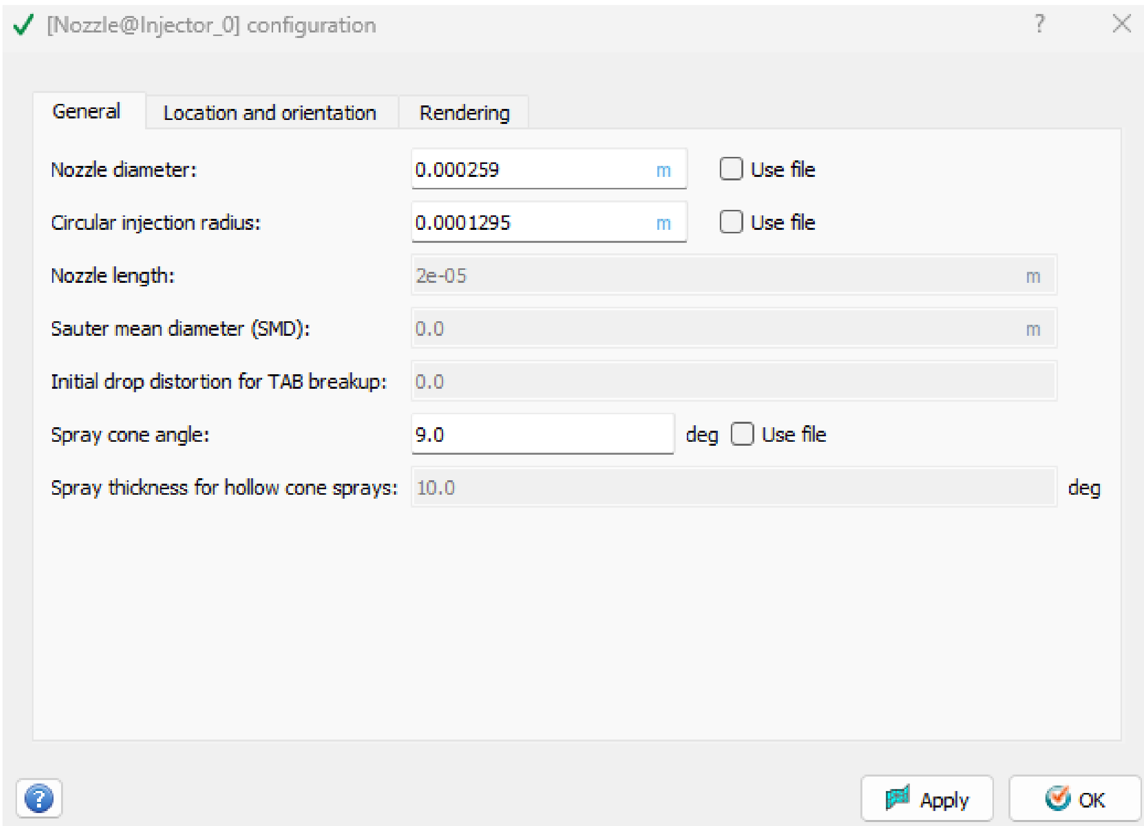

Under 'Location and orientation' for Nozzle@Injector_0, the nozzle is positioned with a radial position of 0.00097 m, an axial position of 0 m, and azimuthal position of 0 degrees. The tilt angle in the XZ plane is set to 62.5 degrees, which effectively angles the nozzle to optimize spray penetration and fuel distribution within the combustion chamber [12]. This configuration is crucial for directing the spray to target areas in the cylinder, enhancing mixing efficiency and ensuring a more uniform combustion process. By carefully tuning the nozzle orientation, the setup can mitigate issues such as wall wetting and uneven air-fuel mixing that could lead to inefficient combustion or increased emissions.

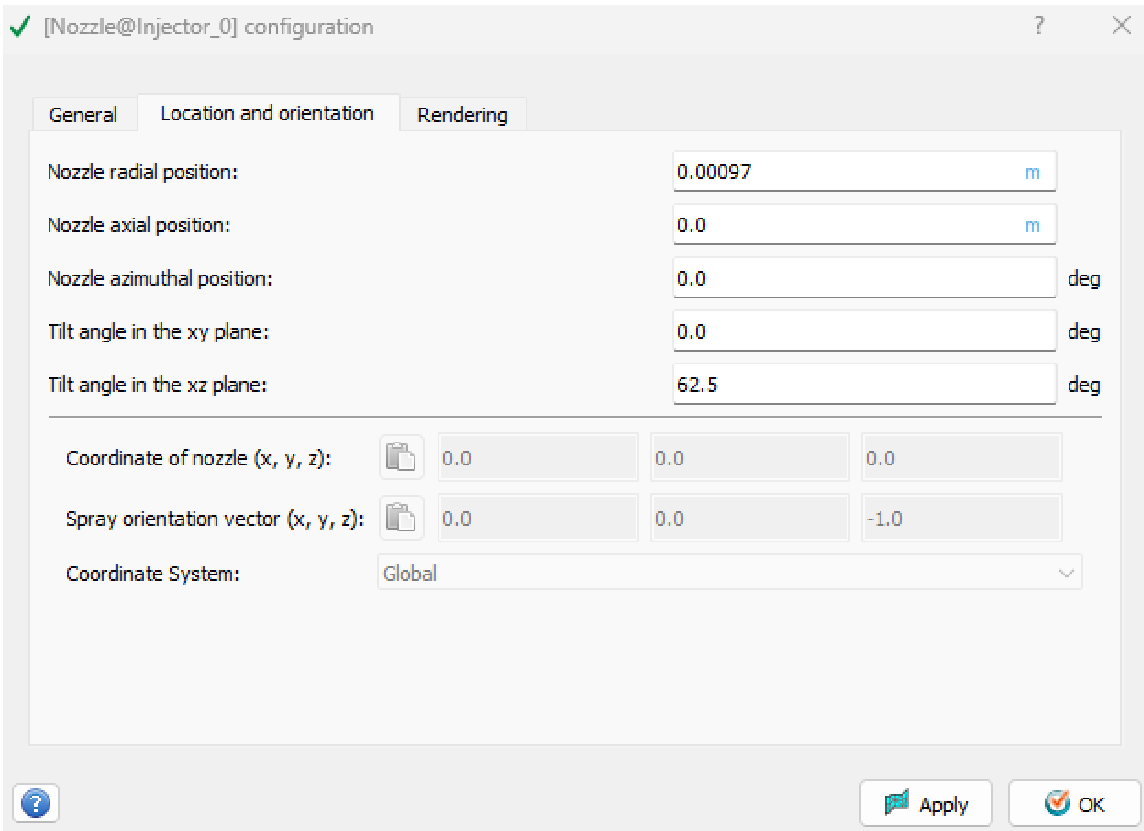

Under 'Rendering,' the configuration shows that the spray cone is visualized, with specific nozzle and label colors chosen, and the opacity set to 1. This setting is purely for visualization purposes, allowing the operator to clearly view and differentiate the spray cone during setup and analysis. Displaying the spray cone helps in verifying that the spray coverage is as expected and aligns correctly within the engine geometry. The color and opacity choices do not affect the simulation results but are vital for confirming that the spray's spatial parameters align with the intended design.

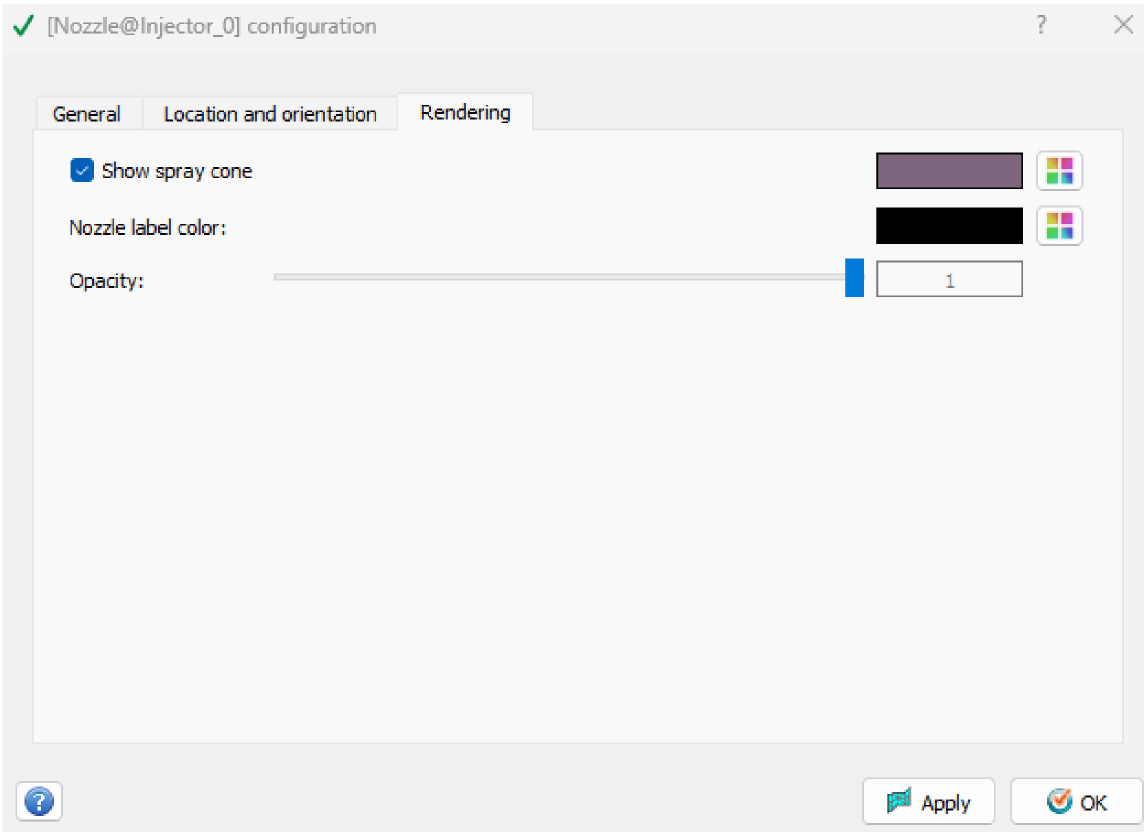

Under 'Misc' tab in the Injector editor for Injector_0, the injection spray type is set to 'Solid cone spray,' with no dynamic cone angle adjustments and a swirl fraction of 0.0. This setup creates a robust and consistent spray pattern, ensuring that the fuel is atomized in a controlled manner throughout the injection event. The solid cone spray type is commonly used in scenarios where a dense spray is needed to penetrate deep into the combustion chamber, aiding in better mixing with air [13]. The absence of swirl indicates that the spray will not have a rotational component, simplifying the spray dynamics and reducing computational complexity while still achieving effective fuel distribution.

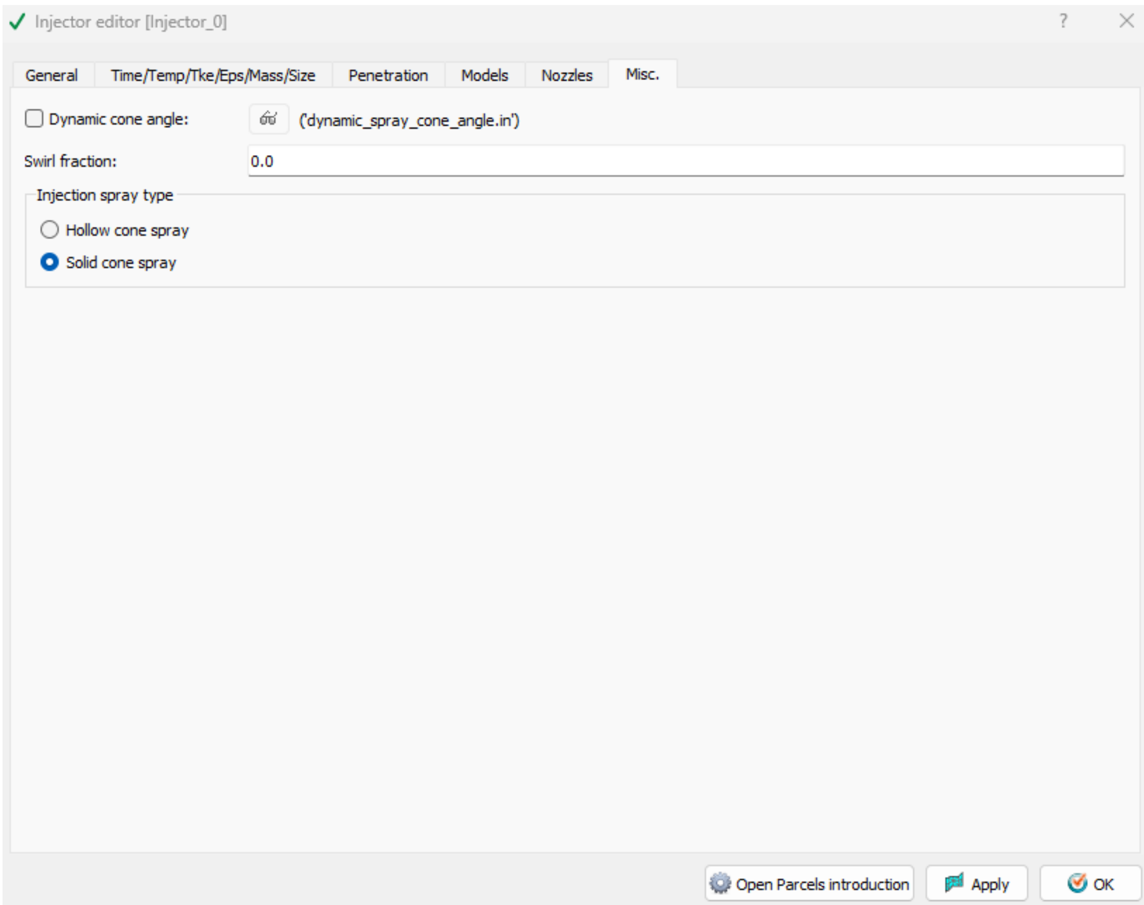

The following images illustrate the injector and nozzle setup within the simulation for each piston configuration, highlighting the spray cone extending outward from the nozzle. The injector's angled position and visible spray cone confirm the proper orientation to optimize fuel delivery and mixing in the combustion chamber.

1. **Open-W Piston**

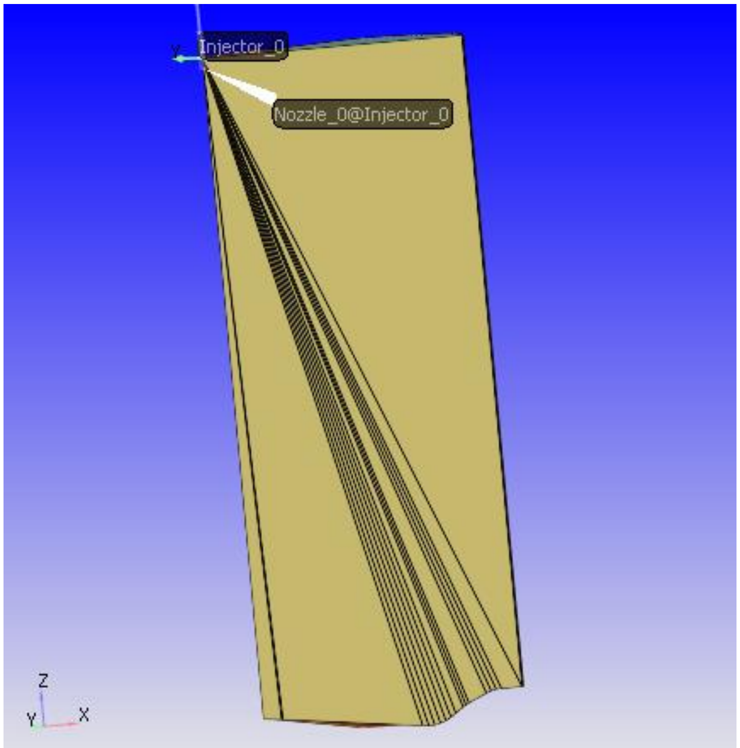

2. **Omega Piston**

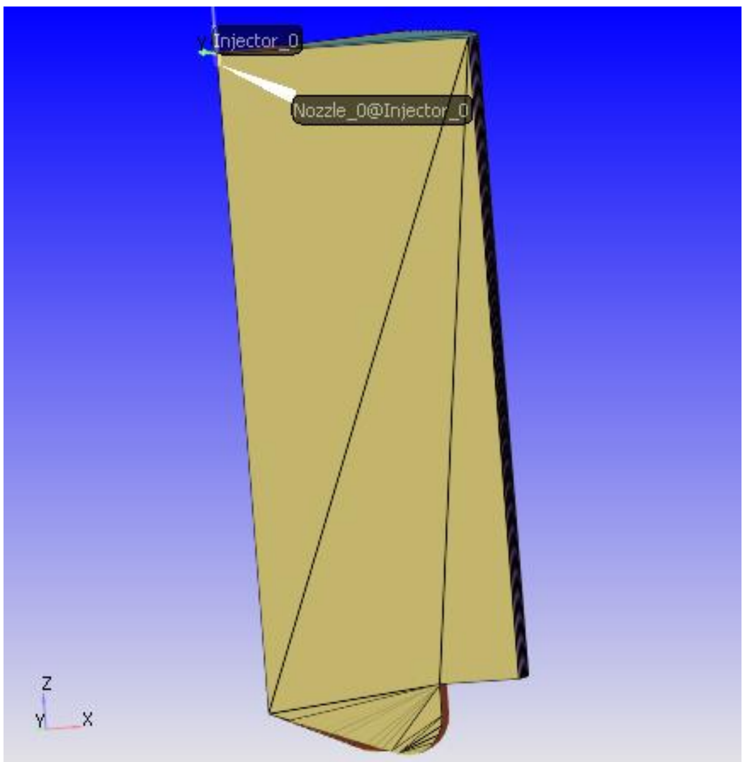

- Combustion modeling

Use the provided 'combust.in' file to configure the combustion modeling parameters. Alternatively, set them manually as reflected in the subsequent configuration windows.

The combustion modeling settings specify the combustion parameters essential for the simulation. In the general settings, the fuel species used is C_7H_{16} (heptane), indicating that heptane is the primary fuel for this simulation. The temporal type is set to SEQUENTIAL with a start time of -10.0 degrees and an end time of 135.0 degrees, which defines the temporal window for the combustion process. The combustion temperature cutoff is set at 600 K, ensuring that combustion calculations only occur above this temperature, preventing unrealistic reactions at lower temperatures. The emissions model is activated, allowing for the tracking of emissions such as NO_x and soot during the combustion process. Other parameters in tabs not presented are automatically managed by CONVERGE CFD with no alterations required.

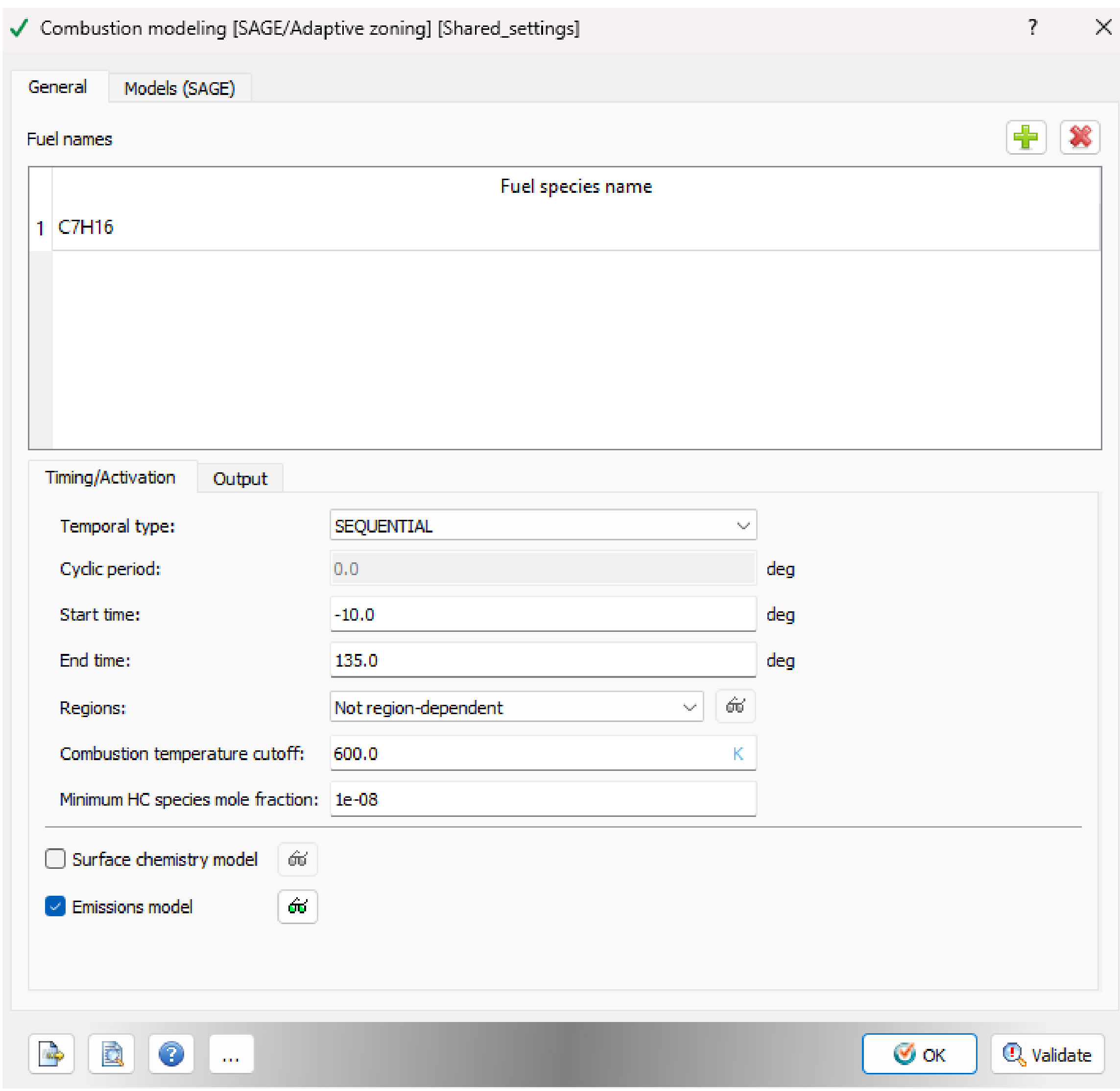

The SAGE detailed chemistry solver is used for combustion modeling, leveraging advanced capabilities for simulating complex chemical reactions [14]. The re-solve option is configured to re-solve the chemistry only if the temperature changes by 2.0 degrees, optimizing computational efficiency without compromising accuracy. The solver employs the CVODES with a dense solver, recommended for scenarios with less than or equal to 100 species, operating under constant volume conditions, which is suitable for capturing the combustion dynamics accurately. Analytical Jacobian is used to enhance the convergence and stability of the solution. Other configurations, such as reaction multipliers and advanced solver options, are set by default in CONVERGE CFD.

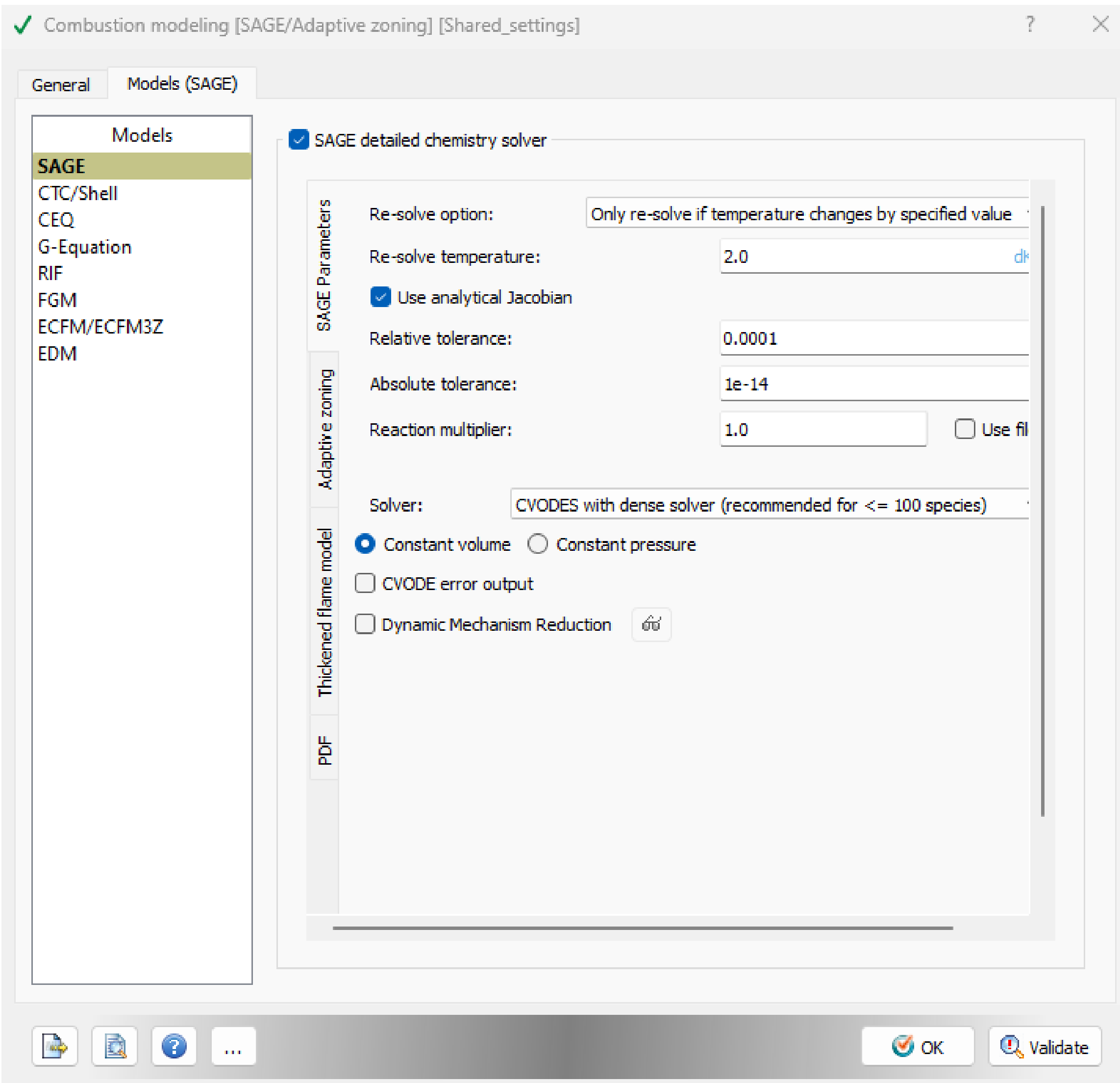

Adaptive zoning is activated with a dimension of 2, which allows for dynamic adjustment of the computational grid based on the temperature and reaction rate gradients, optimizing the accuracy and efficiency of combustion modeling. The temperature bin size is set to 5.0 K and the reaction ratio bin size to 0.05, fine-tuning the resolution of the adaptive zones. Conserving NO_x during species remap is enabled, which ensures that NO_x concentrations are accurately maintained across the computational domain during mesh adaptations. The adaptive zoning helps in achieving precise resolution where it is most needed, thereby improving the fidelity of the simulation results [15]. All other adaptive zoning parameters not shown are handled automatically by CONVERGE CFD.

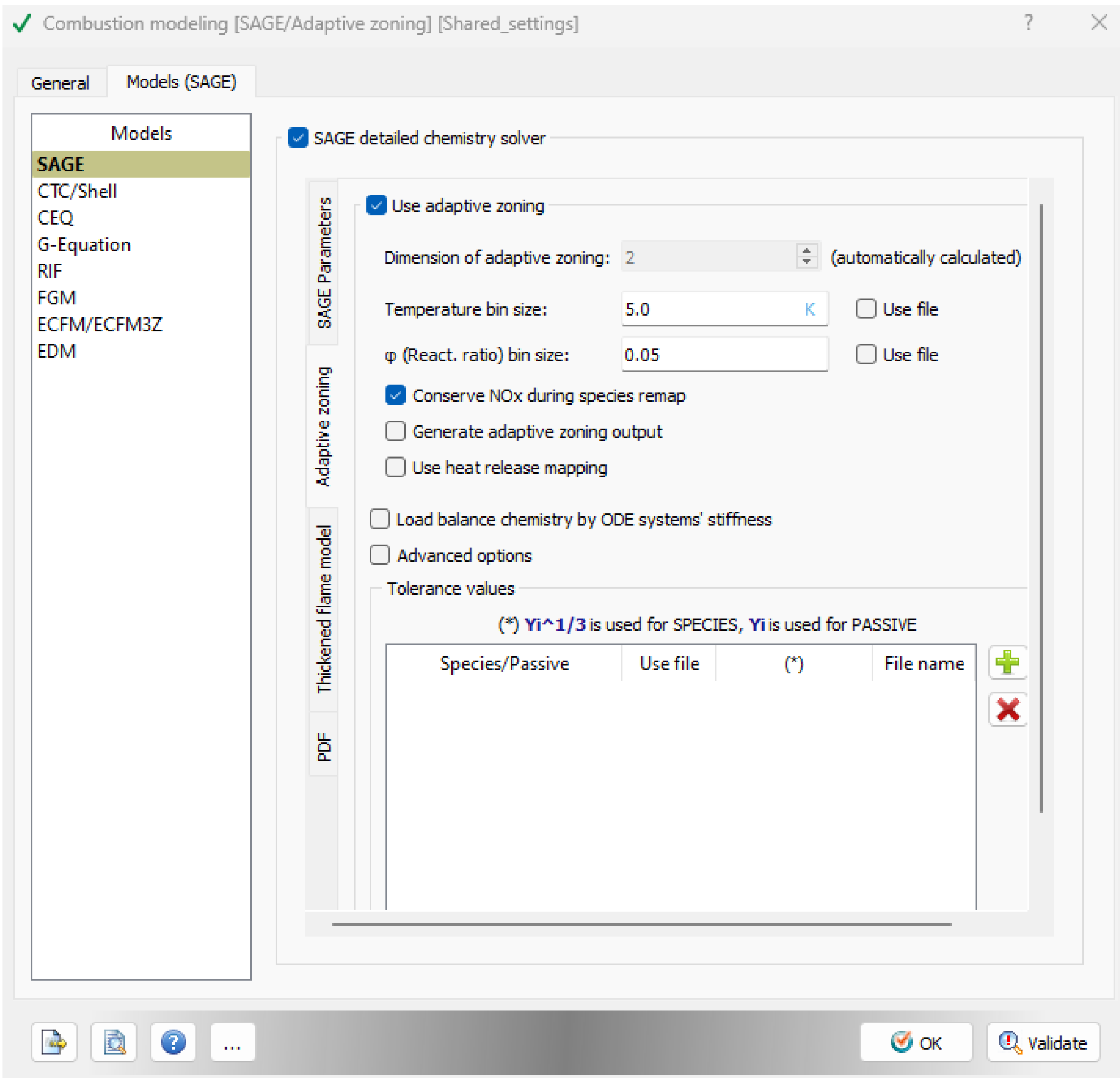

- Emissions modeling

The NO_x modeling configuration employs the Thermal NO_x model (Extended Zeldovich), which is effective for simulating NO_x formation in high-temperature combustion environments [16]. The equilibrium assumption is used for O/OH species, simplifying computational requirements while maintaining accuracy. The mass scaling factor for converting NO to NO_x is set to 1.533, ensuring correct post-processing of NO_x emissions. This setup balances detailed chemical modeling and computational efficiency, making it suitable for systems with significant thermal NO_x formation.

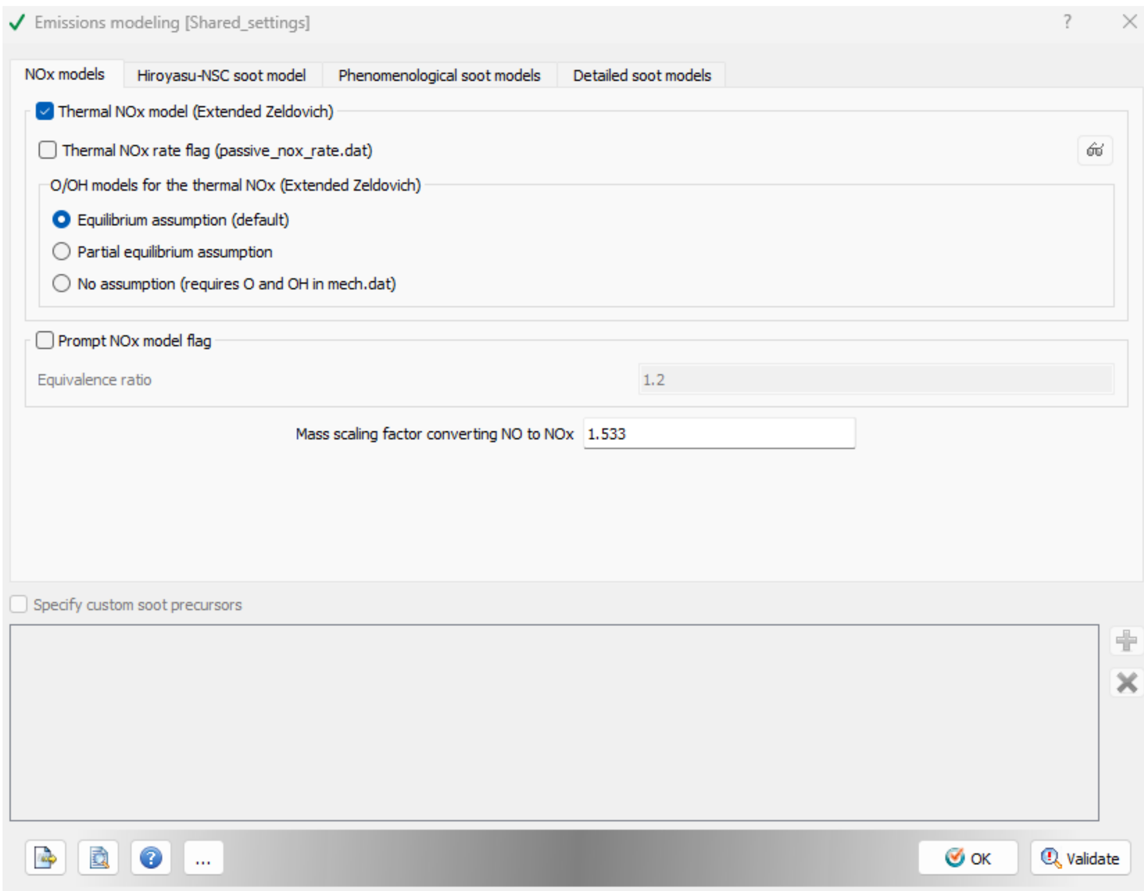

The Hiroyasu-NSC soot model is configured to predict soot formation and oxidation. Parameters such as the pre-exponential factor (350.0 $(s\cdot bar^{0.5})^{-1}$) and activation energy (12,500 cal/mol) are calibrated for accurate formation rates. The soot particle diameter is set to 2.5e^{-06} cm, and the density is 2.0 g/cm^3, ensuring realistic representation of particulate size and mass. Using total hydrocarbons as formation species captures the contribution of all hydrocarbon molecules to soot generation. This model is ideal for applications requiring detailed soot behavior without excessive computational demand.

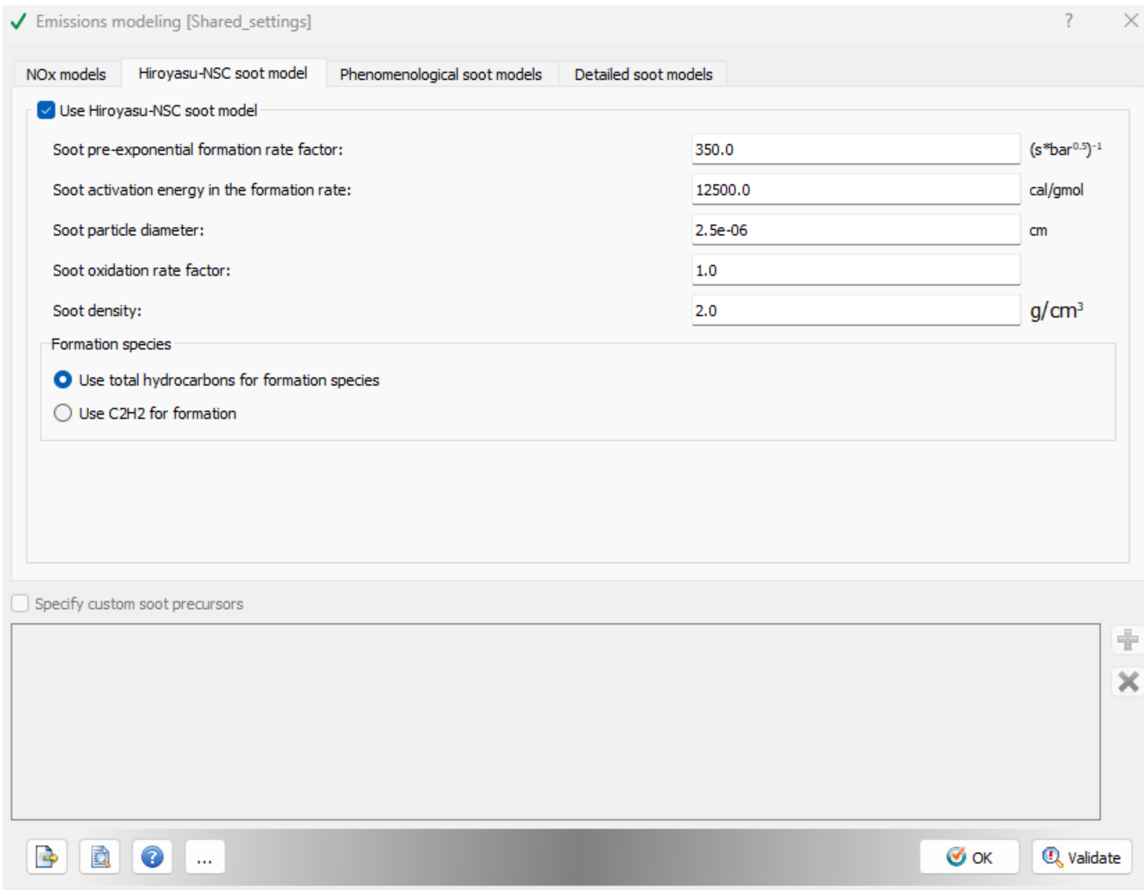

- Turbulence modeling

The RNG k-ε model is selected as the turbulence model, with all turbulence parameters set to their default values as shown in the window.

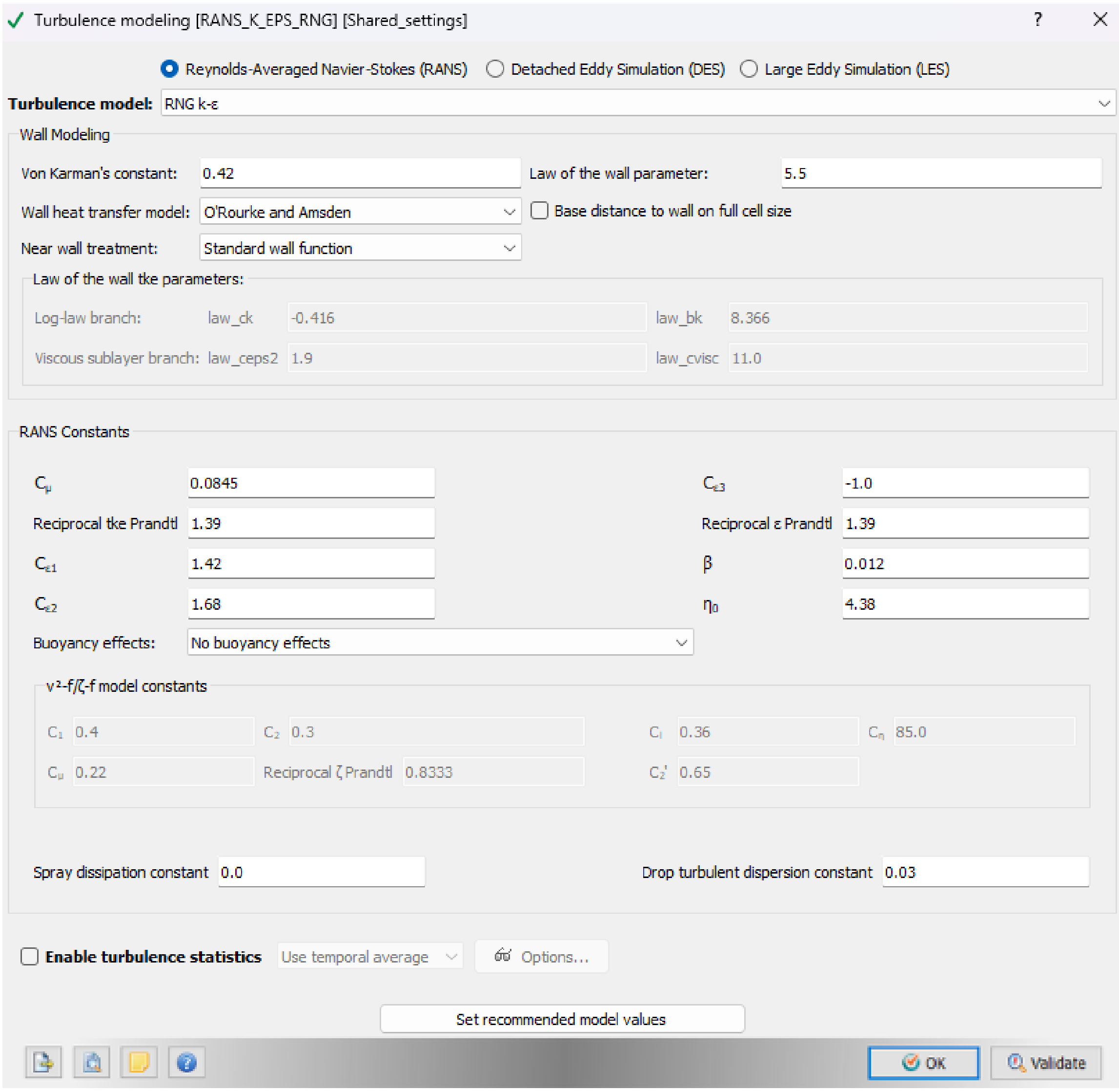

Grid Control

- Base grid

In the Base Grid dialog box, the values for dx, dy, and dz are all set to 0.004 m.

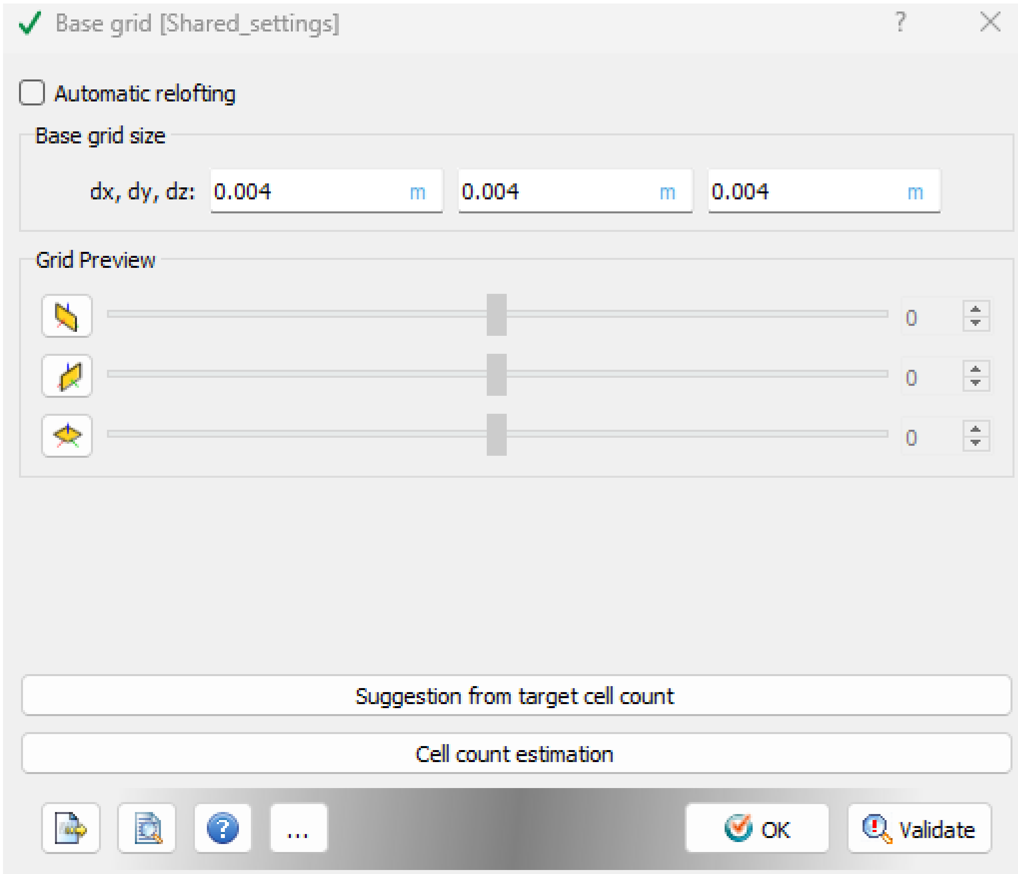

- Adaptive Mesh Refinement

Use the provided 'amr.in' file to configure the adaptive mesh refinement (AMR) parameters. Alternatively, the parameters can be configured manually, as demonstrated in the following windows.

The AMR is set up for the velocity criterion within the 'In_cylinder_region.' The AMR parameters include a steady cycle setting of 100, with minimum and maximum cell counts defined as 1 and 2,000,000 respectively, to control the mesh density dynamically. The embedding frequency is set to 1, indicating mesh refinement updates occur at every simulation time step, while the release frequency is set to 25, allowing for gradual release of refined cells to prevent excessive mesh growth. For the velocity criterion, the embed type is set to 'Sub-grid scale (SGS)' with a maximum embedding level of 2 and a sub-grid criterion of 2 m/s. The timing control type is 'PERMANENT,' meaning that the mesh refinement remains active throughout the entire simulation cycle of 720 degrees, ensuring that regions of high velocity gradients are adequately resolved to capture detailed flow characteristics.

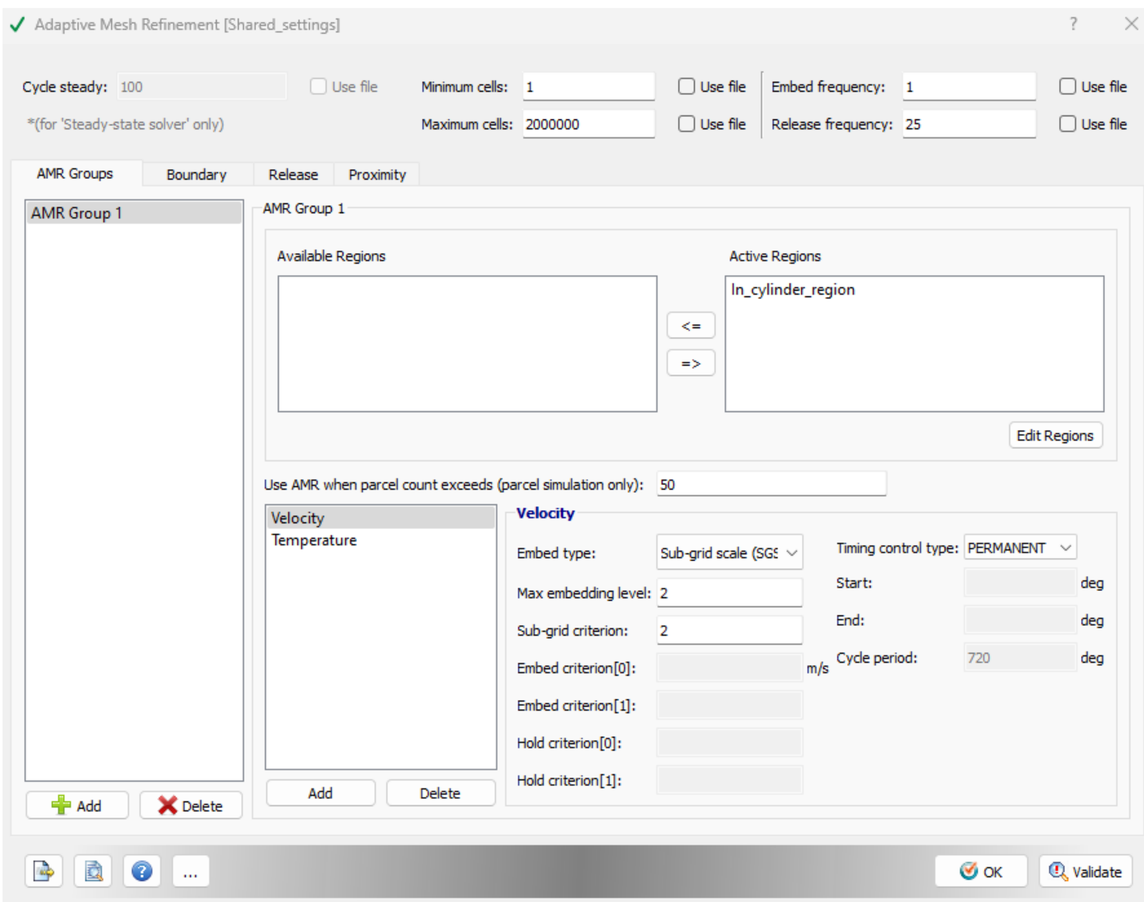

In addition, AMR is configured based on the temperature criterion within the same 'In_cylinder_region.' The overall settings remain consistent with the velocity AMR setup, with cycle steady, minimum, and maximum cell counts, and embedding/release frequencies all similarly defined. However, the temperature-specific refinement uses an embed type of 'Sub-grid scale (SGS)' with a maximum embedding level of 2 and a sub-grid criterion of 5 K. The timing control type for temperature AMR is set to 'SEQUENTIAL,' with an active period from -12 degrees to 180 degrees of the simulation cycle and a cycle period of 720 degrees. This sequential activation allows for targeted mesh refinement during key phases of the simulation, such as during injection and combustion events, to enhance resolution where thermal gradients are most significant. This approach ensures accurate temperature predictions, essential for capturing combustion characteristics and emissions accurately.

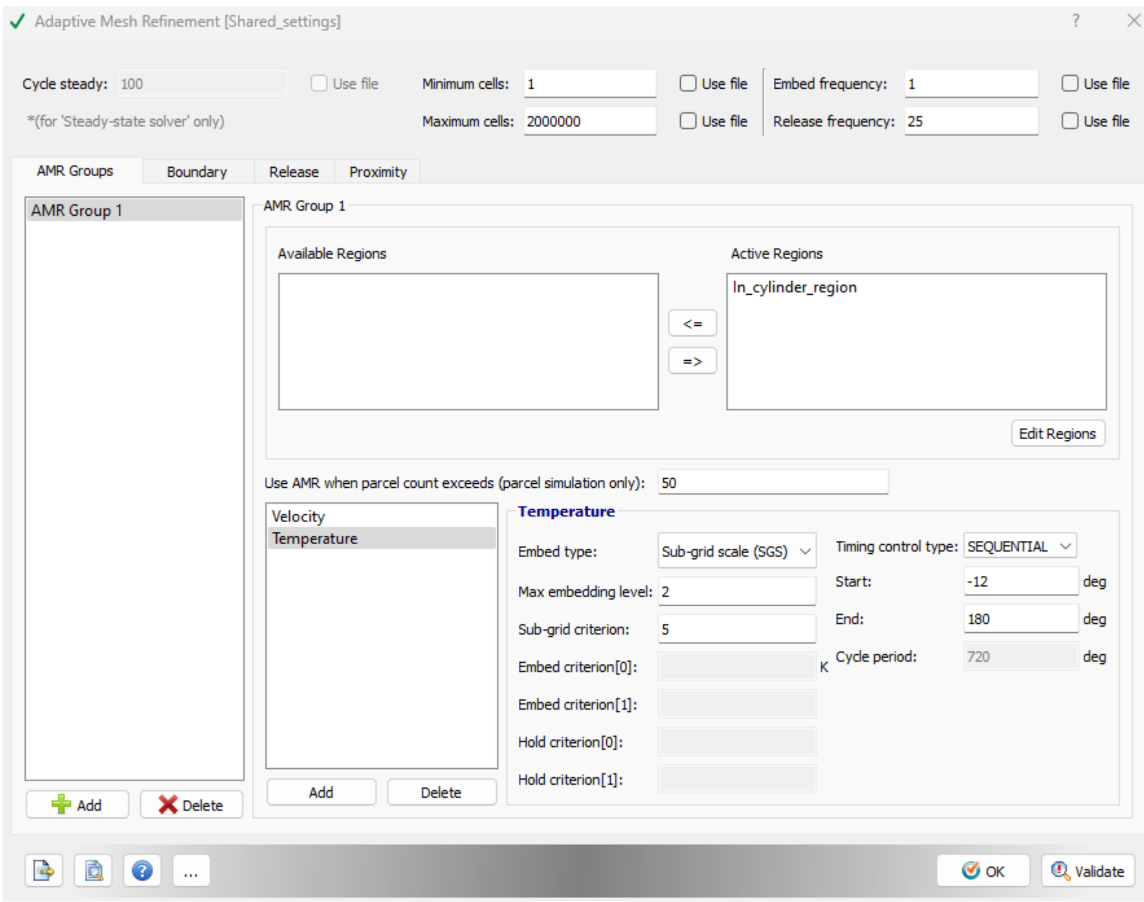

- Fixed embedding

Use the provided 'embedded.in' file to set up the fixed embedding parameters. Alternatively, set them manually as the following windows display.

For Embedding 1, the entity type is set to "NOZZLE," specifically targeting the injector and nozzle identified as Injector_0 and Nozzle@Injector_0, respectively. The mode is set to SEQUENTIAL, allowing dynamic mesh refinement based on the temporal progression of the injection event. The settings include a scale factor of 2, indicating that the mesh will be refined by a factor of 2 times the base grid size. The start time is set at -12 degrees, while the end time is 15 degrees, ensuring that the mesh refinement is applied during the critical phases of the injection process. The radius and length parameters define the spatial extent of the mesh refinement, optimizing the computational resources by focusing on the spray region. These parameters ensure detailed resolution in the region of interest, enhancing the accuracy of spray and combustion simulations.

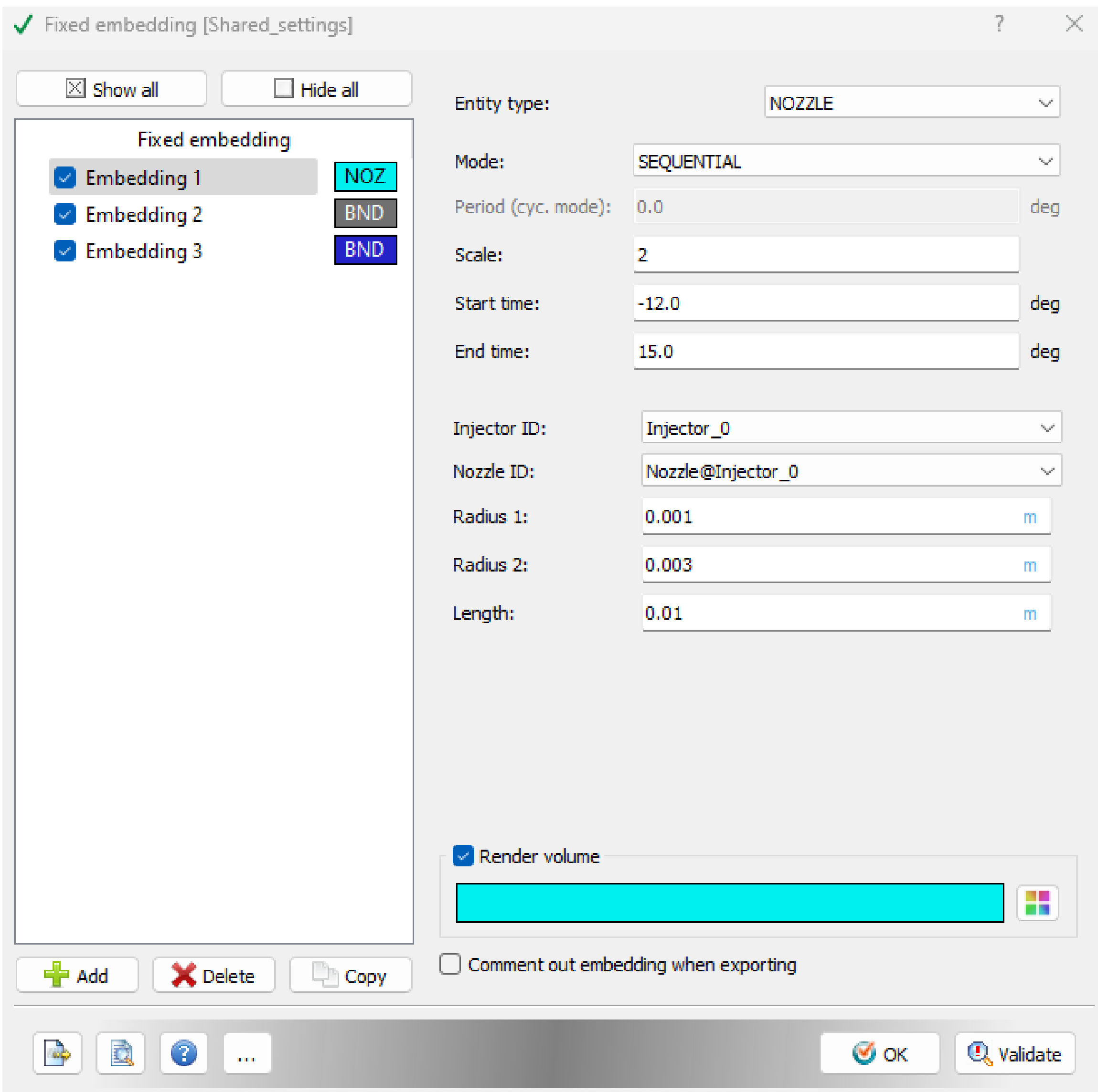

The image below illustrates the applied fixed embedding (Embedding 1) configured around the nozzle. This visualization confirms that the mesh refinement correctly envelops the critical areas of spray development, enhancing the fidelity of the simulation in predicting spray penetration, droplet breakup, and vaporization. The visual representation helps in validating the spatial configuration of the embedding settings, ensuring that the refinements are effectively targeting the regions of interest for accurate and computationally efficient simulations.

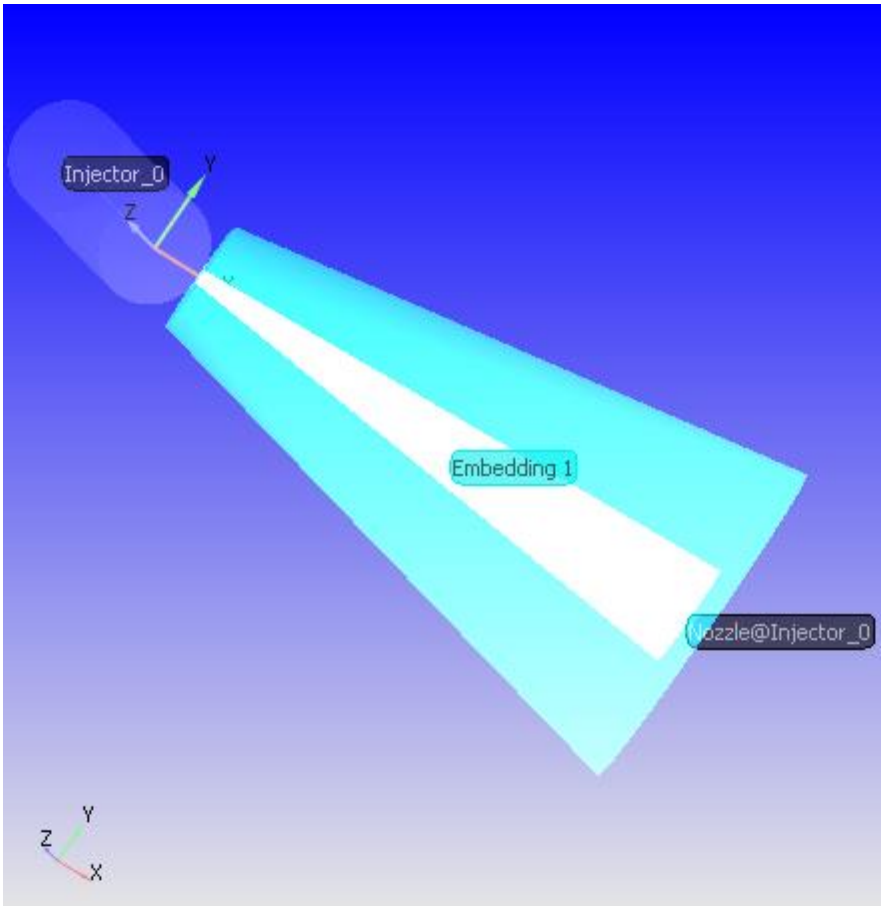

Embedding 2 is configured with the entity type "BOUNDARY," and it is applied to the "Piston" boundary. The mode remains SEQUENTIAL, with settings that match the temporal aspects of the engine cycle, beginning at -20 degrees and ending at 180 degrees. This embedding uses a scale of 1 and a single embed layer, refining the mesh at the piston boundary to capture fine-scale interactions between the spray and the piston surface during the combustion cycle. This refinement is crucial for accurately modeling the heat transfer, fluid flow, and potential impingement effects on the piston, contributing to a more detailed and realistic simulation outcome.

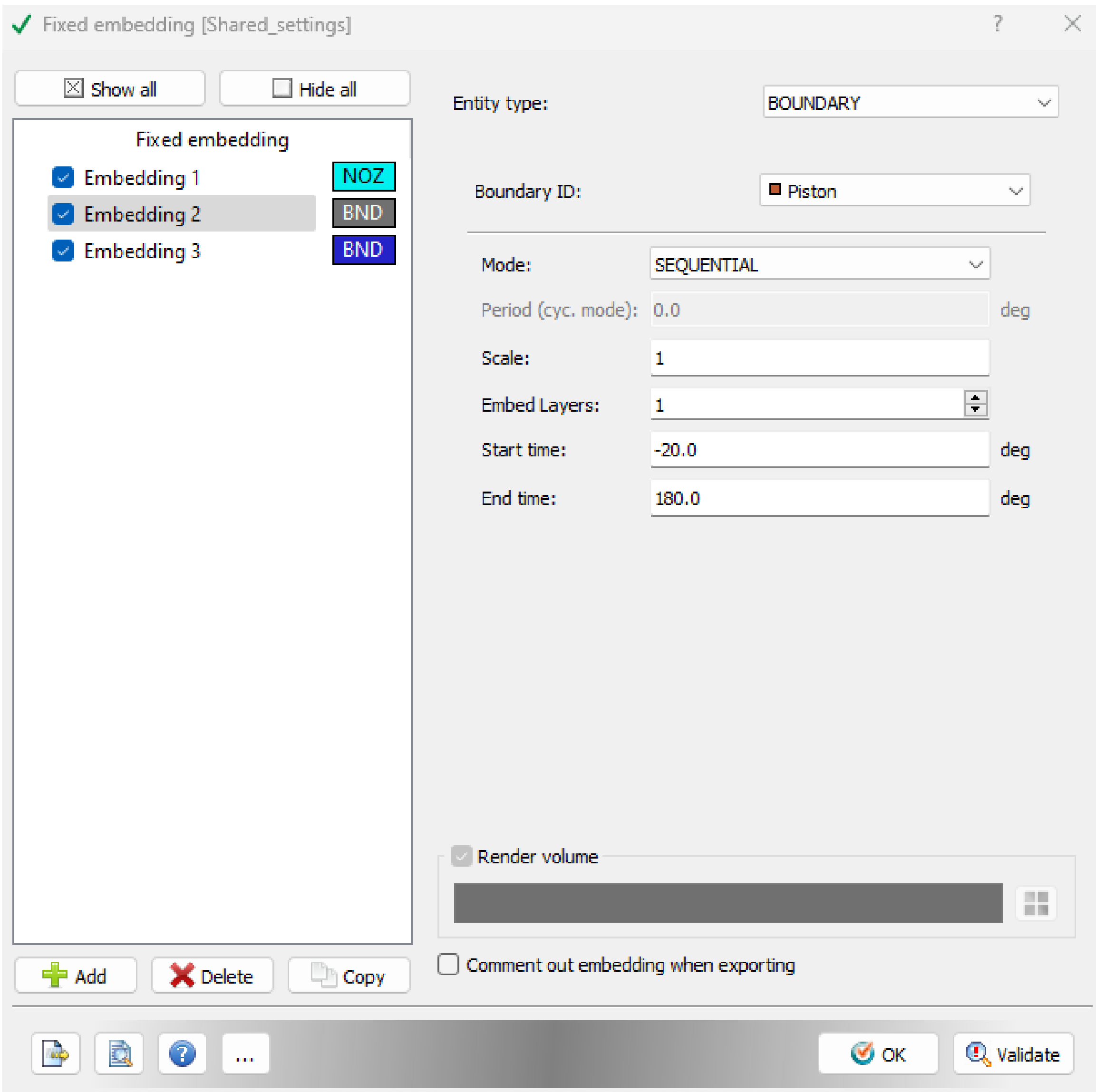

Embedding 3 targets the "Cylinder Head" boundary with similar settings as Embedding 2, maintaining consistency across critical engine components. The sequential mode, with the same time range from -20 degrees to 180 degrees, ensures that the mesh refinement aligns with the operational timing of the engine cycle. The scale and embed layers are kept at 1, focusing the mesh refinement on the cylinder head to accurately resolve the interactions between the injected fuel spray, in-cylinder flow, and the cylinder head. This setting is essential for capturing the complexities of the combustion process near the top of the combustion chamber.

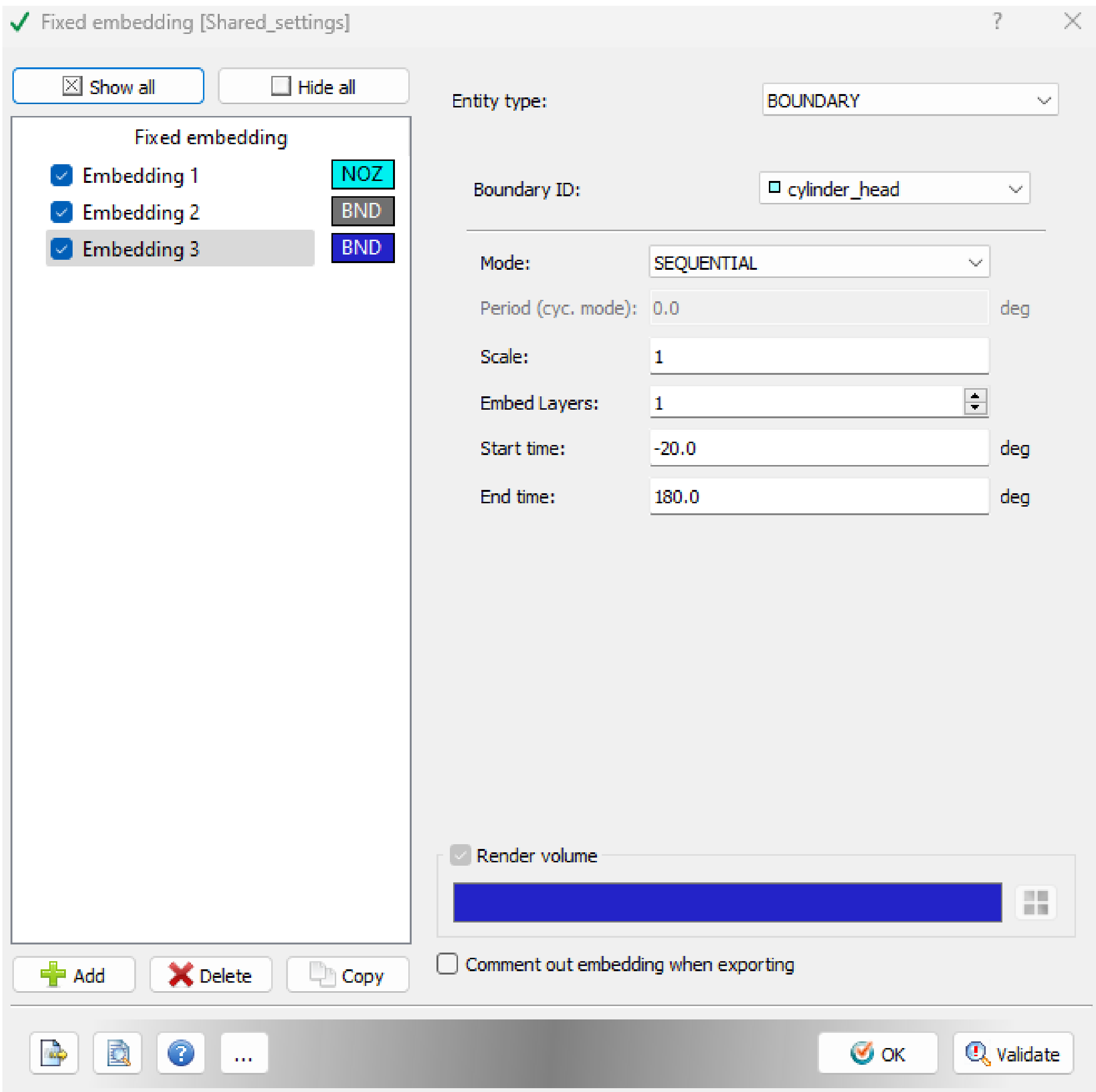

Output/Post-Processing

- Post variable Selection

Use the provided 'post.in' file to configure the post-processing variable selection. This approach ensures that all relevant variables are correctly set up, as shown in the subsequent configuration windows.

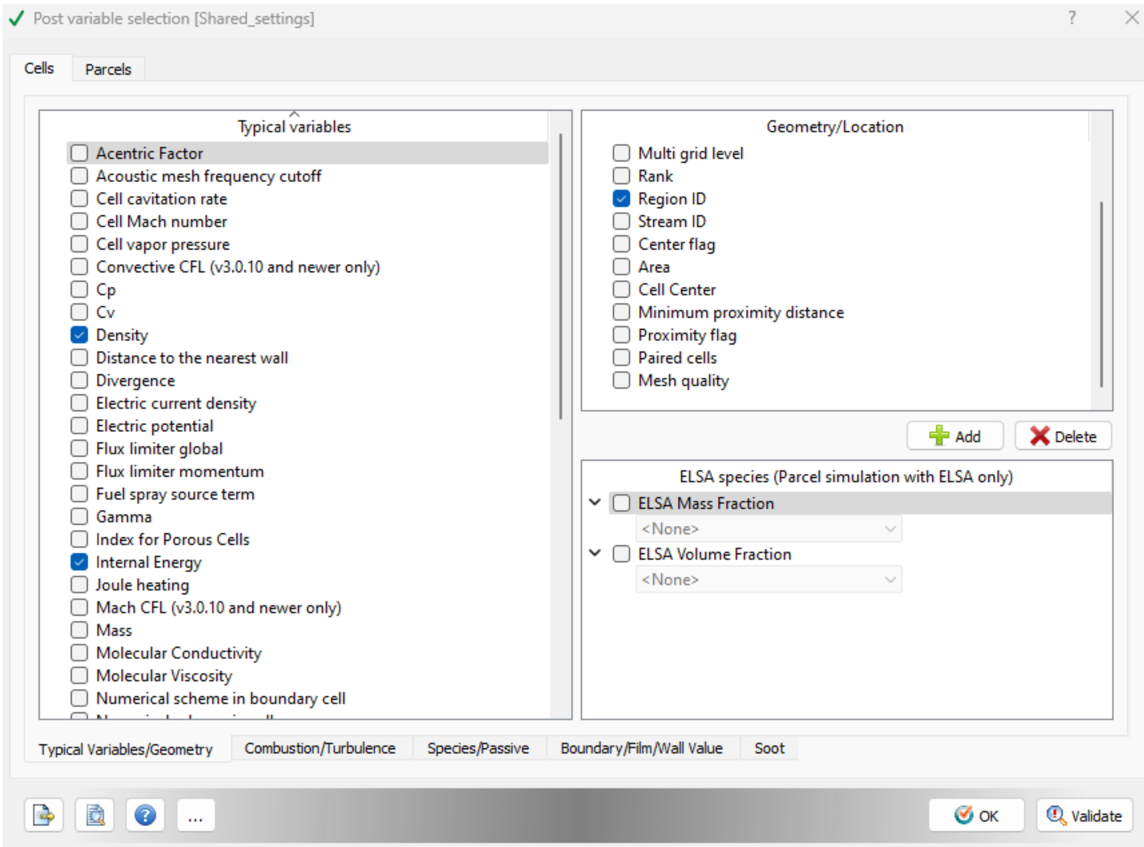

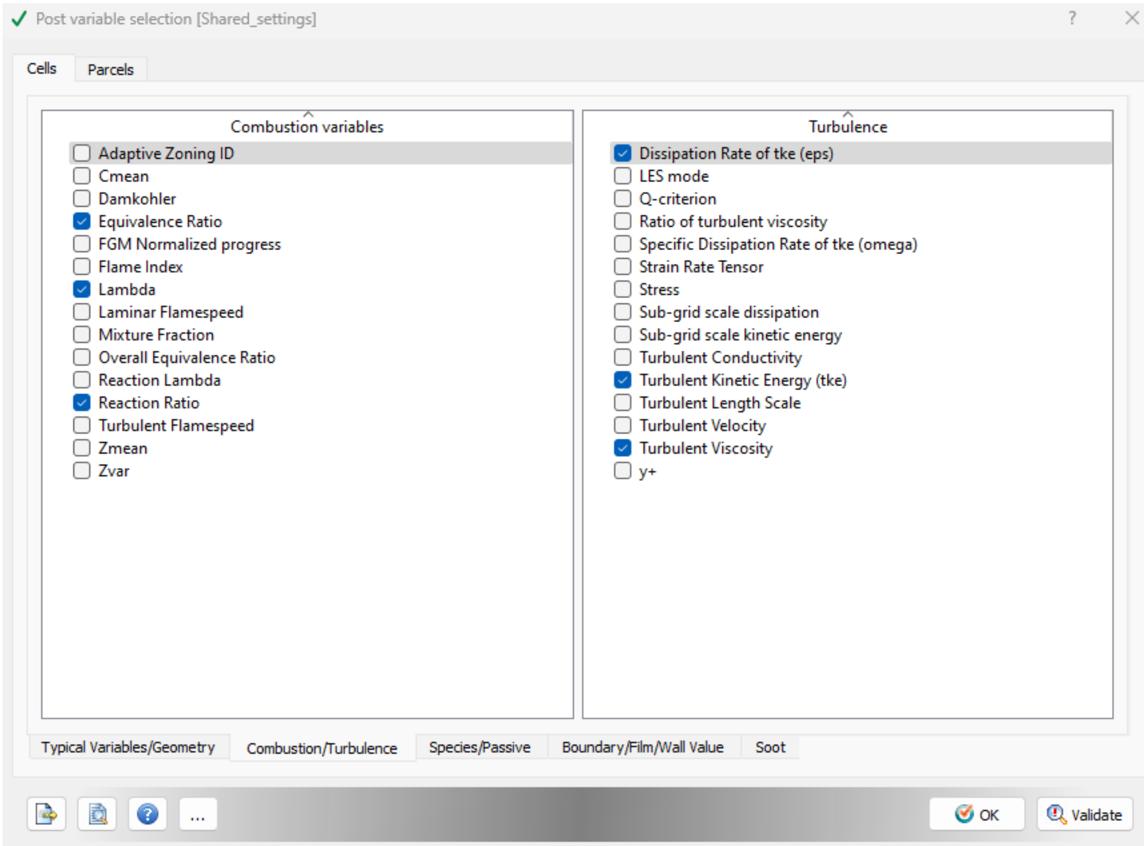
Post variable selection [Shared_settings]
Cells
Parcels
Combustion variables
Adaptive Zoning ID
Cmean
Damkohler
Equivalence Ratio
FGM Normalized progress
Flame Index
Lambda
Laminar Flamespeed
Mixture Fraction
Overall Equivalence Ratio
Reaction Lambda
Reaction Ratio
Turbulent Flamespeed
Zmean
Zvar
Turbulence
Dissipation Rate of tke (eps)
LES mode
Q-criterion
Ratio of turbulent viscosity
Specific Dissipation Rate of tke (omega)
Strain Rate Tensor
Stress
Sub-grid scale dissipation
Sub-grid scale kinetic energy
Turbulent Conductivity
Turbulent Kinetic Energy (tke)
Turbulent Length Scale
Turbulent Velocity
Turbulent Viscosity
y+
Typical Variables/Geometry
Combustion/Turbulence
Species/Passive
Boundary/Film/Wall Value
Soot
...
OK
Validate

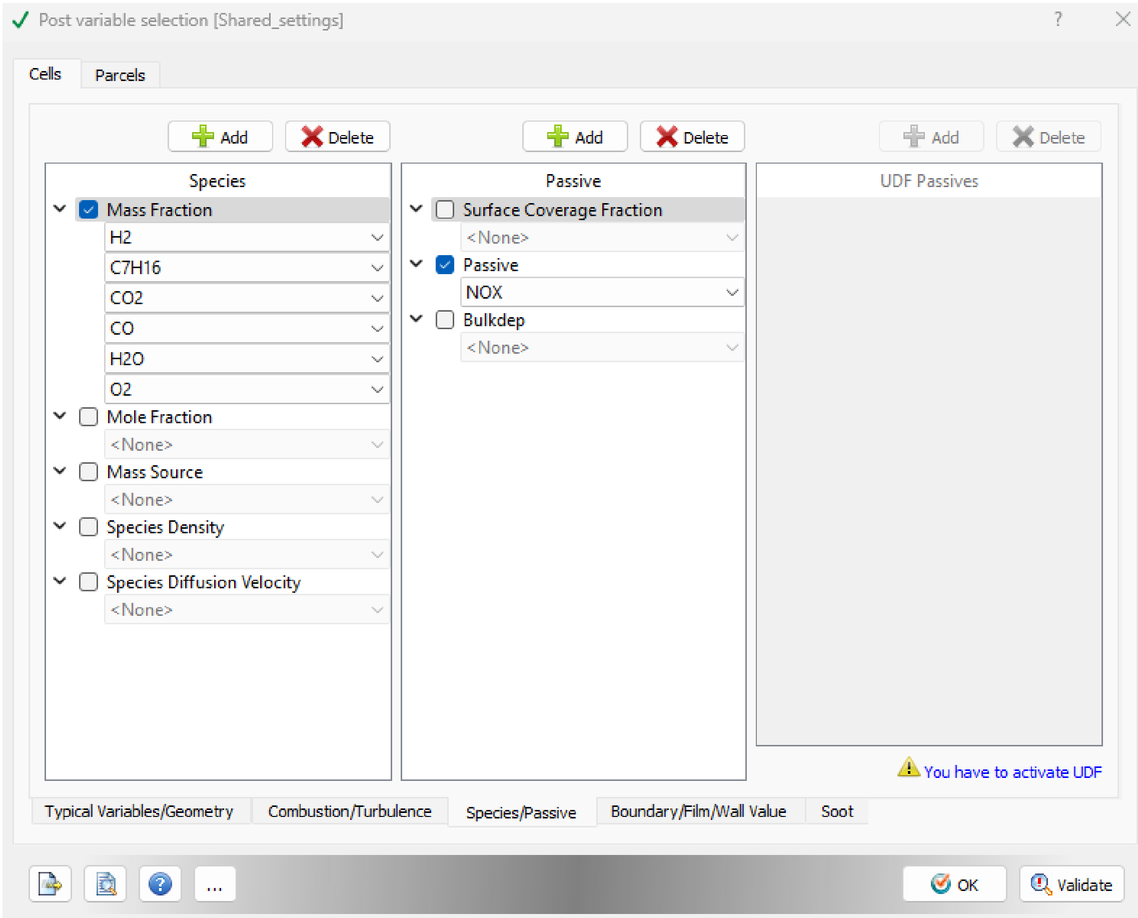
Post variable selection [Shared_settings]
Cells
Parcels
Add
Delete
Add
Delete
Add
Delete
Species
Mass Fraction
H2
C7H16
CO2
CO
H2O
O2
Mole Fraction
<None>
Mass Source
<None>
Species Density
<None>
Species Diffusion Velocity
<None>
Passive
Surface Coverage Fraction
<None>
Passive
NOX
Bulkdep
<None>
UDF Passives
You have to activate UDF
Typical Variables/Geometry
Combustion/Turbulence
Species/Passive
Boundary/Film/Wall Value
Soot
...
OK
Validate

- Output files

Use the provided 'inputs.in' file to configure the selection of output files. This method ensures that all relevant variables are accurately set up, as demonstrated in the subsequent configuration windows.

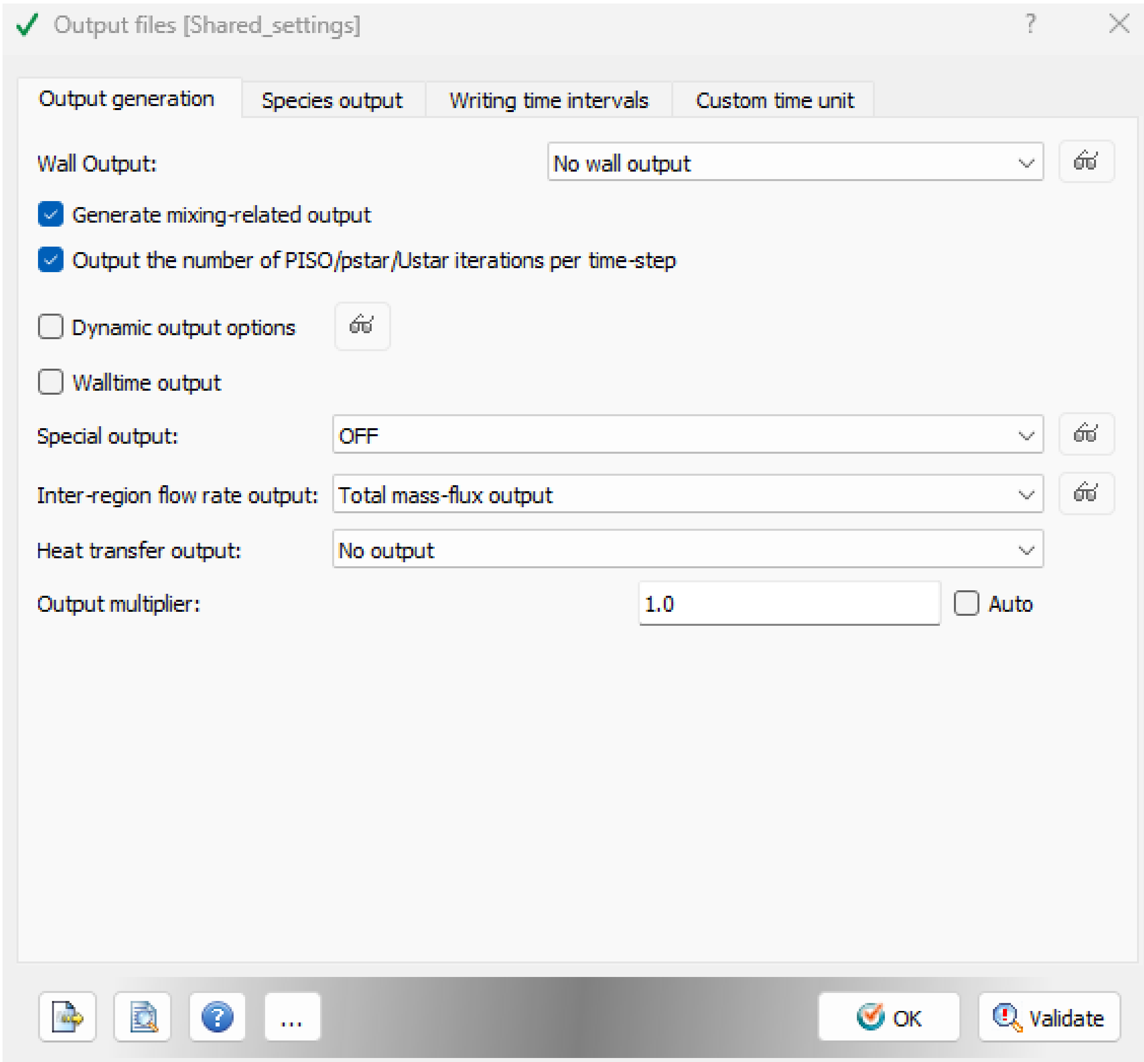

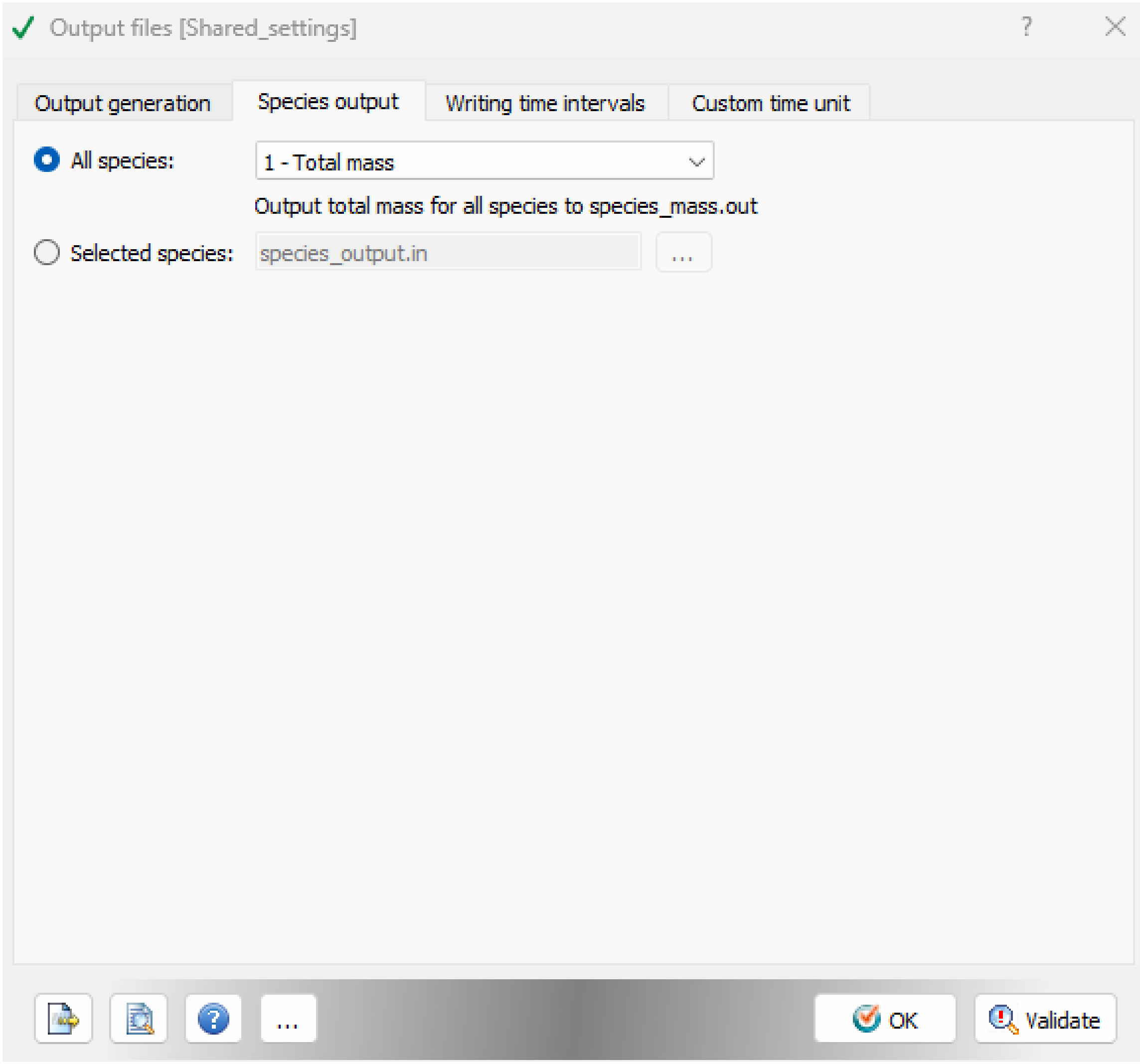
Output files [Shared_settings]
Output generation
Species output
Writing time intervals
Custom time unit
All species:
1 - Total mass
Output total mass for all species to species_mass.out
Selected species:
species_output.in
...
...
OK
Validate

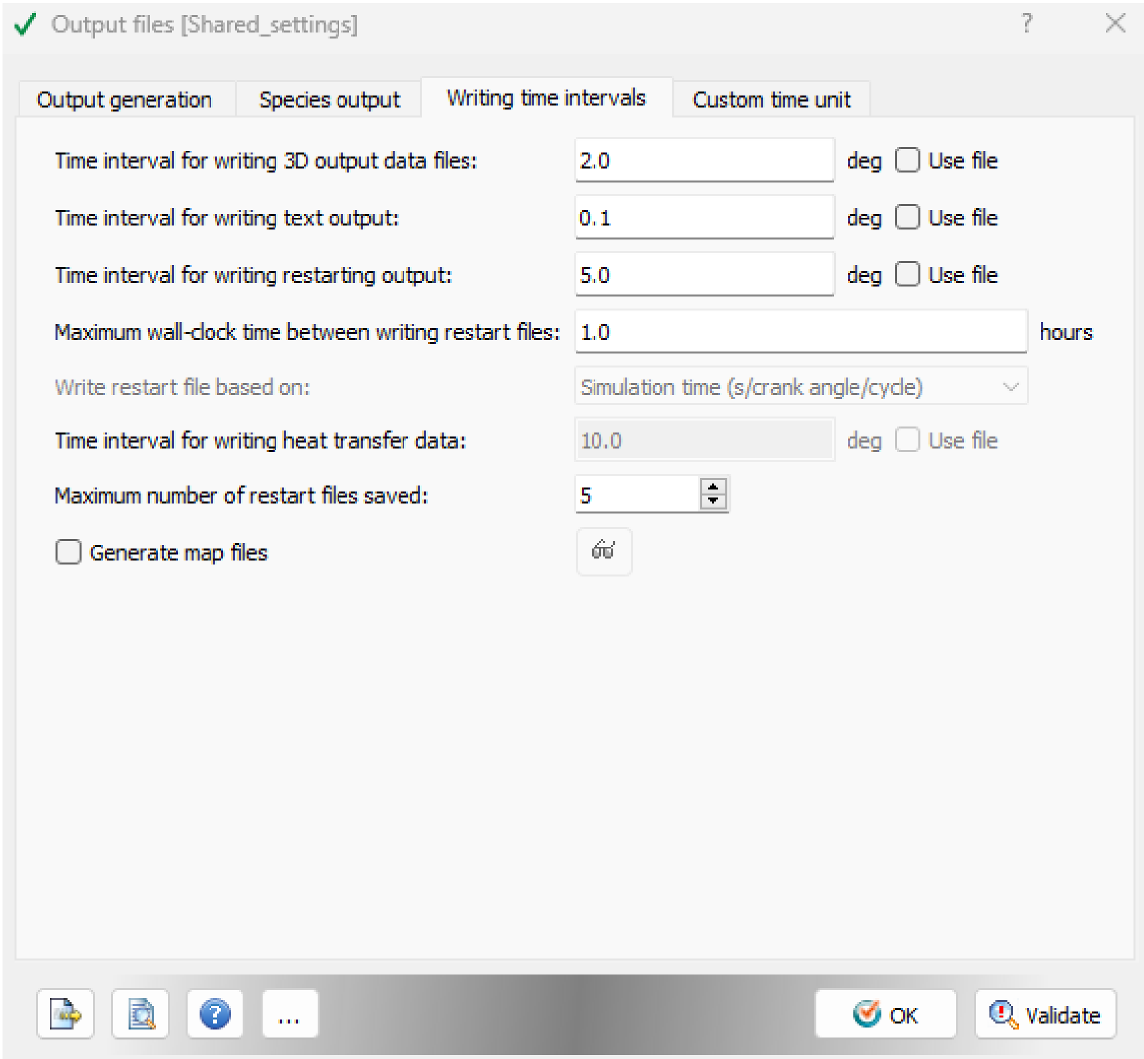
Output files [Shared_settings]
Output generation
Species output
Writing time intervals
Custom time unit
Time interval for writing 3D output data files:
2.0
deg
Use file
Time interval for writing text output:
0.1
deg
Use file
Time interval for writing restarting output:
5.0
deg
Use file
Maximum wall-clock time between writing restart files:
1.0
hours
Write restart file based on:
Simulation time (s/crank angle/cycle)
Time interval for writing heat transfer data:
10.0
deg
Use file
Maximum number of restart files saved:
5
Generate map files
...
OK
Validate

Exporting Input Files

File > Export > Export Input Files

These files will be used in Cygwin to execute the simulation, as CONVERGE CFD relies on an external solver. This approach is applied to the Open-W piston case and similarly to the Omega piston case.

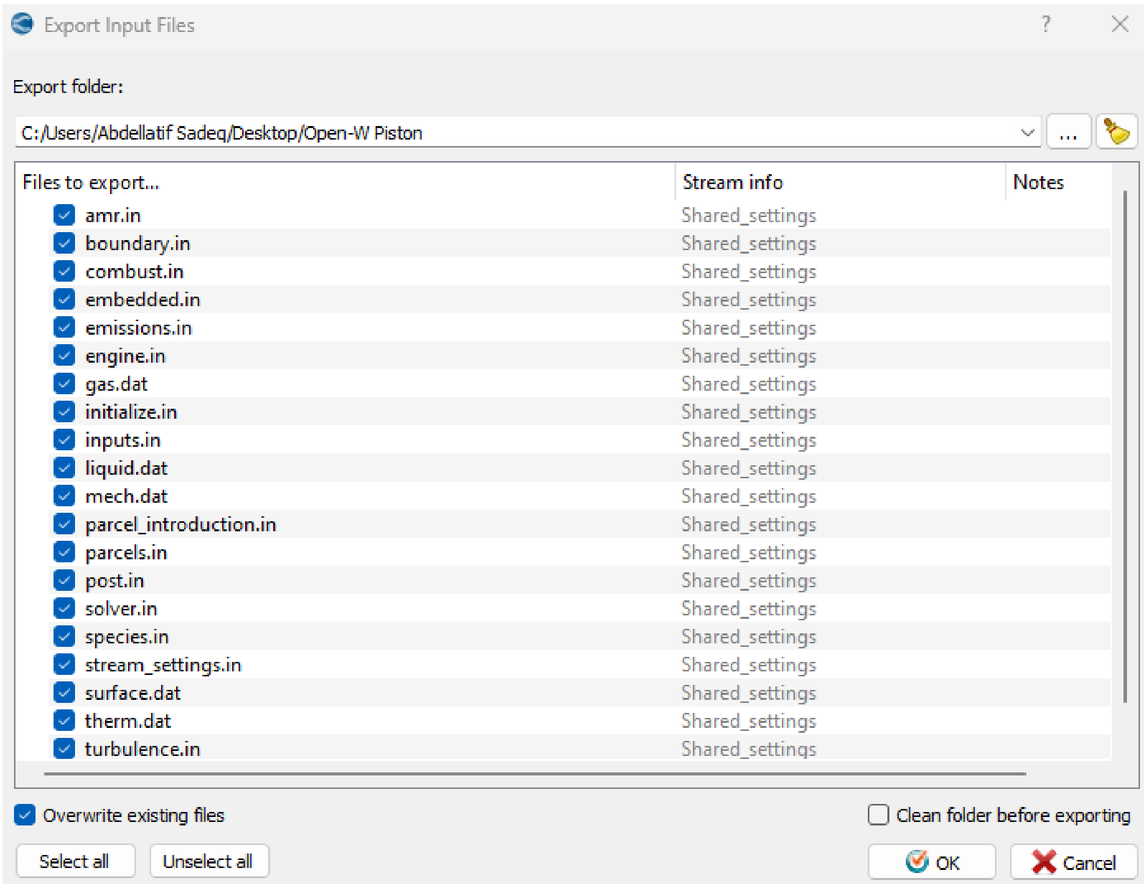

After navigating Cygwin to the directory containing the simulation input files, the following command is used to perform the simulation:

```
mpiexec -n 4 converge --license explore
```

Post Conversion

Files are converted for post-processing using CONVERGE CFD software. To begin, navigate to the 'Post-Processing 3D' tab, specify the directory containing the case files, and select the desired output format for the post-processing software. The same procedure applies to the Omega piston case.

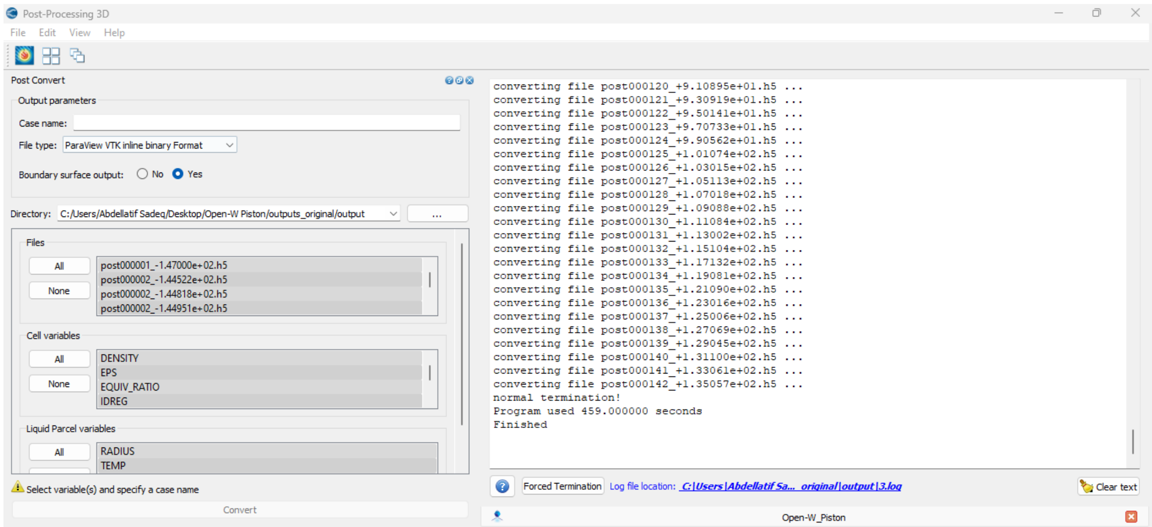

ParaView - Post Processing

The case is now prepared for post-processing. To begin post-processing in ParaView, select the .vtm group file. This approach is applied for the Open-W piston case and is applied in a similar manner to the Omega piston case.

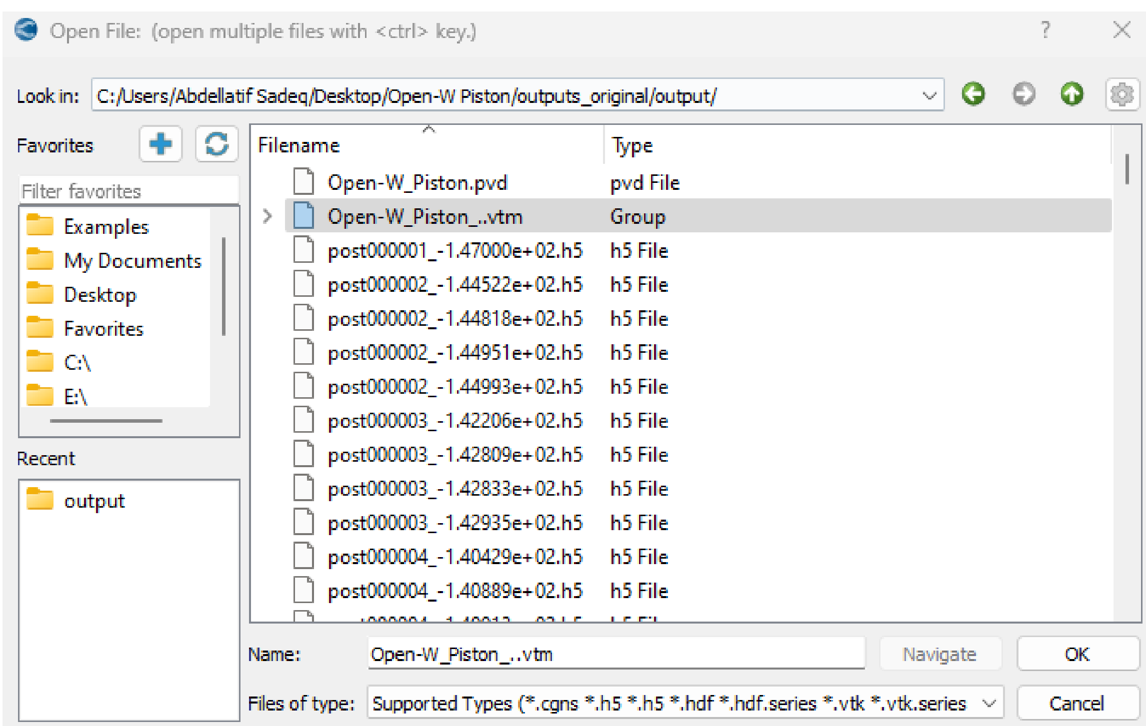

- **Mesh Refinement**

1. Open-W Piston

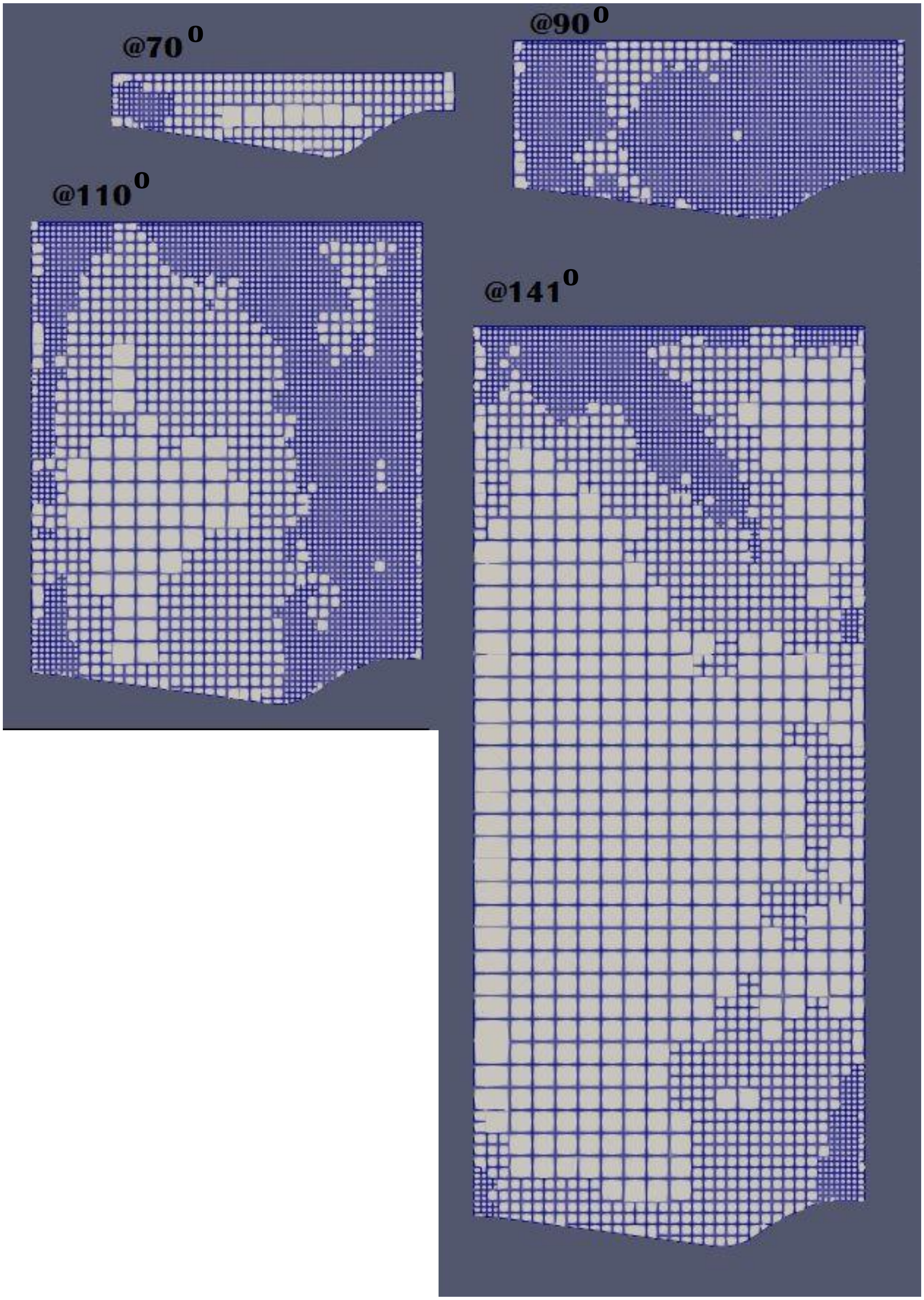

2. Omega Piston

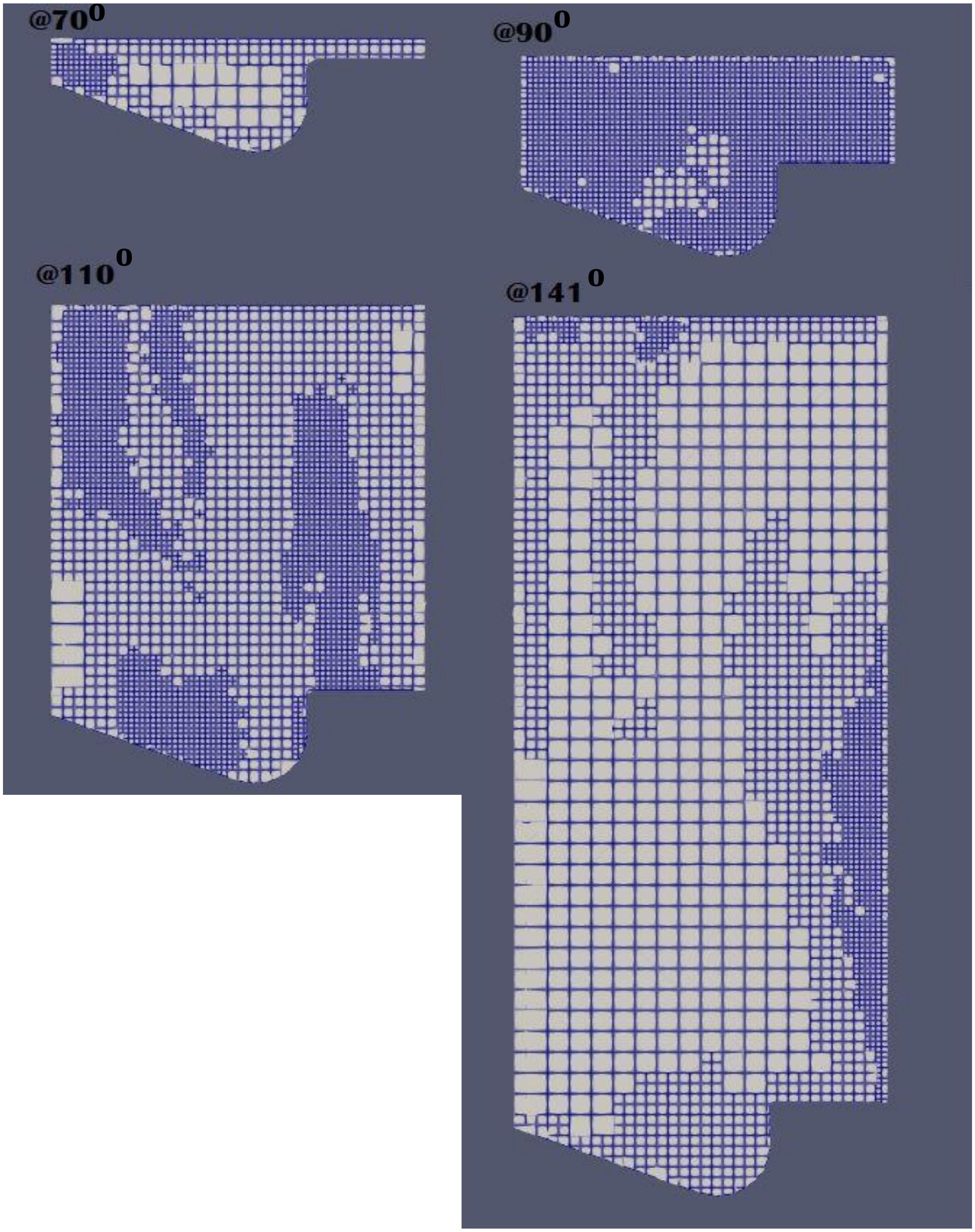

The mesh refinement combines AMR for resolving dynamic high-gradient regions and fixed embedding for consistent detail in critical areas, ensuring accuracy and efficiency for both piston configurations [17].

Results and Discussions

The results and discussions presented in this section aim to provide a comprehensive evaluation of the thermodynamic, combustion, emission, and performance characteristics of the Open-W and Omega piston configurations. By analyzing critical parameters such as in-cylinder pressure, temperature profiles, heat release rates, and emissions, the study highlights the influence of piston geometry on combustion efficiency and pollutant formation. The findings are contextualized to demonstrate trade-offs between performance metrics and environmental impacts, offering insights for optimizing diesel engine designs.

1. Thermodynamic and Combustion Dynamics Analysis

This first part presents a comparative analysis of key combustion parameters, including in-cylinder pressure, mean temperature, heat release rate (HRR), and integrated heat release rate (IHRR), to evaluate the thermodynamic and combustion dynamics of the Open-W and Omega piston configurations.

- **In-cylinder Pressure**

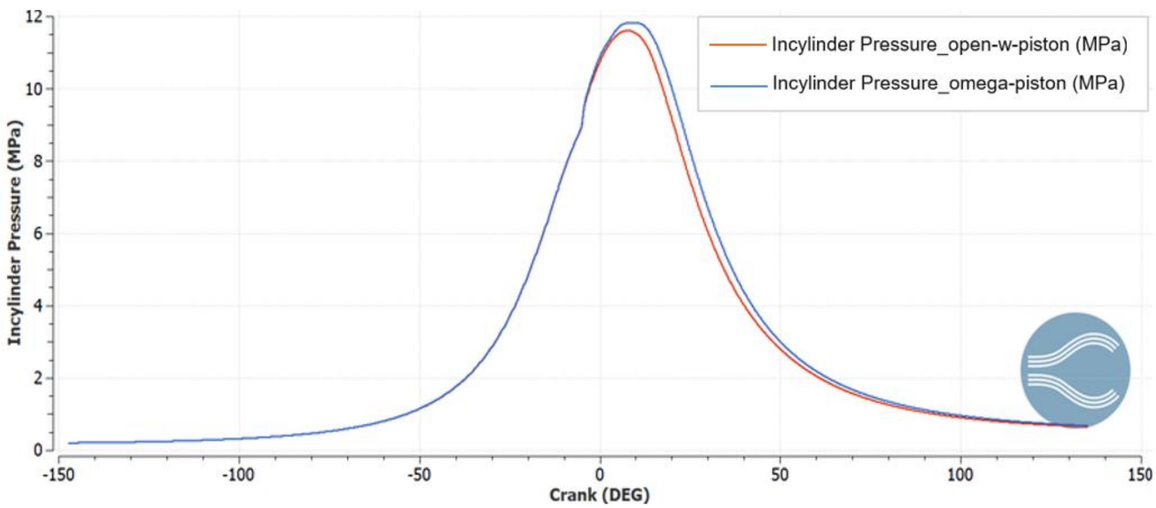

The in-cylinder pressure plot highlights a marginally higher peak pressure for the Omega piston compared to the Open-W piston. This indicates that the combustion in the Omega piston achieves slightly higher instantaneous energy conversion at its peak. This could be attributed to the geometric characteristics of the Omega piston, which potentially promotes a shorter but more intense combustion phase. However, this observation does not necessarily translate into better performance, as other factors, such as heat release and temperature distribution, need to be considered for a holistic evaluation.

- **Mean Temperature**

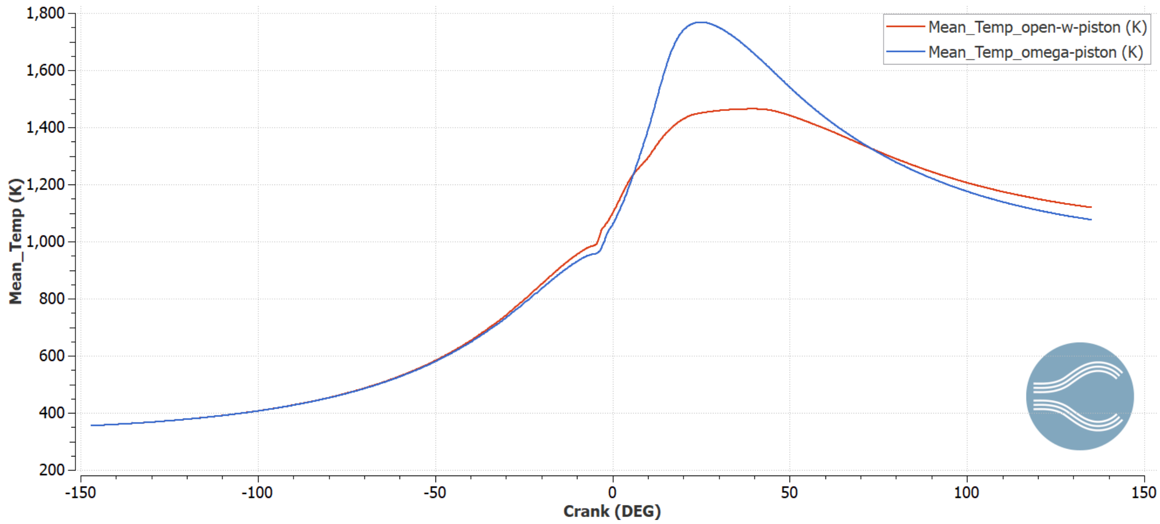

The mean temperature plot reveals significantly higher peak temperatures for the Omega piston, attributed to its bowl profile, which enhances swirl and turbulence, thereby improving air-fuel mixing and combustion efficiency. In contrast, the Open-W piston's simpler geometry results in less efficient mixing and evaporation. This leads to more localized fuel trapping and late combustion events, which cause higher localized temperatures in specific regions. While the Omega piston's design ensures better overall combustion and lower localized peaks, the Open-W piston's geometry inherently leads to uneven combustion patterns that affect temperature distribution [1]. However, the lower overall temperature in the Open-W piston, despite less efficient combustion, can have the advantage of reducing NO_x emissions.

- **Heat Release Rate (HRR)**

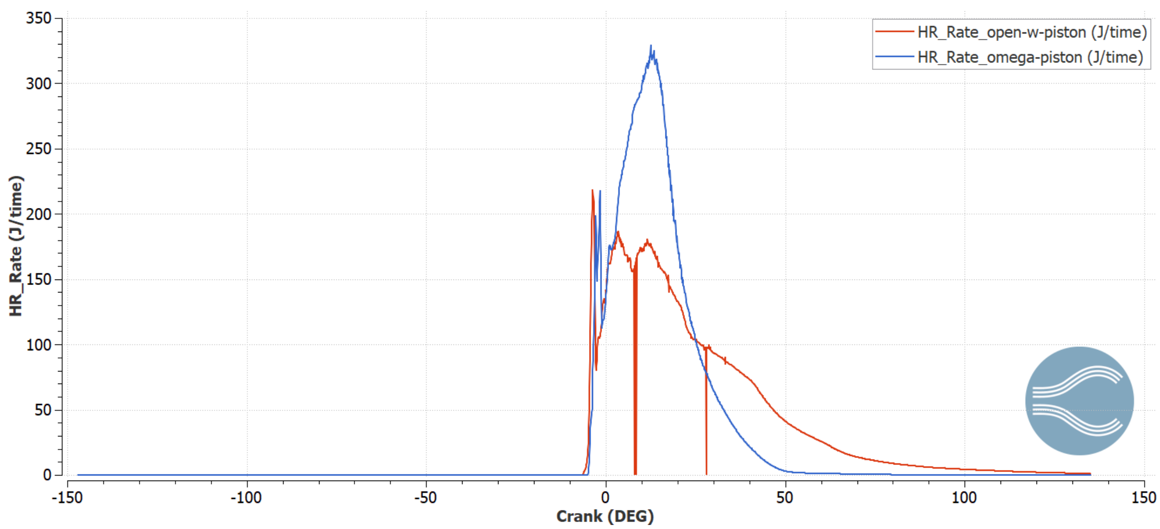

The HRR plot, after discounting the sharp noise-induced spike in the Open-W piston, shows that the Omega piston achieves a higher overall HRR. This aligns with its enhanced swirl and turbulence, promoting efficient combustion and contributing to the higher peak temperatures observed earlier. In contrast, the lower HRR of the Open-W piston reflects less efficient combustion, consistent with its lower overall temperatures and slower energy release.

- **Integrated Heat Release Rate (IHRR)**

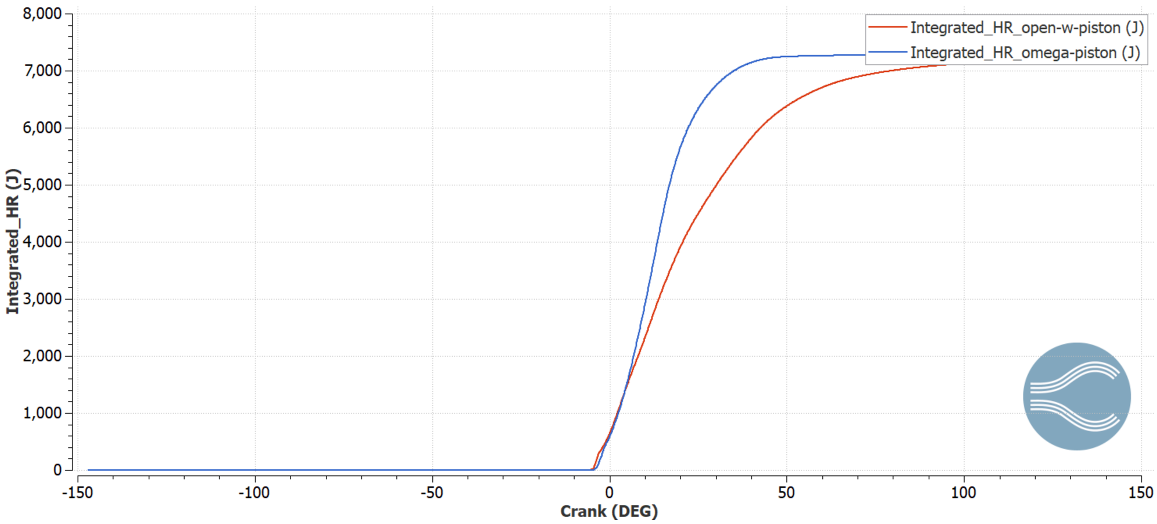

The IHRR curve provides a cumulative measure of energy release during the combustion process [18]. The Omega piston curve consistently remains above that of the Open-W piston, demonstrating its ability to release more total energy per cycle. Despite the same fuel injection quantity, the Omega piston shows an additional 67.56 Joules of energy per cycle compared to the Open-W piston. This additional energy, though advantageous in terms of overall efficiency, highlights the unutilized fuel in the Open-W piston, which accumulates across cycles and results in diminished long-term performance. However, the higher IHRR in the Omega piston underscores the importance of optimizing fuel utilization while managing the associated challenges of higher temperatures and potential NO_x emissions.

2. Emission Profiles

This second part examines the emission characteristics of NO_x, CO, and soot for the Open-W and Omega piston configurations. By analyzing these profiles, insights into the effects of piston geometry, combustion temperature, and air-fuel mixing on emission formation are provided, highlighting the trade-offs between combustion efficiency and pollutant generation.

- **NO_x Emission**

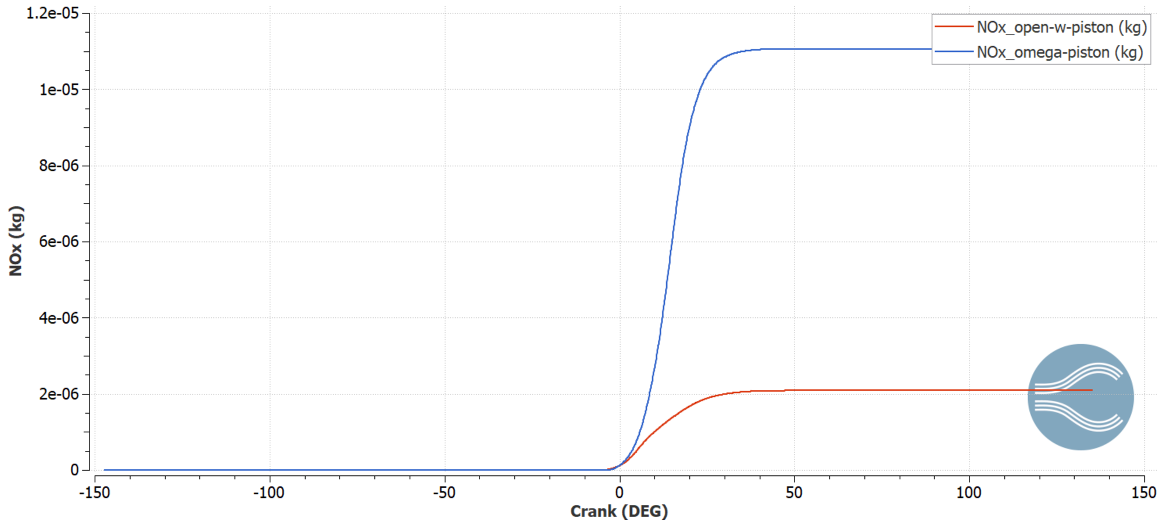

The production of NO_x in an engine cylinder depends on factors such as equivalence ratio, piston bowl geometry, combustion temperature, and peak pressure [19]. The plot shows the NO_x mass produced in the diesel engine cylinder, with higher NO_x concentrations observed in the Omega piston configuration. This increase is primarily attributed to the higher combustion temperatures and peak pressures achieved in the Omega piston, both of which accelerate the thermal NO_x formation pathway (Zeldovich mechanism) [16]. The plot further illustrates that NO_x formation begins with the onset of combustion and intensifies shortly after the occurrence of peak cylinder pressure, coinciding with the conditions conducive to NO_x production.

- **CO Emission**

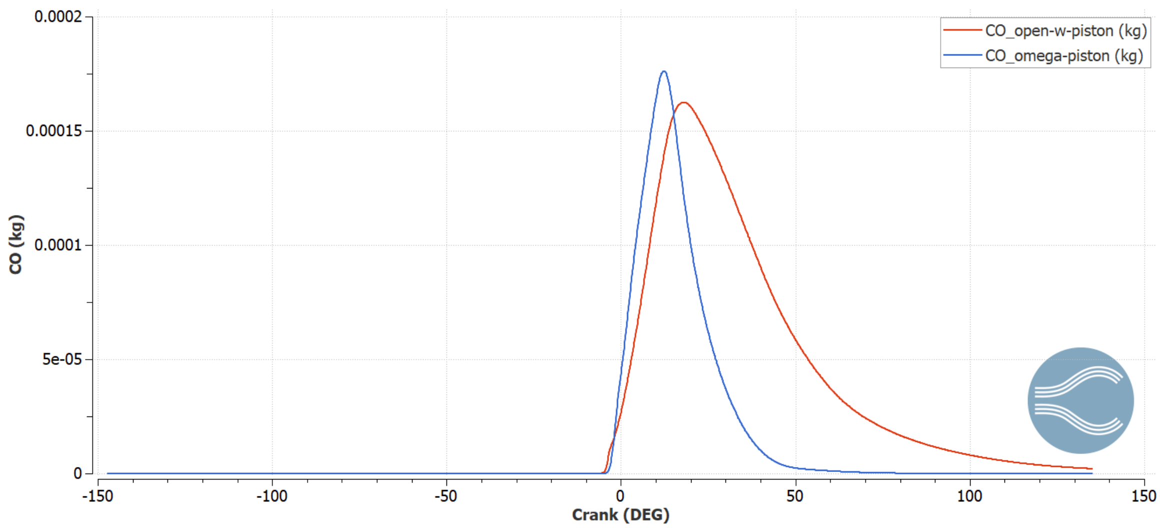

The formation of CO primarily results from incomplete combustion and improper air-fuel mixing [20]. In the engine cylinder with the Open-W piston, the simpler geometry leads to less efficient mixing of the air-fuel mixture, which reduces the reaction rate and results in lower combustion temperatures. These lower temperatures hinder effective flame propagation, causing incomplete fuel combustion and the production of a higher concentration of CO.

- **Soot Emission**

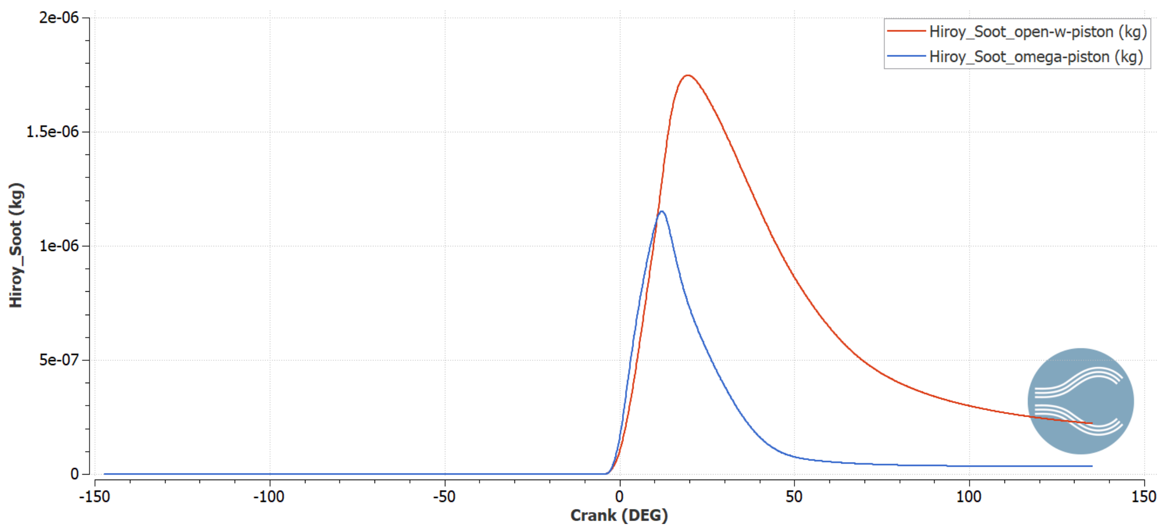

The incomplete combustion of fuel results in the formation of soot, often visible as black smoke, which primarily consists of carbon particles [21]. The plot compares the soot mass formed in the engine cylinders of Open-W and Omega piston configurations. It is evident that the engine with the Open-W piston produces a higher amount of soot. This can be attributed to its lower cylinder temperature, which limits the oxidation of soot precursors and hinders complete combustion. Additionally, the Open-W piston's simpler geometry leads to less efficient air-fuel mixing, further contributing to soot formation. In contrast, the Omega piston's enhanced swirl and turbulence promote better mixing and combustion, reducing soot production despite higher peak temperatures.

3. Performance Metrics

Using the engine performance calculator available in CONVERGE CFD, the power, torque, and IMEP are calculated and compared for the Open-W and Omega piston configurations.

- **Open-W Piston**

To calculate the power, the following formula is used [22]:

$$Power\ (P) = \frac{Work\ (W)}{Time\ (t)}$$

Based on the engine performance calculator,

Cycle (number)	CA From (deg)	CA To (deg)	Duration (deg)	Gross Work (N*m)	IMEP (Gross) (Pa)	CA10 (deg)	CA50 (deg)	CA90 (deg)	PFP (MPa)	PFP CA (deg)	HRR peak (J/deg)	HRR peak CA (deg)
1	-135.153	135.003	270.156	3028.53	1.24257e+06	0.70348	17.8347	53.0275	11.5373	5.90962	217.947	-3.59515

1. **Work Output (*W*):**

   W = 3028.53 N·m (calculated from engine performance metrics).

2. **Duration of Work (θ):**

   The work duration spans θ = 270.156 degrees of crankshaft rotation.

3. **Engine Speed (*N*):**

   Engine speed is specified as *N* = 1600 RPM (Revolutions Per Minute).

4. **Rotational Speed (*f*):**

   To convert to revolutions per second (RPS):

$$f = \frac{N}{60} = \frac{1600}{60} = 26.667 \text{ RPS}$$

5. **Angular Velocity (ω):**

   Total angular displacement per second is:

$$\omega = f * 360 = 26.667 * 360 = 9600 \text{ degrees per second}$$

6. **Time Duration (*t*):**

   To calculate the time for the given crank angle duration:

$$t = \frac{\theta}{\omega} = \frac{270.156}{9600} = 0.02814 \text{ seconds}$$

7. **Power (*P*):**

   To calculate the power, divide the work per time:

$$P = \frac{W}{t} = \frac{3028.53}{0.02814} = \mathbf{107.62\ KW}$$

Torque (T) Calculation:

$$P = \frac{(2\pi N T)}{60},$$

$$T = \frac{(P * 60)}{(2\pi N)} = \frac{(107.62 * 1000 * 60)}{(2 * 3.14 * 1600)} = \mathbf{642.64\ N \cdot m}$$

This value suggests a low-speed, high-torque engine, which is common for diesel engines.

- **Omega Piston**

Based on the engine performance calculator,

Cycle (number)	CA From (deg)	CA To (deg)	Duration (deg)	Gross Work (N*m)	IMEP (Gross) (Pa)	CA10 (deg)	CA50 (deg)	CA90 (deg)	PFP (MPa)	PFP CA (deg)	HRR peak (J/deg)	HRR peak CA (deg)
1	-135.153	135.018	270.171	3409.28	1.39878e+06	1.00833	12.5019	27.5283	11.2583	12.6081	329.543	12.6081

1. **Work Output (*W*):**

   W = 3409.28 N·m (calculated from engine performance metrics).

2. **Duration of Work (θ):**

   The work duration spans θ = 270.171 degrees of crankshaft rotation.

3. **Engine Speed (*N*):**

   Engine speed is specified as *N* = 1600 RPM (Revolutions Per Minute).

4. **Rotational Speed (*f*):**

   To convert to revolutions per second (RPS):

$$f = \frac{N}{60} = \frac{1600}{60} = 26.667 \text{ RPS}$$

5. **Angular Velocity (ω):**

   Total angular displacement per second is:

$$\omega = f * 360 = 26.667 * 360 = 9600 \text{ degrees per second}$$

6. **Time Duration (*t*):**

   To calculate the time for the given crank angle duration:

$$t = \frac{\theta}{\omega} = \frac{270.171}{9600} = 0.02814 \text{ seconds}$$

7. **Power (*P*):**

   To calculate the power, divide the work per time:

$$P = \frac{W}{t} = \frac{3409.28}{0.02814} = \mathbf{121.14\ KW}$$

Torque (T) Calculation:

$$P = \frac{(2\pi NT)}{60},$$

$$T = \frac{(P * 60)}{(2\pi N)} = \frac{(121.14 * 1000 * 60)}{(2 * 3.14 * 1600)} = \mathbf{723.37\ N \cdot m}$$

The following bar plot presents a comparison of power, torque, and IMEP between the Open-W and Omega piston configurations.

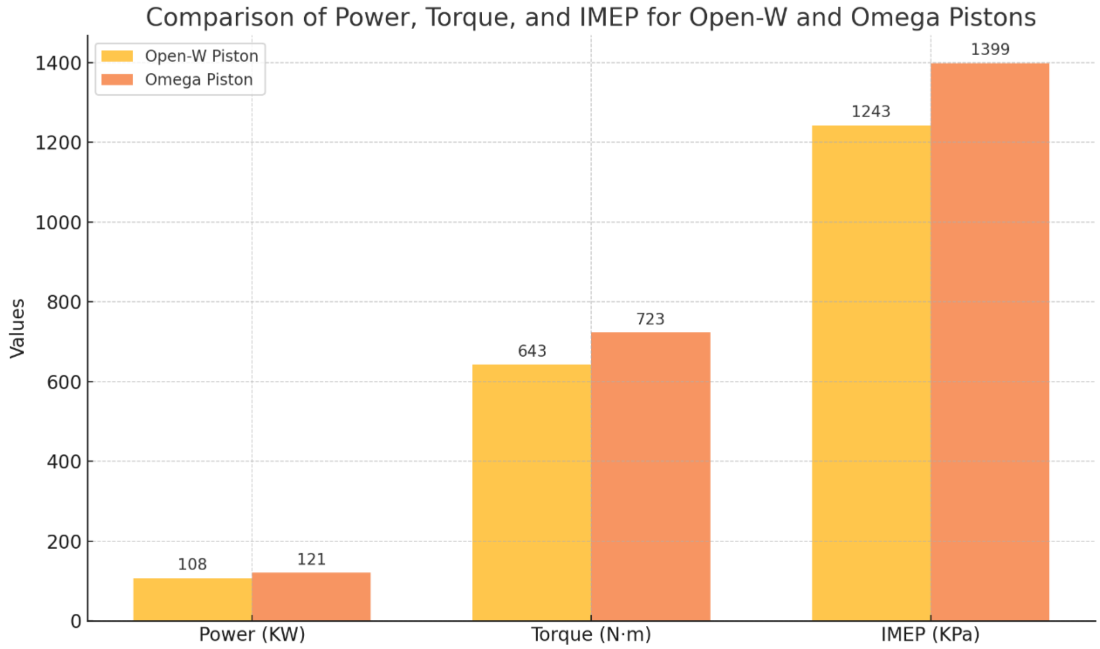

The bar plot highlights the performance differences between the Open-W and Omega piston configurations in terms of power, torque, and IMEP. The Omega piston demonstrates superior performance across all metrics, primarily due to its advanced bowl geometry, which enhances swirl, turbulence, and air-fuel mixing during combustion. This leads to a more efficient energy conversion process, as reflected in the higher power output and torque. Additionally, the increased IMEP indicates improved pressure distribution and sustained combustion efficiency in the Omega piston. These findings emphasize the critical role of piston geometry in optimizing engine performance while balancing emissions and thermal management.

Final Comparison

Table 1 provides a comprehensive comparison of the thermodynamic, combustion, emission, and performance metrics for the Open-W and Omega piston configurations. It highlights key parameters such as in-cylinder pressure, mean temperature, HRR, and IHRR, as well as emission characteristics like NO_x, CO, and soot emissions. Additionally, the table evaluates the overall performance in terms of power output, torque, and IMEP.

Table 1: Comparative Analysis of Thermodynamic, Combustion, Emission, and Performance Metrics for Open-W and Omega Pistons.

Parameter	Open-W Piston	Omega Piston	Selected Configuration
In-cylinder Pressure	Slightly lower peak pressure.	Marginally higher peak pressure due to intense combustion phase.	✔ Omega Piston
Mean Temperature	Lower overall temperatures; less swirl and mixing. Reduced NO_x emissions.	Higher peak temperatures due to enhanced swirl and turbulence. Increased NO_x emissions.	✔ Omega Piston
Heat Release Rate (HRR)	Lower overall HRR, less efficient combustion.	Higher HRR due to improved air-fuel mixing and sustained combustion.	✔ Omega Piston
Integrated HRR (IHRR)	Lower total energy release; unutilized fuel accumulation.	Higher total energy release per cycle, indicating better combustion efficiency.	✔ Omega Piston
NO_x Emission	Lower NO_x emissions due to lower combustion temperatures and pressures.	Higher NO_x emissions due to higher temperatures and pressures, promoting the Zeldovich mechanism.	✔ Open-W Piston
CO Emission	Higher CO emissions due to incomplete combustion and poor air-fuel mixing.	Lower CO emissions due to better combustion efficiency and mixing.	✔ Omega Piston

Parameter	Open-W Piston	Omega Piston	Selected Configuration
Soot Emission	Higher soot formation due to lower temperatures and incomplete combustion.	Lower soot formation due to efficient combustion and reduced soot precursor oxidation.	✔ Omega Piston
Power (KW)	107.62 KW	121.14 KW	✔ Omega Piston
Torque (N·m)	642.64 N·m	723.37 N·m	✔ Omega Piston
IMEP (KPa)	1243 KPa	1399 KPa	✔ Omega Piston

The comparative analysis in Table 1 demonstrates that the Omega piston configuration consistently outperforms the Open-W piston across most thermodynamic, combustion, emission, and performance metrics. While the Open-W piston exhibits advantages in reducing NO_x emissions due to its lower combustion temperatures, it suffers from higher CO and soot emissions, as well as lower overall power, torque, and IMEP. In contrast, the Omega piston leverages its advanced bowl geometry to enhance swirl, turbulence, and air-fuel mixing, resulting in superior energy conversion and combustion dynamics. However, the higher temperatures and pressures associated with the Omega piston demand careful optimization to balance performance gains with emission control. These findings underscore the critical role of piston design in achieving an optimal trade-off between engine efficiency and environmental impact.

Videos

The following videos were uploaded to YouTube, illustrating simulation results for the Open-W and Omega piston configurations over a cut-plan:

1. Open-W Piston

- **Mesh Animation:** A visualization showcasing the computational mesh used for the Open-W piston, highlighting the grid structure employed to capture combustion dynamics and fluid flow.

  Available at: https://youtu.be/DDiMa48QvLE

- **NO_x Formation:** This video illustrates the spatial and temporal distribution of NO_x concentrations within the Open-W piston, depicting regions with significant formation due to combustion processes.

  Available at: https://youtu.be/pAgTwTPCVaw

- **CO Formation:** This video shows the distribution of CO concentrations, emphasizing areas where incomplete combustion occurs and highlighting the resulting CO formation.

  Available at: https://youtu.be/nnWvOjHq4gQ

- **Soot Formation:** This video highlights the formation of soot within the Open-W piston, showing areas where carbon particles are generated due to combustion characteristics.

  Available at: https://youtu.be/QszYVyjJ4Wg

2. Omega Piston

- **Mesh Animation:** A visualization displaying the computational mesh used for the Omega piston, detailing the grid structure and its role in simulating combustion processes and fluid flow.

  Available at: https://youtu.be/1c0DOockaQ0

- **NO_x Formation:** This video demonstrates the distribution of NO_x concentrations within the Omega piston, highlighting areas where NO_x is formed during combustion.

  Available at: https://youtu.be/wzkpWpFq6zQ

- **CO Formation:** This video presents the CO concentration distribution, illustrating the generation of CO within the Omega piston due to specific combustion conditions.

  Available at: https://youtu.be/72juQ0yBLhQ

- **Soot Formation:** This video shows the regions where soot particles are formed within the Omega piston, depicting the combustion characteristics leading to carbon particle generation.

  Available at: https://youtu.be/-2idbXfH3oQ

References

1. V. C. Pham, J. K. Kim, W.-J. Lee, S.-J. Choe, V. V. Le, and J.-H. Choi, "Effects of Piston Bowl Geometry on Combustion and Emissions of a Four-Stroke Heavy-Duty Diesel Marine Engine," *Applied Sciences*, vol. 12, no. 24, p. 13012, Dec. 2022. DOI: 10.3390/app122413012.

2. A. Jamil, M. B. Baharom, and A. R. A. Aziz, "IC engine in-cylinder cold-flow analysis – A critical review," *Alexandria Engineering Journal*, vol. 60, no. 3, pp. 2921–2945, Jun. 2021. DOI: 10.1016/j.aej.2021.01.040.

3. C. Xu, M. A. Kalam, and H. Cho, "The Study on the Effect of the Piston Shapes through Biodiesel Mixture Combustion in Diesel Engine," *E3S Web of Conferences*, vol. 53, no. 4, p. 03022, Jan. 2018. DOI: 10.1051/e3sconf/20185303022.

4. D. P. Schmidt and C. Rutland, "A New Droplet Collision Algorithm," *Journal of Computational Physics*, vol. 164, no. 1, pp. 62–80, Oct. 2000. DOI: 10.1006/jcph.2000.6568.

5. M. H. H. Ishak, F. Ismail, S. Che Mat, M. S. Abdul Aziz, M. Z. Abdullah, and A. Abas, "Numerical study on the influence of nozzle spray shape on spray characteristics using diesel and biofuel blends," *Biofuels*, vol. 12, pp. 1–13, Apr. 2019. DOI: 10.1080/17597269.2019.1583717.

6. S. Y. Deng, "Comparing Simulation for Turbulent Dispersion and Coalescence of Droplets within a Spray with Two Models," *Applied Mechanics and Materials*, vol. 353, pp. 2473–2476, Aug. 2013. DOI: 10.4028/www.scientific.net/AMM.353-356.2473.

7. M. Dodd, D. M. Khorassani, A. Ferrante, and M. Ihme, "Analysis of droplet evaporation in isotropic turbulence through droplet-resolved DNS," *International Journal of Heat and Mass Transfer*, vol. 172, p. 121157, Jun. 2021. DOI: 10.1016/j.ijheatmasstransfer.2021.121157.

8. S. Wadekar, A. Yamaguchi, and M. Oevermann, "Large-Eddy Simulation Study of Ultra-High Fuel Injection Pressure on Gasoline Sprays," *Flow Turbulence and Combustion*, vol. 107, pp. 149–174, Jun. 2021. DOI: 10.1007/s10494-020-00231-0.

9. R. B. Stull, "Turbulence Kinetic Energy, Stability and Scaling," in *An Introduction to Boundary Layer Meteorology*, vol. 13, Springer, Dordrecht, 1988, DOI: 10.1007/978-94-009-3027-8_5.

10. A. V. Demidovich, S. S. Kralinova, P. P. Tkachenko, N. E. Shlegel, and R. S. Volkov, "Interaction of Liquid Droplets in Gas and Vapor Flows," *Energies*, vol. 12, no. 22, p. 4256, Nov. 2019. DOI: 10.3390/en12224256.

11. C. Harms, H. Fazeli, and J. Vanaken, "The Characteristics of Flow Discharge Coefficient of Plain Orifice Geometries on Pintle Injector Design," *International Journal*

of Fluid Mechanics Research, vol. 48, no. 5, Jan. 2021. DOI: 10.1615/InterJFluidMechRes.2021039337.

12. M. Medina, A. Bautista, M. Wooldridge, and R. Payri, "The Effects of Injector Geometry and Operating Conditions on Spray Mass, Momentum and Development Using High-Pressure Gasoline," *Fuel*, vol. 294, p. 120468, Jun. 2021. DOI: 10.1016/j.fuel.2021.120468.

13. C. Bekdemir, L. M. T. Somers, and P. Goey, "Numerical Modeling of Diesel Spray Formation and Combustion," *Brain Research*, Jan. 2009.

14. A. Piano, A. Scalambrò, F. Millo, F. Catapano, P. Sementa, S. Di Iorio, and A. Bianco, "CFD-Based Methodology for the Characterization of the Combustion Process of a Passive Pre-Chamber Gasoline Engine," *Transportation Engineering*, vol. 13, p. 100200, Sep. 2023. DOI: 10.1016/j.treng.2023.100200.

15. T. Yang, H. Zhou, Y. Yin, and Z. Ren, "Zone-Adaptive Modeling of Turbulent Flames with Multiple Chemical Mechanisms," *Proceedings of the Combustion Institute*, vol. 39, no. 2, pp. 2409–2418, 2023. DOI: 10.1016/j.proci.2022.09.034.

16. L. Anetor, C. Odetunde, and E. Osakue, "Computational Analysis of the Extended Zeldovich Mechanism," *Arabian Journal for Science and Engineering*, vol. 39, pp. 8287–8305, Nov. 2014. DOI: 10.1007/s13369-014-1398-7.

17. A. Pappa, A. Verhaeghe, P. Bénard, W. De Paepe, and L. Bricteux, "Adaptive Mesh Refinement Towards Optimized Mesh Generation for Large Eddy Simulation of Turbulent Combustion in a Typical Micro Gas Turbine Combustor," *Energy*, vol. 301, p. 131550, Aug. 2024. DOI: 10.1016/j.energy.2024.131550.

18. G. R. Srinivasan, R. Jambulinga, A. Gacem, A. Ahmad, J. K. Bhutto, K. K. Yadav, A. Mezni, O. K. R. Alharbi, S. Islam, Y. Ahn, and B.-H. Jeon, "Effect of Fuel Preheating on Engine Characteristics of Waste Animal Fat-Oil Biodiesel in Compression Ignition Engine," *Polymers*, vol. 14, no. 18, p. 3896, Sep. 2022. DOI: 10.3390/polym14183896.

19. M. N. Nabi, M. G. Rasul, M. A. Arefin, M. W. Akram, M. T. Islam, and M. W. Chowdhury, "Investigation of major factors that cause diesel NO_x formation and assessment of energy and exergy parameters using e-diesel blends," *Fuel*, vol. 292, p. 120298, May 2021. DOI: 10.1016/j.fuel.2021.120298.

20. İ. A. Reşitoğlu, K. Altinişik, and A. Keskin, "The pollutant emissions from diesel-engine vehicles and exhaust aftertreatment systems," *Clean Techn Environ Policy*, vol. 17, pp. 15–27, Jan. 2015. DOI: 10.1007/s10098-014-0793-9.

21. F. A. Atiku, E. J. S. Mitchell, A. R. Lea-Langton, J. M. Jones, A. Williams, and K. D. Bartle, "The Impact of Fuel Properties on the Composition of Soot Produced by the Combustion of Residential Solid Fuels in a Domestic Stove," *Fuel Process. Technol.*, vol. 151, pp. 117–125, Oct. 2016. DOI: 10.1016/j.fuproc.2016.05.032.

22. H. Tanweer, B. Soomro, D. Muhammad, A. Fatah, M. Waseem, and A. Ateeque, *Experimental Analysis of Diesel and Dual-Fuel Engine*, Oct. 2020.